Fabrication of 3D Hybrid Architectures Composed of sp^2-Carbon and Inorganic Materials

by

S. Mahyar Mazloumi Sadat

A thesis

presented to the University of Waterloo

in fulfillment of the

thesis requirement for the degree of

Doctor of Philosophy

in

Chemistry - Nanotechnology

Waterloo, Ontario, Canada, 2013

Declaration

I hereby declare that I am the sole author of this thesis. This is a true copy of the thesis, including any required final revisions, as accepted by my examiners. I understand that my thesis may be made electronically available to the public.

Abstract

Three dimensional (3D) hybrid architectures are new types of materials that have a number of technological applications. However, the synthesis of such materials has been problematic to date. The objective of this study is to fabricate 3D hybrid architectures composed of sp^2-carbon nanomaterials and inorganic nanostructures using a convenient microwave assisted technique.

Sp^2-Carbon nanomaterials such as carbon nanotubes (CNTs), graphene and its derivative graphene oxide (GO), have been explored by researchers as major components of hybrid materials due to their exceptional electrical, thermal, mechanical and biological properties. However, most of the research has been devoted to the hybrids with randomly dispersed phases. The present study explores the feasibility of using aligned 3D sp^2-carbon structures in a bottom-up microwave-assisted chemical synthesis approach to fabricate various 3D sp^2-carbon/inorganic hybrid architectures. The carbon nanostructures, either tubular or planar, not only contribute to the functionalities of the hybrids, but also template the ordered assembly of phases on nanometer scale.

Mimicking nature is a key to develop novel types of materials with enhanced physical and mechanical properties suitable for advanced applications (e.g. lightweight and yet tough materials that are extensively needed in automotive and aerospace industries). One approach to obtain such materials or devices is to mimic nature processes and synthesize hybrid materials with ordered structures on the nanometer scale. Those functional structures are fabricated in this thesis through an in-situ microwave synthesis of inorganic materials on 3D sp^2-carbon architectures. Generally, in chapter 1, it was shown and discussed the procedures to fabricate 3D architectures of carbon nanotubes and graphene oxide as basic components for template

synthesis of the hybrids. Then in chapter 2 the microwave chemical synthesis approach was introduced as a convenient route for fabricating inorganic materials such as zinc oxide (ZnO) which was shown to be used as UV sensors.

Through photolithography patterning of the iron catalyst thin films on Si/SiO_2 substrates, 3D aligned CNT structures were fabricated and were coated in-situ with inorganic materials such as cobalt oxide, zinc oxide and manganese oxide using a microwave synthesis approach (chapter 3). The obtained aligned strips of CNT/Co_3O_4 were chosen as an example to illustrate the application of such 3D hybrids in energy storage applications. The capacitance of the aligned CNT/Co_3O_4 strips was measured to be 123.94 F/g.

Using graphene oxide as template for manufacturing the 3D sp^2-carbon/inorganic hybrid structures, interesting novel layered configurations are obtained that are similar to the layered structures of exoskeleton of the mollusks nacre. The layered hybrid structure shown to be mechanically improved compared to its constituents (chapter 4). Finally in chapter 5, some of the future routes have been proposed for further research on this novel field of 3D hybrid materials composed of sp^2-carbons and inorganic nanomaterials.

Dedication

I would like to dedicate this dissertation to my parents (Reza and Marzieh) and my lovely sisters (Mahsan and Mahnoosh) who are always supportive to me and trust me in reaching my dreams. Also, to all my friends who showed me the real meaning of friendship and are always kind and helpful to me.

Table of contents

Contents

List of Figures

List of Abbreviations

1D	One Dimensional
2D	Two Dimensional
3D	Three Dimensional
AFM	Atomic Force Microscopy
ALD	Atomic Layer Deposition
BET	Brunauer-Emmett-Teller
CNTs	Carbon Nanotubes
CV	Cyclic Voltammetry
CVD	Chemical Vapor Deposition
DWNTs	Double Walled Carbon Nanotubes
EDX	Energy Dispersive X-ray spectroscopy
GO	Graphene Oxide
HA	Hydroxyapatite
MBE	Molecular Beam Epitaxy
MO	Metal Oxide
MOCVD	Metal-Organic Chemical Vapor Deposition
MWNTs	Multi Walled Carbon Nanotubes
NHE	Normal Hydrogen Electrode
PDMS	Polydimethylsiloxane
PC	Polycarbonate
PECVD	Plasma Enhanced Chemical Vapor Deposition
PET	Polyethylene Terephthalate

PLD   Pulsed Laser Deposition

PMMA   Poly(methyl methacrylate)

SEM   Scanning Electron Microscopy

SOI   Semiconductor-On-Insulator

SWNT   Single Walled Carbon Nanotubes

TEM   Transmission Electron Microscopy

VLS   Vapor-Liquid-Solid

XRD   X Ray Diffraction

CHAPTER 1. Background

1.1. Introduction

During the past decade, lots of important and exciting fore-front fields have emerged in Physics, Chemistry, Engineering and Biology due to the advancements in nanotechnology which deals with the structure and properties of materials at nanometer scale (less than 100 nm). The scaling down of materials and devices through nanotechnology hold the promise of not only reducing the manufacturing costs compared to conventional technologies, but also increasing the efficiency of the systems and making them more environmental friendly (1).

Carbon allotropes (eg. Carbon nanotubes, Graphene sheets, Diamonds and Buckyballs) in this regard have received huge attention (2). Among them, more research has been devoted to carbon nanotubes (CNTs, 1D) and graphene structures (2D) owing to their exceptional properties including high electrical conductivity and mechanical strength. They have been used widely as components of composites to obtain new categories of materials with superior characteristics than the constituents (3). As it was mentioned before, the essence of fabricating new materials that can fulfill the requirements of advanced applications led to the development of hybrid structures composed of different components with diverse properties (4). The hybrid structures which are inspired from nature have unique features resembling the biological systems i.e. self-assembly of the building blocks, hierarchy and multi-functionality of the structures (5). Such novel hybrid materials are favorable mechanically and have potential applications in various fields for instance in energy storage or electronics (6–10). Chapter 1 of the current thesis deals with the background information and literature review on the synthesis processes and parameters

that affect the production of carbon nanotubes, graphene oxide films, inorganic nanoparticles and their hybrid structures.

1.2. Carbon nanotube

1.2.1. What are carbon nanotubes?

Carbon nanotubes are the tubular allotrope of carbon with sp^2 hybrid C-C bonds. They can be formed as single walled (SWNT), double walled (DWNT), or multi walled (MWNT) concentric carbon tubes with different chiralities, diameters, lengths, and be organized into various shapes such as films, mats, forests, and yarns (11–14). Figure 1.1.a shows a TEM image of the DWNTs and MWNTs with different diameters and number of walls. Figure 1.1.b shows schematically the hexagonal order of the carbon atoms in the graphene sheet.

Basically carbon nanotubes can be defined as 1D materials composed of rolled-up graphene sheets. Depending on the direction and vector that the graphene sheet rolls around, the chirality of the obtained CNT is determined. The chirality of SWNTs is defined by a vector called chiral vector $\vec{C}$:

$$\vec{C} = n\vec{a_1} + m\vec{a_2} \qquad\qquad (1)$$

in which n and m are integers and $\vec{a_1}$ and $\vec{a_2}$ are the unit cell vectors in the two dimensional lattice of graphene sheet (15). The CNT axis is perpendicular to the chiral vector $\vec{C}$. The value of (n,m) determines the chirality of a CNT (i.e. armchair, zigzag and chiral) and it's electrical, optical and mechanical properties.

2
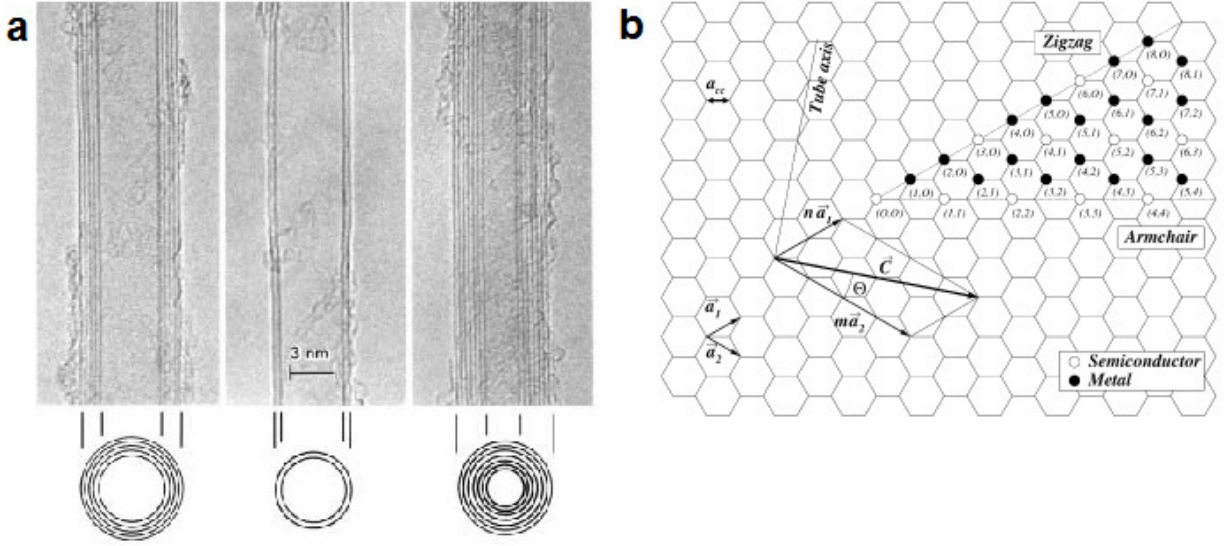
Figure 1.1. (a) TEM images of double wall and multi wall carbon nanotubes(Adopted from ref. (16) with permission). (b) Schematic image of hexagonal order of carbon atoms in the graphene sheet showing the chiral vector $\vec{C}$ and chiral angel θ for a (2,4) nanotubes(Adopted from ref. (17) with permission).

For instance if |n-m|=3p, the CNTs are metallic and if |n-m|=3p±1, the CNTs are semiconducting (p is an integer). The circumference of the CNTs is equal to the chiral vector length (15):

$$c = |\vec{c}| = a\sqrt{n^2 + nm + m^2} \qquad (2)$$

Therefore the diameter of the CNTs can be obtained by the following formula:

$$D = \frac{c}{\pi} \qquad (3)$$

MWNTs can be considered as a tubular structure with several concentric SWNTs which are observed in TEM images (Figure 1.1). The intertubular distance between the concentric SWNTs is defined as:

$$d = 0.344 + 0.1\exp\left(-\frac{c}{4\pi}\right) \qquad (4)$$

in which $\frac{c}{4\pi}$ is the radius of the CNTs and c is the length of chiral vector.

3

Not all the (n,m) combinations in the chiral vector are defined for MWNT chirality. The structure and electronic properties of MWNTs are not as diverse as SWNTs and they are metallic (18).

1.2.2. CNT synthesis

SWNTs and MWNTs have been produced through various processes among which arc discharge, laser ablation and chemical vapor deposition are the most relevant ones for mass production.

1.2.2.1. Arc discharge

Arc discharge is the method that CNTs were first discovered with in 1991 by Iijima (16). In this method CNTs are produced when a direct-current arc voltage is applied between two graphitic electrodes placed in an inert gas such as Helium or Argon (Figure 1. 2). At a temperature of about 4000K, the solid carbon atoms evaporate from the electrodes and consequently the CNTs form during the condensation of hot gaseous carbon atoms. Buckyballs, MWNTs and SWNTs can be made through this process. When the pure graphitic electrodes are used, buckyballs are produced inside the chamber and MWNTs on the cathode. In order to synthesize SWNTs, a metal catalyst is needed (Fe, Co or their mixtures) with a pure graphite cathode (11,19). Although the arc-discharge method is very simple and common, it's hard to separate the obtained CNTs from the crude product including soot, catalytic metals, and various side products such as buckyballs, amorphous carbon and graphite particles.
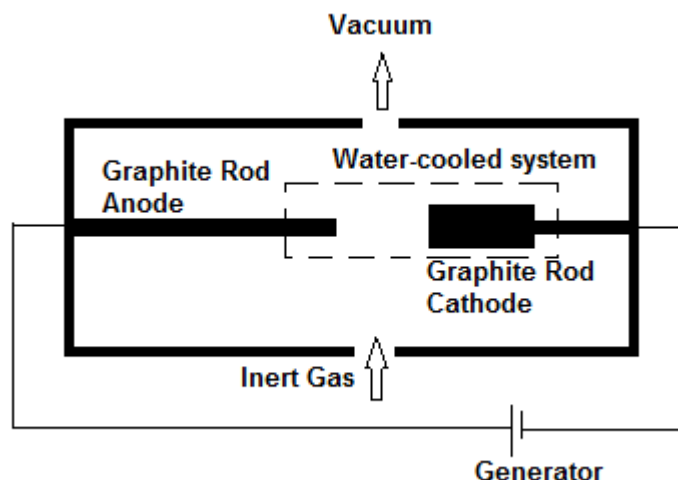
Figure 1. 2. Schematic drawing of an arc discharge oven for CNT synthesis.

1.2.2.2. Laser ablation

Laser ablation technique involves the evaporation of solid graphitic electrodes into a hot carbon gas under inert atmosphere using a pulsed or continuous laser beam. The carbon gases condense on a collector as soot that has CNTs in it. The same as arc discharge, here the pure graphite electrodes produce MWCNTs and the electrodes mixing with catalyst particles (Fe, Co), produce SWCNTs (20). While the quality of the MWCNTs depend on temperature more effectively when the pure graphite electrode is used, the quality of SWCNTs depend on the catalyst particles (20).

However, these two methods (arc discharge and laser ablation) are less favored for production of CNTs since they need expensive instruments and they consume a lot of energy. Also, only entangled bundles of nanotubes in powder form can be produced and it's less favored for controlled synthesis of ordered CNT structures on substrates (11).

1.2.2.3. Chemical vapor deposition

In chemical vapor deposition (CVD) method, a volatile compound of carbon such as ethanol or a hydrocarbon like ethylene or acetylene decompose at high temperature (500 to 1100 °C) assisted by catalyst particles (Fe, Co, Mo or mixtures) which also act as nucleation site for CNT growth (Figure 1. 3) (11,20).
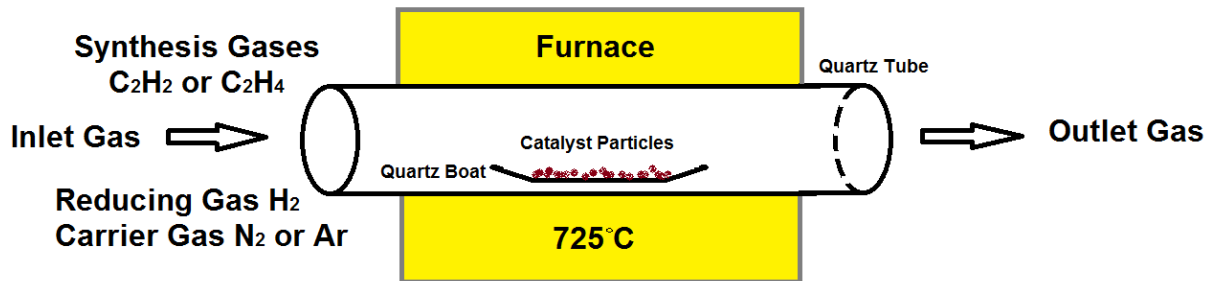
Figure 1. 3. Schematic drawing of a chemical vapor deposition (CVD) chamber.

Both SWNTs and MWNTs can be well made through CVD process and it's possible to control and manipulate the morphology and structure of the obtained nanotubes. For instance various forms of CNTs e.g. mats (21), yarns (22), vertically aligned CNTs (23), horizontal CNT arrays (24) and patterned CNT structures (25) have been synthesized through CVD method.

Using plasma CVD instead of thermal CVD, the growth temperature can be reduced and it is possible to grow individual, free-standing, vertical CNTs. When the gases are in the plasma state, they become ionized and have high energy electrons (few electron volts). These electrons supply the energy needed for chemical reactions while the gas itself is relatively cooler (300-500 K) compared to that in thermal CVD methods (26).

1.2.3. Aligned Carbon Nanotubes

Improvements have been made to CVD methods to reduce the production of amorphous carbon on the catalyst particles and therefore increase the growth yield of nanotubes (13,14). It has been shown that small amounts of water vapor or oxygen together with the synthesis gases can reactivate the catalysts and enhance their performance to produce nanotubes. Therefore longer CNTs can be obtained (14,27). Also using thin film catalysts instead of nanoparticles results in the formation of aligned CNT structures. At growth temperature, catalyst thin films turn into catalyst nanoparticles dispersed homogenously all over the substrate. The density and size of the catalyst nanoparticles depend on the thin film thickness and the annealing temperature and therefore defines the final morphology of the CNTs. A denser catalyst dispersion leads to a more compact CNT structure, because the nanotubes lean on each other during the growth via van der Waals forces (28). Wei et al. (28) have shown that the thinner the catalyst film, the smaller the particles are during thermal annealing and the denser are the obtained CNTs (Figure 1. 4).

It has been reported that presence of a thin alumina supporting layer enhances the catalyst activity and density of the CNTs as well as their length and these features are influenced by the porosity of the alumina layer (29). It's possible to grow CNTs as tall as 1 millimeter with the help of alumina supporting layer (30).
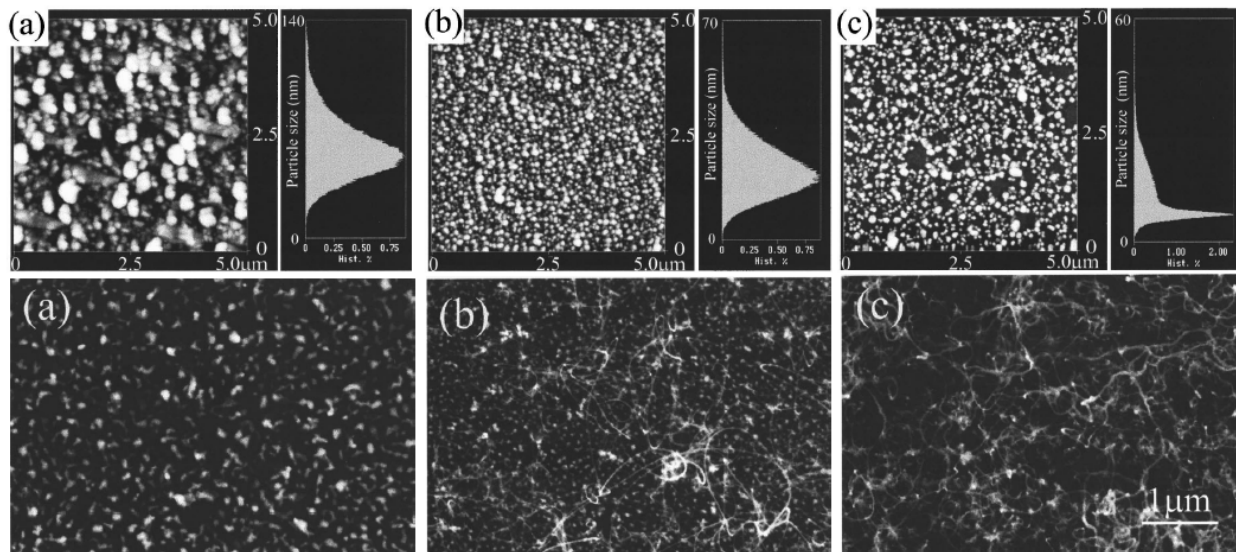
Figure 1. 4. AFM images (top) of Fe catalyst particles on a Si(100) substrate with 500 nm thick SiO$_2$ layer after thermal annealing at 660 ˚C for 10 minutes. SEM images (bottom) of the corresponding CNTs grown on the substrates shown above. The thickness of Fe films are (a) 20 nm, (b) 10 nm and (c) 5 nm (Adopted from ref. (28) with permission).

1.2.4. Patterned Aligned CNT Structures

Owing to the advancements in Micro and Nanotechnology, several fabrication techniques have been developed to use the patterning processes in designing various catalyst configuration and shapes on the wafer substrates. Photolithography is a technique in which a substrate with a desired pattern design is made that can be deposited later with a catalyst thin film. The patterned catalyst, when it's used for CNT growth result in a patterned CNT structure with a three dimensional configuration.

Basically the substrate is coated with a light-sensitive chemical called "photo-resist", or simply "resist". Later, a light source (UV for example) is used to transfer a geometric pattern from a photo-mask to the photo-resist coated on the substrate. Then the exposed area is treated chemically either to stabilize and fix the patterned design on the photo-resist or to etch it away, depending on the photo-resist type (i.e. negative or positive respectively, Figure 1. 5).

8
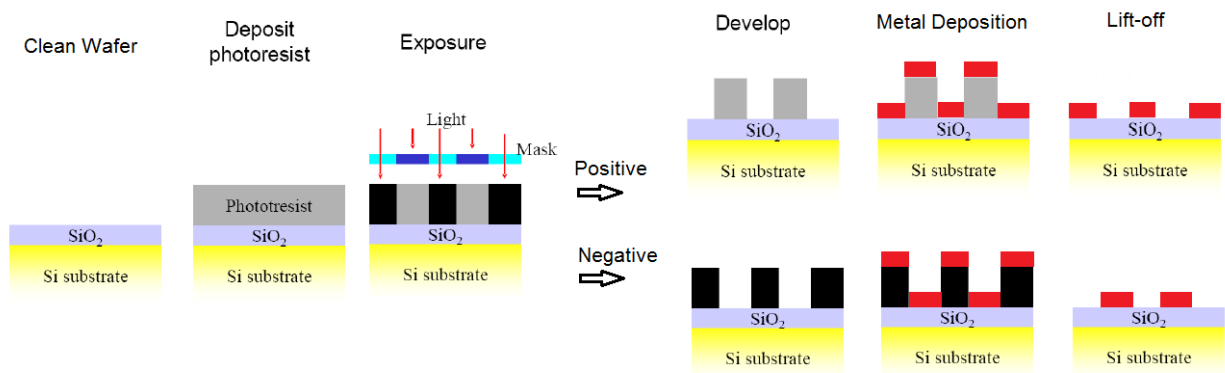
Figure 1. 5. Schematic steps in photolithography and design of a patterned catalyst substrate.

The obtained pattern on the substrate can be coated with a metal catalyst through electron beam deposition or sputtering techniques. At the end, when the photo-resist is gone at the lift-off step, the patterned designs of the desired metallic catalyst remain on the substrate. The obtained substrate with the patterned catalyst design can be used to grow CNTs through CVD process. Figure 1. 6 shows typical structures of the aligned CNTs grown through a CVD method on a patterned design of Fe catalysts on a Si/SiO$_2$ substrate. It has been shown schematically that during the growth in the CVD chamber and at high temperatures, synthetic gases dissociate on the catalyst patterns on the substrate, dissolve in it and later CNTs only grow at those areas where catalyst film presents. Therefore lots of different shapes of aligned CNTs can be made with this technique which can be beneficial for various applications and will be discussed later in chapter 3.
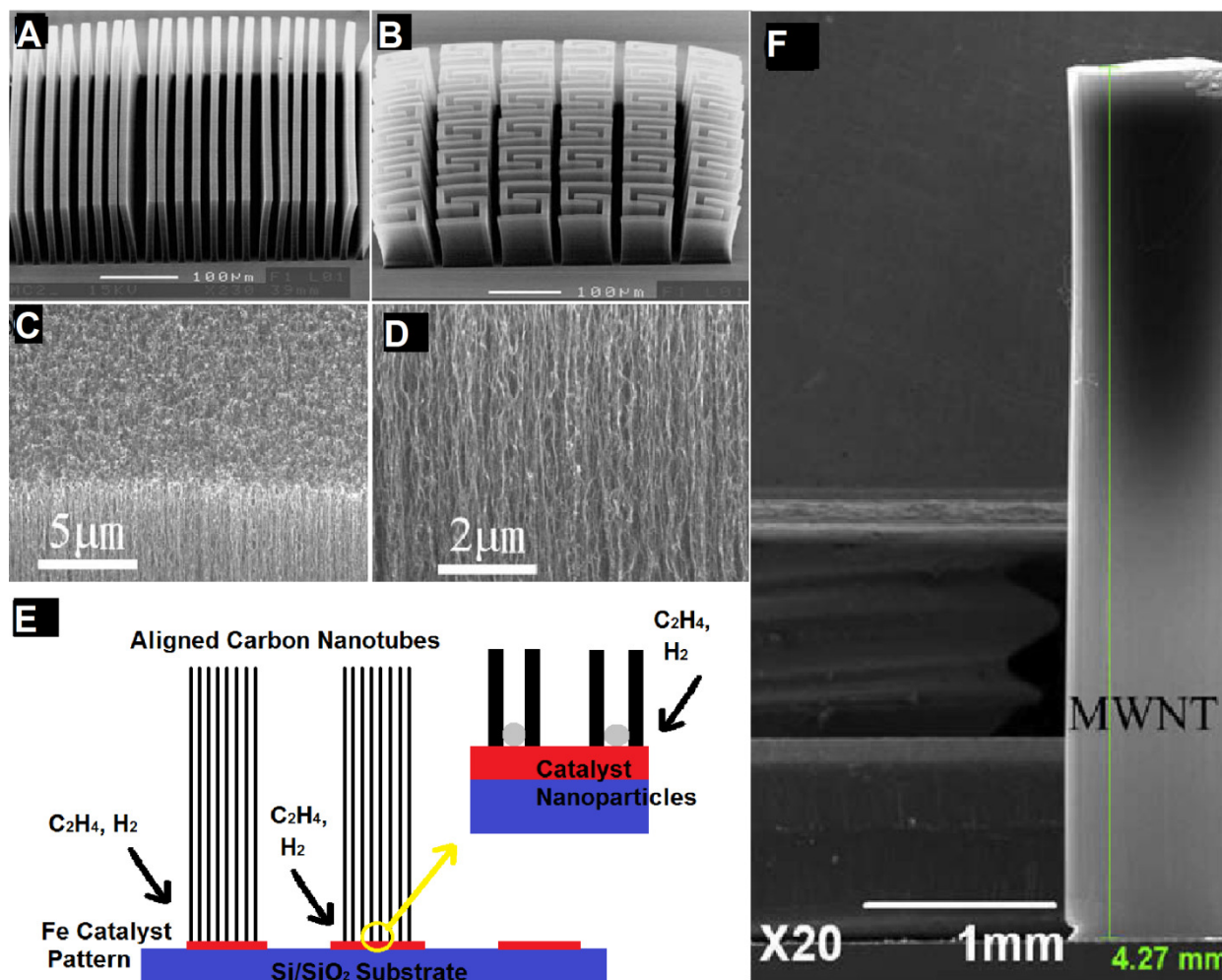
Figure 1. 6. SEM images of the patterned aligned CNT structures grown on a Si/SiO₂ substrate by CVD method. (a) CNT wall shape structures, (b) Maze-like CNT pillars, (c&d) typical zoomed-in image of aligned CNTs, (e) schematic representation of the growth mechanism of the patterned aligned CNTs on the Si/SiO₂ substrate, (f) ultra-tall CNT forest. (a&b adopted from ref. (25) with permission. c,d&f adopted from ref. (31) with permission).

1.2.5. Transfer of CNT patterns

One of the major applications of CNT structures is in electronic circuits as for example inter-connects. The vertical alignment of nanotubes can enhance the isotropic electrical behavior of the devices built with such patterns. In advanced applications, flexible substrates are of great importance to make modern light weight flexible devices. Therefore it's useful to find a way to transfer CNT structures from a rigid substrate (used in CVD) to a soft polymeric substrate. Zhu

10

et al. (32) transferred aligned CNTs to different substrates such as glossy paper, cloth, polymers, glass slides, iron and copper foils at low temperatures using polydimethylsiloxane (PDMS) as an intermediate. They first coated the target substrate with PDMS mixture and then inverted a piece of the patterned CNT array on it and pressed. Then the whole substrate was subjected to a curing process at 90-120 ˚C for 10 min. After the PDMS polymerization, they lifted off the Si substrate and the CNTs were left on the target substrate (32).

In another approach Tsai and co-workers (33) transferred aligned CNTs directly to a polycarbonate (PC) or polyethylene terephthalate (PET) flexible substrate. They heated the substrates to temperatures slightly higher than glass transition of the polymers while they are inverted and pressed on the aligned CNTs. The surface of the polymers melts down gradually and the CNTs penetrate into the polymers and they can be taken off the original substrate when the polymer cools down (Figure 1. 7). Sunden et al. (34) showed that the transfer of the CNT patterns can also be done through a microwave assisted heating. During microwave irradiation, localized heating zones induced at the silicon/CNT interface result in local temperature exceeding the glass transition temperature of the polymer. At the same time the pressure is applied by the weight of the silicon substrate. Therefore CNTs penetrate into the polymer and when cooled down, they can be lift-off the silicon substrate (34).
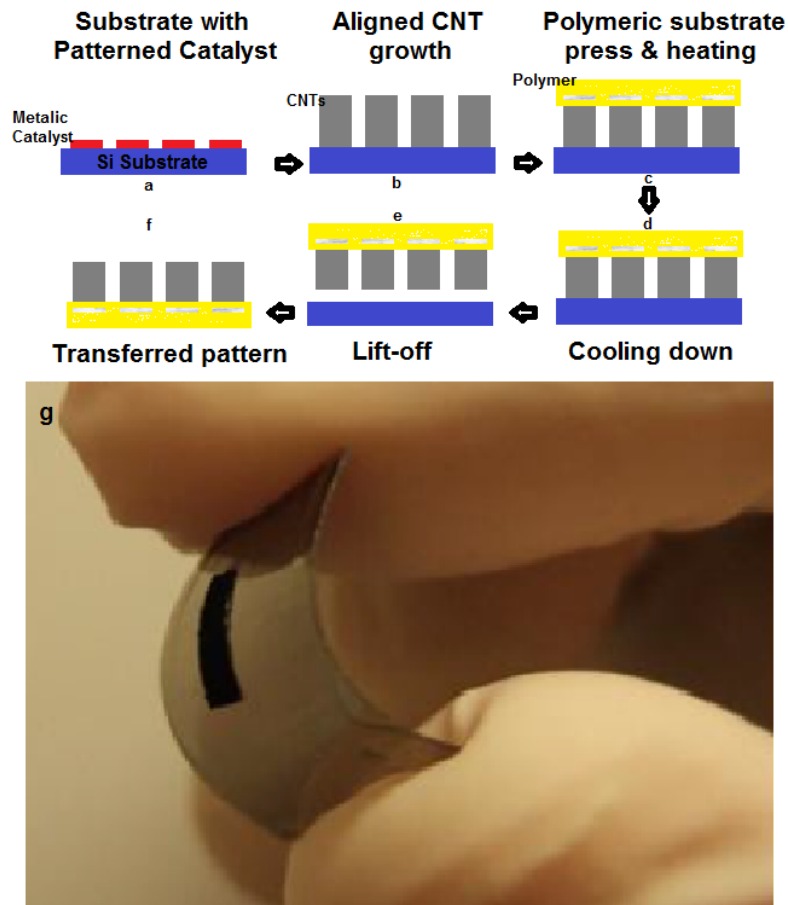
Figure 1. 7. Schematic drawing of direct transfer of CNT patterns into flexible polymeric substrates. (a) Deposition of a patterned catalyst on Si substrate. (b) Growth of vertically aligned CNTs on the catalyst patterns through CVD method. (c) Putting a flexible polymeric substrate on the CNT patterns and heating above glass transition temperature. (d) Cooling down. (e and f) Lift-off the polymeric substrate from the Si substrate. (g) Optical image of a transferred CNT forest on the PDMS substrate (adopted from ref. (32) with permission).

1.2.6. Capillary Condensation and Bending of CNTs

The meso and microporous gaps between aligned nanotubes can be places for diffusion of liquids through capillary and van der Waals forces. During drying these forces compress the nanotubes together and form solid bundles of aligned nanotubes (35–39). In CNT films, the shrinkage and condensation of the nanotubes result in a cellular pattern structure of random
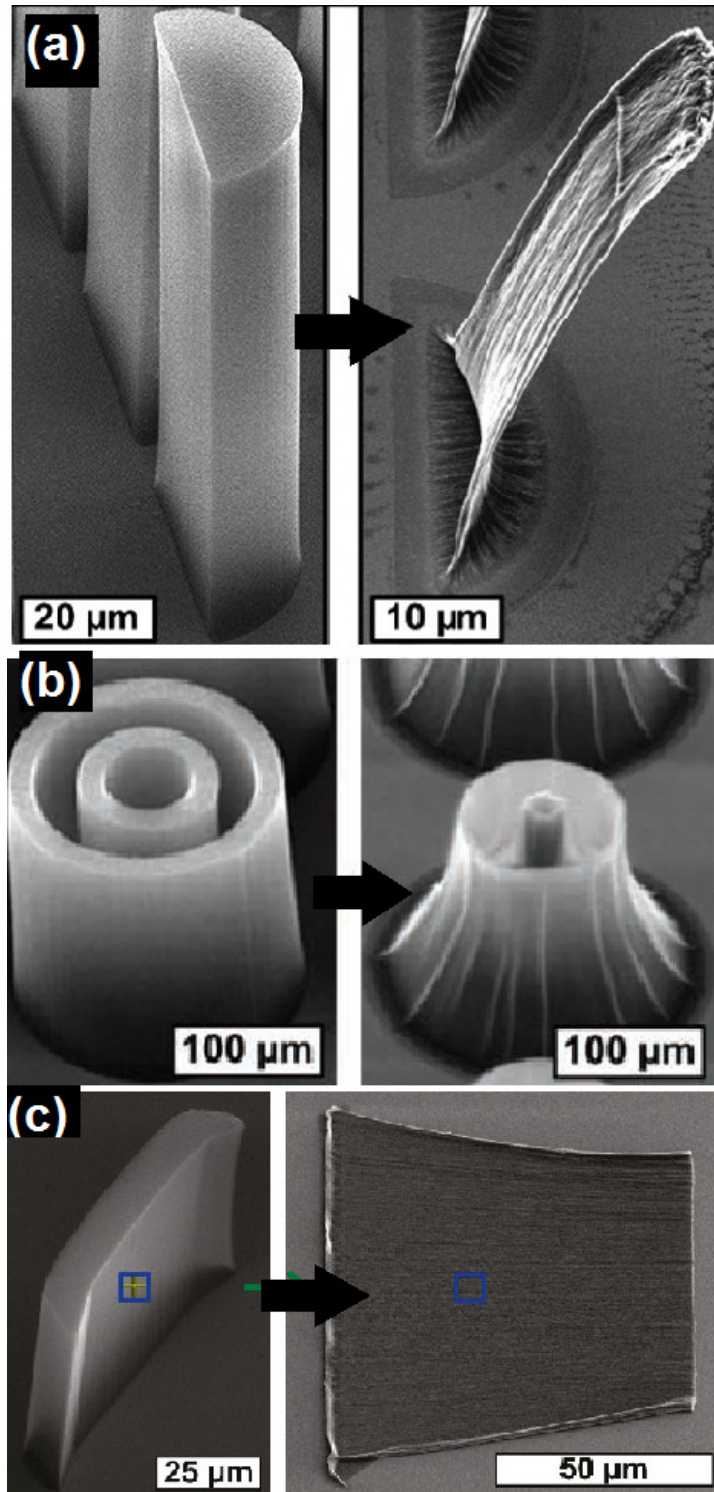
Figure 1. 8. SEM images of aligned CNTs structures before and after capillary induced condensation and bending (a) semi-rod (Adopted from ref. (40) **with permission), (b) concentric circular hollow rods (Adopted from ref.** (39) **with permission), (c) Solid walls (Adopted from ref.** (38) **with permission).**

13

perturbations. However condensation of patterned aligned nanotubes leads to interesting new architectures.

Figure 1. 8 shows scanning electron microscopy images of the aligned CNT structures before and after condensation with water vapor. Volder et al. (39) demonstrated that with controlling the initial shape and size of the CNT patterns as well as the density of the nanotubes in the aligned structures, it's possible to design and obtain various three dimensional architectures which are difficult to fabricate via conventional routes. Also using the capillary and surface tension forces, the aligned CNT patterns can be folded and bent on a substrate at a desired direction (38) (Figure 1.8c). In chapter 4 of this thesis, it's further discussed how this approach was used to make aligned strips of CNT/Inorganic hybrids.

1.3. Graphene

Graphene is the 2D single atomic layer allotrope of carbon which has a honeycomb structure of C-C bonds with sp^2 molecular orbital. It can be considered as the building block of other allotropes of carbon such as buckyballs, carbon nanotubes and graphite (which is stack of graphene layers). Graphene has been theoretically studied for over sixty years now but it was just in recent years that Novoselov and Geim turned it to an experimental tool and started a new era in graphene research (41,42). In 2010, Novoselov and Geim were awarded the Nobel Prize in Physics for "groundbreaking experiments regarding the two-dimensional material graphene".

Graphene has superior electrical (intrinsic mobility~200000 $cm^2v^{-1}s^{-1}$), mechanical (Young's modulus~ 1.0 TPa), thermal (thermal conductivity~5000$Wm^{-1}K^{-1}$) and optical properties (optical transmittance~ 97.7%) as well as a high specific surface area (~2630 m^2g^{-1})

(43). To obtain those properties and fabrication of graphene based devices, graphene should be isolated properly as a single layer sheet. Several approaches have been developed including gas phase deposition on catalytic substrates (44), mechanical cleavage of graphite (45), and chemical exfoliation of graphite flakes. The last two have received more attention due to the inexpensive procedure they require (46). The challenge to exfoliate the graphite structure is to overcome the hydrophobicity (most importantly to chemically exfoliate in water) and the exfoliation energy resulted from the van der Waals attraction between the graphitic layers. The exfoliation energy is about 61 meV/C atom and the interlayer distance is 3.34 Å (47). To address this problem, one approach is to oxidize the graphite to graphite oxide which has wider interlayer distance and is also hydrophilic due to the polar oxygen groups formed on it. Later, the obtained graphite oxide is dispersed and exfoliated through sonication in water to form isolated graphene oxide sheets (GO). The GO sheets are soluble in water and can be chemically modified via various wet chemistry approaches. Also the GO sheets can be reduced partially to the graphene sheets (43). In this thesis, GO solutions are made chemically and used as precursors to make GO/Inorganic layered hybrid materials (Chapter 5). Therefore next section is devoted to the literature data on the chemical synthesis of GO.

1.3.1. Synthesis of Graphene Oxide (GO)

Chemical exfoliation of graphite in solvents is an interesting approach to make single graphene layers due to its inexpensive precursor material (graphite powder) and its high yield. GO is an interesting material by itself too, since it can be chemically modified and functionalized and therefore be used as an organic material in chemical reactions.

Several approaches have been developed to synthesize graphite oxide, in which all of them are similar in terms of oxidation of graphite flakes with a strong oxidative agent (48). One uses potassium chlorate ($KClO_3$) and nitric acid (HNO_3) to oxidize graphite (Brodie and Staudenmaier methods), and the other one (Hummers method) uses potassium permanganate ($KMnO_4$) and sulfuric acid (H_2SO_4) (43). The obtained graphite oxide is hydrophilic (due to the presence of hydroxyl, carboxyl and epoxy groups bonding on its surface) and is composed of stacks of so called GO sheets and can be easily exfoliated in an aqueous environment with simple sonication or stirring.

In this thesis a modified Hummers method was used to produce GO solutions which will be discussed further in Chapter 4. As in the case of other nanomaterials, large scale handling and applications need integration and assembly of the nanomaterials into 3D architectures. Graphene derivatives also should be made in 3D assemblies for industrial applications. To address this issue, several approaches have been developed and various structures such as films, foams, and sponges have been made (49). In the current study, layered GO films have been used as initial components to make GO-Inorganic layered hybrid architectures (Chapter 4). The literature survey on how such layered films can be produced is presented here.

1.3.2. Graphene Oxide (GO) Films and Papers

Similar to carbon nanotubes films, GO sheets can be made into thin film. Dikin and co-workers (50) first used vacuum filteration of GO solution through an Anodisc filter to make the GO films with different thicknesses ranging from 1 to 30 µm. Through a slow filtration process, GO sheets stack together and make a layered thin film. Water is removed through filter as well as

evaporation from the surface. The sheets that are placed on the filter first orient randomly because the water goes down rapidly at the very first moments of filtration. But as a very thin film forms, the filtration speed slows down and therefore the GO sheets have more time to sediment and stack together and make a uniform layered structure. Thus, the obtained final film have a more ordered structure in the middle (50).

Figure 1. 9 illustrates the SEM and digital images of a typical free-standing GO film which is made through vacuum filtration on an Anodisc membrane. The surface of the film as it can be seen is more crumpled and wrinkled and the middle part is more uniformly layered. After filtration and during drying, the GO sheets bond together via van del Waals forces. The obtained film is mechanically strong and the tensile modulus can be as high as 32-42 GPa (50).
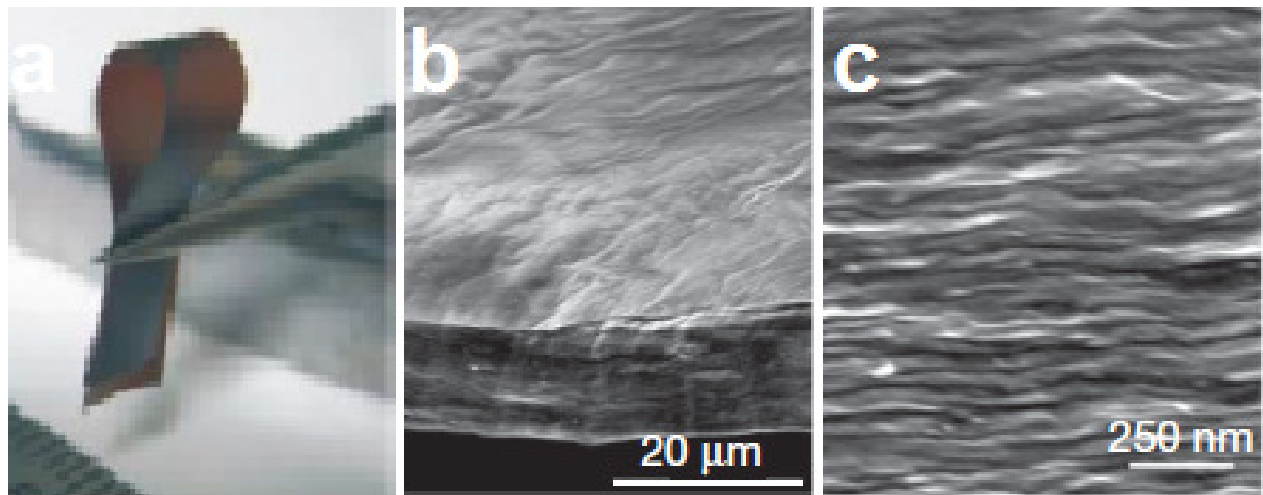
Figure 1. 9. (a) Digital image of the free-standing GO film, (b&c) SEM images of the GO film made by vacuum filtration (Adopted from ref. (50) with permission).

Another approach to produce GO films and papers which is relatively faster than the filtration technique is simply heating of the GO solution. During heating and as water evaporates, a film forms at the air/water interface (49) (Figure 1. 10).
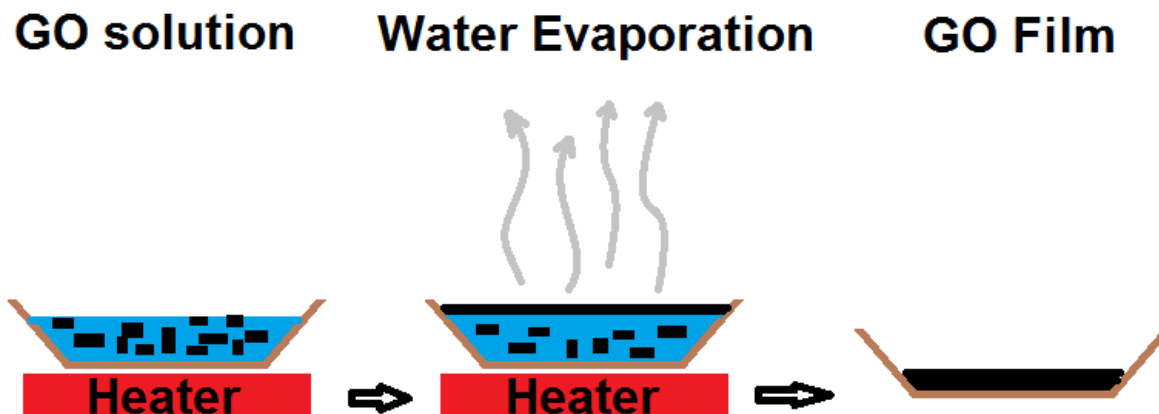
Figure 1. 10. Schematic drawing of GO film fabrication through evaporation.

In the current study, GO films were fabricated through vacuum filtration and were used as templates to make layered GO/Inorganic hybrids via nanostructure synthesis approaches (Chapter 4). The inorganic synthesis approaches are discussed in the following section briefly.

1.4. Chemical Synthesis of Inorganic Nanostructure Materials

Chemical approaches are convenient routes to produce inorganic nanostructure materials due to their inexpensive process and the ability to control the morphology and assembly of the constituents as well as the density of the obtained material easily. Several ways have been developed in order to fabricate lots of different inorganic materials with enormous morphological variations. Different 0D, 1D, 2D and 3D architectures have been produced and used in

18

experimental and industrial applications. The main routes however utilized similar activation energies for the synthesis such as temperature and pressure (hydrothermal synthesis) (51), microwave energy (microwave synthesis) (52), ultrasound energy (ultrasonic synthesis) (53) or their combinations (microwave-hydrothermal synthesis). The affecting parameters can be pressure, temperature, concentration of precursor materials, pH, and the solvent type. These processes can be either templated (directed self-assembly using soft or hard templates) or template-free (54–61). Here in this study, microwave synthesis was used as a facile approach to fabricate inorganic nanostructures such as ZnO, Co_3O_4, MnO_2, Ag, Fe_3O_4, and hydroxyapatite. In chapter 2, patterned synthesis of ZnO nanostructures is demonstrated as an example for UV-sensory applications. In chapters 3 and 4, the CNT/inorganic and GO/inorganic hybrids were fabricated through the microwave synthesis approach.

CHAPTER 2. Microwave-assisted Chemical Synthesis of Zinc Oxide Patterns

2.1. INTRODUCTION

During recent years considerable attention has been devoted to the preparation of semiconductor micro/nano structures, e.g. Zinc oxide (ZnO), on Si/SiO$_2$ substrates for electronic and photonic applications (62,63). Different top-down and bottom-up approaches, such as vapor-liquid-solid (VLS), metal-organic chemical vapor deposition (MOCVD) and self assembled layers, have been proposed for site-selective growth of ZnO structures as a prerequisite for the integration into applicable devices (64–66). However these methods are mostly time-consuming and either need high temperature or require a catalyst which may introduce undesirable impurities into the final product (67). Another deficiency is their limitation in morphological and property variations compared to chemical synthesis methods (68). On the other hand, ZnO is a promising material for using in photovoltaic devices and sensors, due to its intrinsic UV and photo-sensitivity arising from its large band gap and exciton binding energy (69). Therefore finding a simple and rapid way to make patterned arrayed structures is beneficial in developing advanced devices and sensors.

In the current Chapter (Chapter 2), a fast and scale-upable approach is demonstrated for direct on-substrate patterned growth of ZnO nanostructures, which is a synthesis method designed to be compatible with a wide range of substrates and aimed to easily integrate nanostructures into arrayed devices and circuits. For the rapid production of ZnO nanostructures at controlled densities and locations, this method combines standard micro-fabrication techniques with microwave-assisted chemical synthesis. This microwave-synthesis approach is used later to fabricate CNT/Inorganic and GO/Inorganic hybrids.
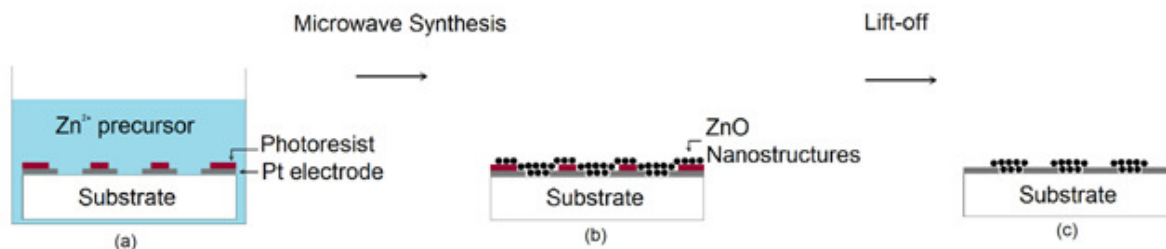
Figure 2.1. Direct on-substrate synthesis of ZnO nanostructures (Adopted from Ref. (56) **with permission).**

2.2. Experimental Procedure

Using a two mask photolithography technique, electric contact (50 nm Pt on 2 nm Ti) and photo-resist (Shipley 1808) patterns were made on a Si/SiO$_2$ substrate (50 nm thermally grown oxide). The substrate was then immersed in a solution with zinc containing precursors and irradiated with microwave using a home-style microwave oven. The substrate, now carrying ZnO nanocrystals, was final washed in acetone (Figure 2.1a-c). The final step rendered patterned ZnO in only designated areas on SiO$_2$ bridging Pt electrodes and thus semiconductor-on-insulator (SOI) type of devices were made and ready for electrical measurements. The detailed synthesis procedure is presented below.

A mixture of ammonia and deionized water was made (1:3 ratio). Then zinc acetate dihydrate powder (ZnAc, Zn(COOCH$_3$)$_2$•2H$_2$O, 1 g, ACS grade) was added to the mixture while vigorously stirring. When all the powder was dissolved, a clear solution was obtained (pH = 12). Then the substrate having the Pt electrodes on it was placed horizontally in the solution in a beaker, put into a microwave oven (2.45 GHz, 900W), and irradiated for 30 s. The solution temperature is about 75 ˚C right after the synthesis. Then it was rinsed repeatedly with DI water and acetone.

21

The microwave-assisted synthesis process (30-60 seconds in duration) is compatible to a wide range of substrates, including glass, plastic (PET), metal (Pt, Au), and polymer (PMMA) thin films.

2.3. Results and discussion

X-ray diffraction (XRD) pattern of the obtained ZnO nanostructures was measured using an X'Pert Pro X-ray powder diffractometer manufactured by PANalatycal and is shown in Figure 2.2. The peaks are attributed to a well crystallized ZnO structure with wurtzite crystal lattice.
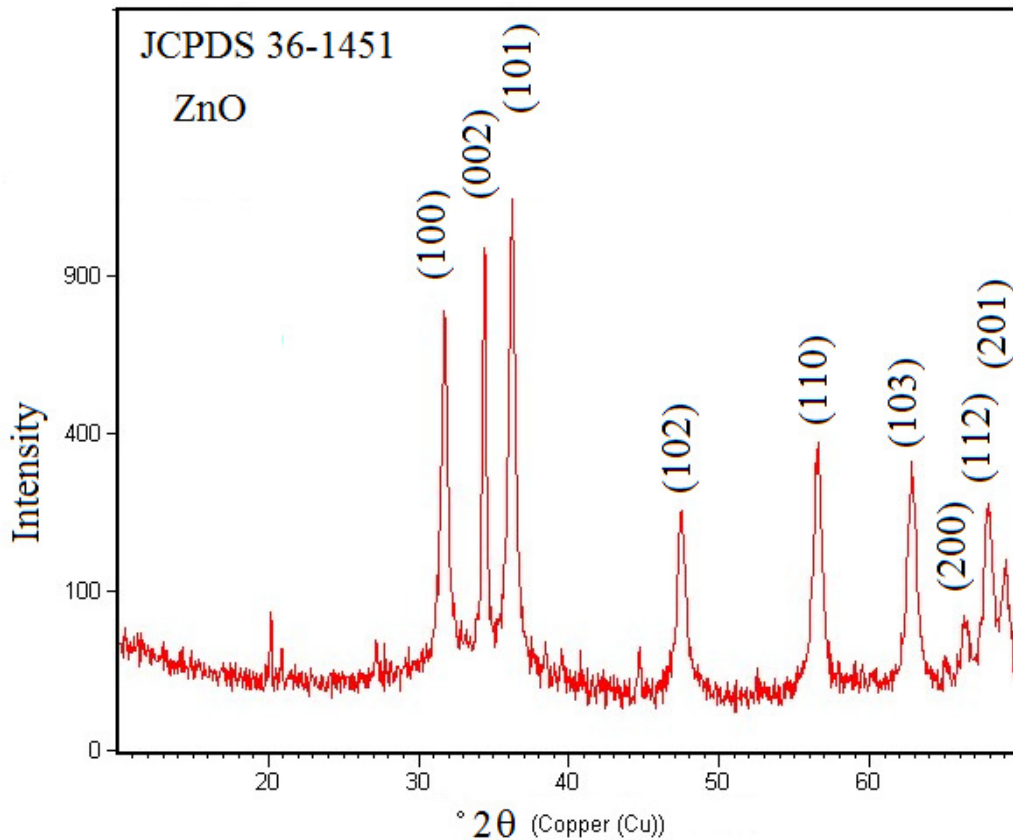
Figure 2.2. XRD pattern of the obtained ZnO nanostructures by microwave-assisted synthesis (Adopted from Ref. (56) **with permission).**

Figures 2.3a-b show the SEM images of a device array with rectangular patches of ZnO nanostructures connected to macroscopic electrodes. The array is a part of a larger circuitry, of which an optical image is shown in Figure 2.3f. The devices have channel length varying from 2 μm to 100 μm. The width of each device is 100 μm. A zoomed-in image of one device shows a monolayer of interconnected ZnO particles bridging two electrodes (Figure 2.3c). The ZnO nanostructures have a flower-like morphology with some hollow petals (Figure 2.3d).

The ZnO synthesis is done in an ammonia water solution:

$$NH_3 + H_2O \longrightarrow NH_4^+ + OH^- \tag{1}$$

After addition of zinc acetate powder, ammonia and hydroxyl ions in the solution form ammonia-zinc complexes and zinc hydroxide ions (70).

$$Zn^{2+} + 4NH_3 \longrightarrow Zn(NH_3)_4^2 \tag{2}$$

$$Zn^{2+} + 4OH^- \longrightarrow Zn(OH)_4^{2-} \tag{3}$$
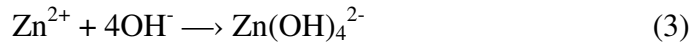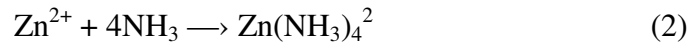
When the mixture is irradiated with microwave $Zn(NH_3)_4^{2+}$ and $Zn(OH)_4^{2-}$ act as growth units for the formation of ZnO structures (71,72).

$$Zn(NH_3)_4^{2+} + 2OH^- \longrightarrow ZnO + 4NH_3 + H_2O \tag{4}$$

$$Zn(OH)_4^{2-} \longrightarrow ZnO + H_2O + 2OH^- \tag{5}$$
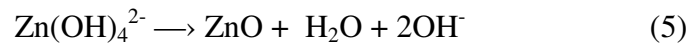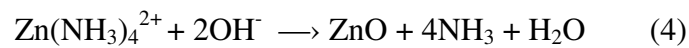
Microwave energy is known to decrease synthesis time and increase the crystallinity of the obtained materials (73–75). Ammonia, which produces a large amount of hydroxyl anions quickly in the aqueous solution, acts as the mineralizer. $Zn(NH_3)_4^{2+}$ and $Zn(OH)_4^{2-}$ physi-absorbed on the substrates act as active sites for ZnO crystallization and further serve as nucleation sites for the growth of star-shaped or flower-like structures (Figure 2.3). ZnO formed

on SiO$_2$, glass, and Pt surfaces are alike, which indicates that the exact chemical composition of substrates is not important.
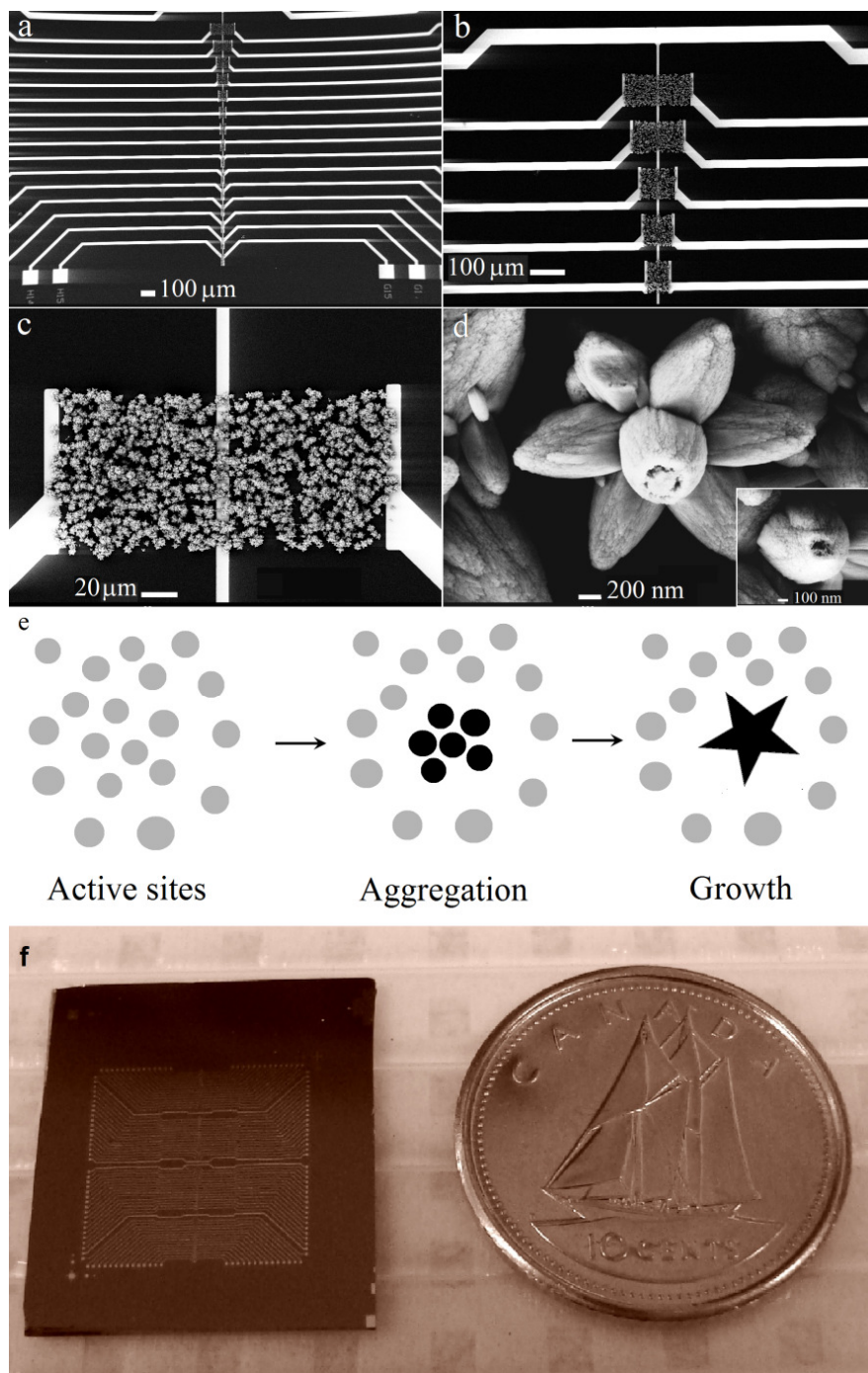
Figure 2.3. SEM and digital images of the integrated device array and the ZnO nanostructures. (a-c) ZnO clusters at designated locations with long metal connections. (d) A single ZnO flower-like nanostructure with hollow petals (inset), (e) Schematic of the possible growth mechanism, (f) Digital image of the device with the Pt electrodes patterned on a Si/SiO$_2$ substrate (Adopted from Ref. (56) with permission).

Further, surface-anchored ZnO structures are identical to their counterparts in solution phase, only devoid of large aggregates and therefore more uniform in size. The density and morphology of the on-substrate patterned ZnO can be controlled by adjusting process parameters such as zinc containing precursor concentration and pH. Microwave irradiation can be repeated multiple times to further increase ZnO density if desired. The microwave synthesis condition allows extremely fast growth in a short period of time, thus sharp petal-like structure is favored. The basal (0001) plane, which has the highest growth rate, is believed to result in a sharp tip along c-axis (76).

2.3.1. Photo-response of the patterned ZnO devices

Figure 2.4 shows the typical photo-responsive characteristics of the device with patterned ZnO interconnects. The dark current is about 500 nA at 5V bias. Under UV (wavelength = 358 nm, filtered beam of 100W Hg lamp) illumination, the current is about 100 times higher, demonstrating a large UV response in comparison with white illumination or dark current which implies that the patterned arrays act as a relevant optical switch.

Interestingly all the I-V curves show non-linear, asymmetric patterns which is likely due to Schottky barriers formed by metal-semiconductor contacts. ZnO-Pt Schottky diodes have been reported previously where Schottky contacts were necessary for certain electronic and optoelectronic applications such as UV detector, transistor, sensor and particularly nanogenerators (77–82). In these reports, several gas-phase deposition techniques (e.g. molecular beam epitaxy (MBE) and pulsed laser deposition (PLD)) and post-synthesis transfer were used to

make ZnO-Pt contacts. In this study, arrayed ZnO-Pt Schottky diodes were easily made as optical sensory/switch devices using a microwave-assisted chemical route.
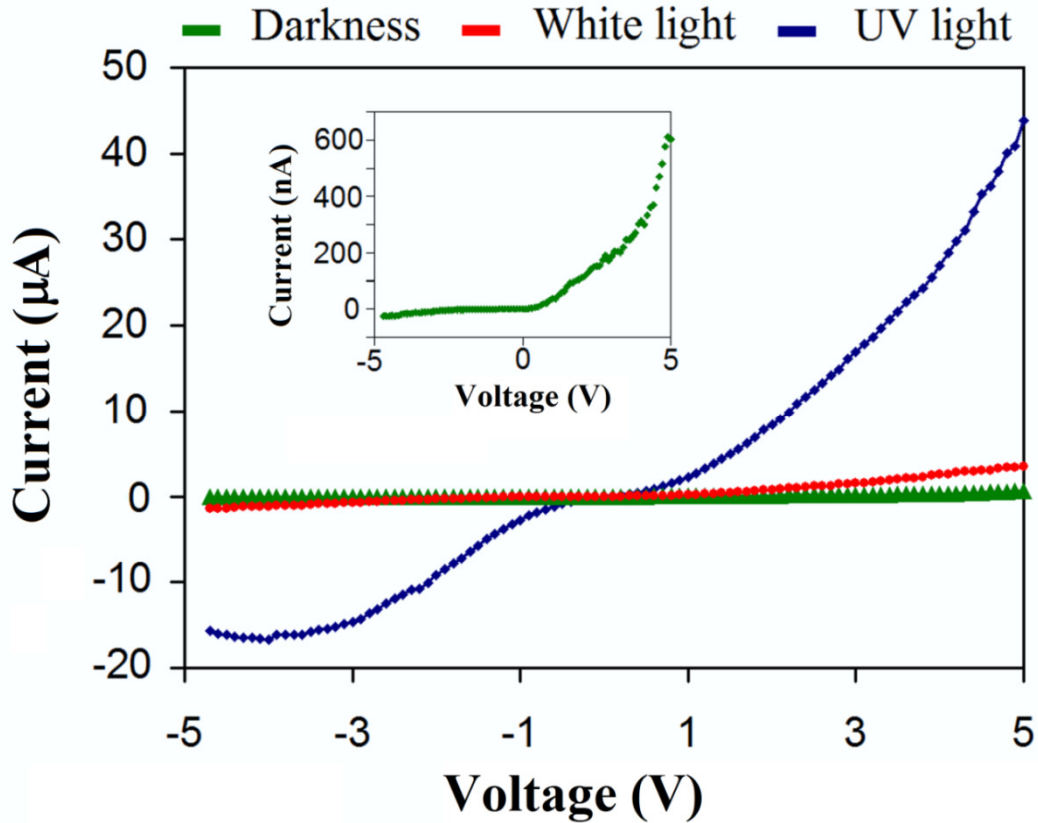
Figure 2.4. I-V curves of a ZnO device in darkness and during exposure to white and UV lights. Inset shows the small dark current (Adopted from Ref. (56) with permission).

The response of current transported through a microdevice to UV was further monitored over time while applying a constant 5V bias across the Pt electrodes (Figure 2.5). The device showed a fast initial response to UV illumination (from ~160 nA to ~210 μA in 120 seconds) and then slowly reached saturation (~250 μA) after about 1000 s. The current decayed rapidly after UV was turned off, indicating a fast recombination of electron-hole pairs in the ZnO nanostructures due to the highly crystallized structure and low surface defects (83). Such device

26

behavior can be beneficial in applications demanding short on-off cycles like optical switches. Figure 2.5b shows the on/off UV-response of the device while it reaches the saturation. The curves show that the rate of increasing current elevates with number of on/off cycles. In other words, the current reaches the saturation faster for more cycles. Figure 2.5c shows the on/off behavior of the device at different time intervals before saturation time (1min, 2min, 30s, 10s, 5s). The current increases both with the number of on/off cycles and larger time intervals. Short on/off times show the fast response of the device to UV light confirming the potential application of the device for rapid UV sensing applications.
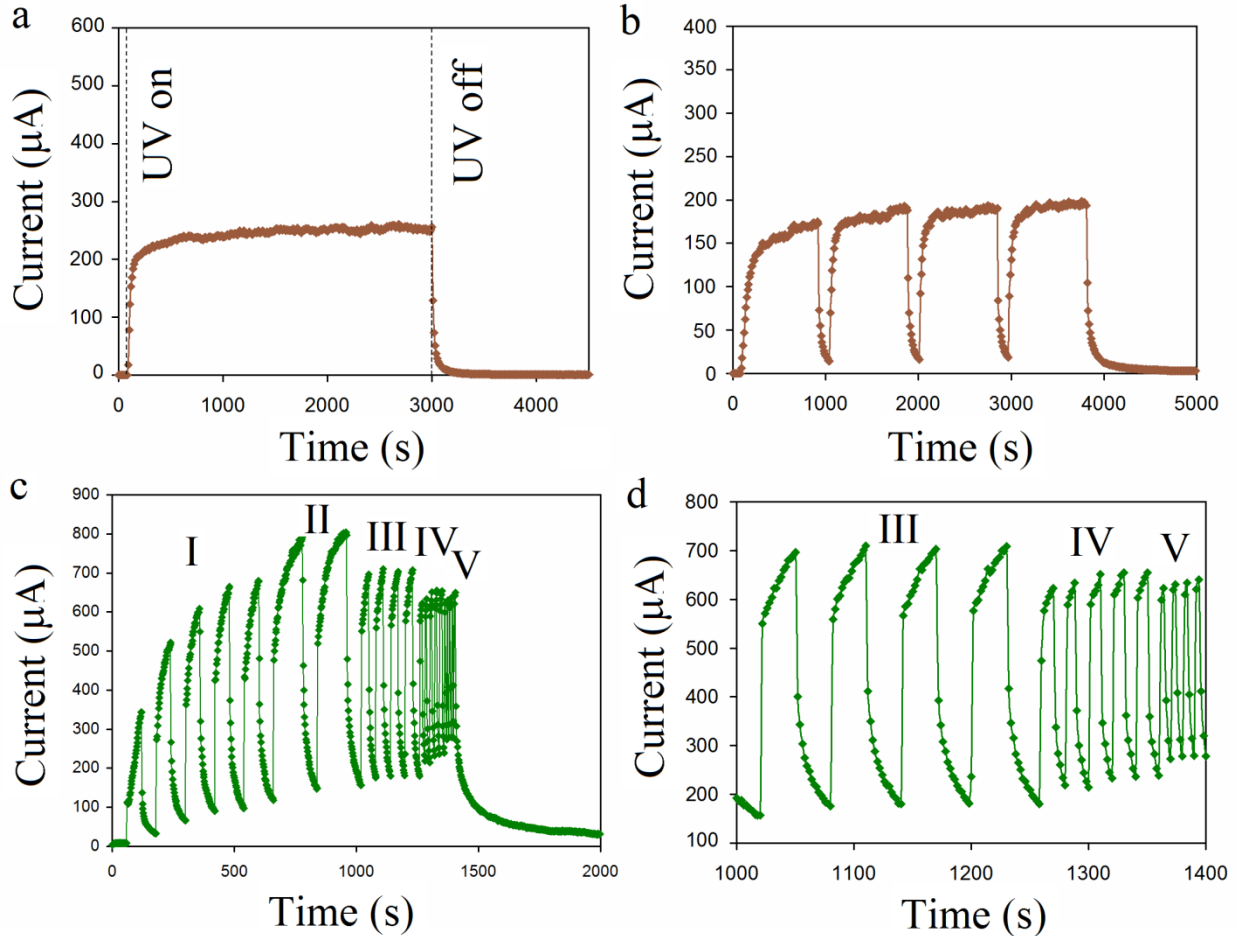
Figure 2.5. I-t curves of a ZnO device in response to UV illumination showing (a) full range, (b) on/off cycle operations to saturation, (c) fast on/off cycles (I:1min, II:2min, III:30s, IV: 10s, V:5s), (d) zoomed area of on/off cycles showing only sections III, IV and V (Adopted from Ref. (56) with permission).

27

2.4. Conclusion

In conclusion, patterning and integration of flower-like ZnO nanostructures into electronic circuits using a rapid microwave-chemical method was reported which can be readily used on wafer scale. Fabrication of ZnO UV sensors with high sensitivity and rapid on/off response time was demonstrated. The microwave-assisted chemical synthesis is compatible to a wide range of substrates and also photo-resists commonly used in lithography. Our results suggest that on-substrate crystallization did not alter the morphology of the ZnO nanostructures compared to those in solution. The microwave synthesis approach presented in this chapter is used to fabricate 3D architectures of CNT/inorganic (Chapter 3) and GO/inorganic hybrids (Chapter 4).

CHAPTER 3. Carbon Nanotube/Inorganic Hybrids

3.1. Introduction

Carbon nanotube (CNT) is considered a class of particularly interesting functional materials for any changes to their surface or structure results in novel materials with improved physical (electric, thermal, and mechanical) and chemical properties for a diverse set of applications. One approach is the enhancement of CNT properties using inorganic materials. This is done through the decoration of the CNT with a thin layer of nanoparticles and fabrication of CNT/Inorganic hybrid materials (84–96).

Ajayan et al. (84) first reported fabrication of CNT/V_2O_5 structures by grinding purified CNT with vanadium oxide powder followed by a sintering step. They made a thin layer of V_2O_5 on the surface and in the inter-tube space of the CNTs (84). Later, several groups reported the decoration of CNTs with inorganic particles such as ZnS (85), ZnO (86–88,96), Cu_2O (89), Ce_2O_3 (90), CoO, NiO (94), Fe_3O_4 (95) and Fe_2O_3 (97).

One can divide these reported synthesis methods into two main categories:

1) ***In-situ synthesis:*** includes the dispersion of CNTs in a metallic precursor solution followed by a direct chemical synthesis of inorganic nanoparticles on the CNT surface using a convenient chemical synthesis approach such as hydrothermal (97,98), microwave synthesis (85) or ultrasonication (86)).

2) ***Ex-situ synthesis:*** is to functionalize CNT sidewalls with organic functional groups followed by the physical or chemical attachment of previously synthesized inorganic nanoparticles on the CNT surface (89,95).

Both categories of methods, however, use dispersed CNT and lead to bulk composite materials with randomly oriented CNT among an inorganic matrix(3). Such structures make a poor connection between the CNTs and the matrix and ultimately affect the hybrid properties. Furthermore, it is not suitable for fabricating 3D architectures and hierarchical nanostructures with specified CNT orientations. To do so, new types of hybrid architectures are introduced with organized orientation and alignment while maintaining their 3D configuration. Such hybrids are fabricated through direct synthesis/coating of inorganic materials on the surface of aligned 3D CNT structures.

3.1.1. Aligned CNT/Inorganic Hybrids

A few studies were reported recently on the decoration of aligned CNTs with metal oxides (MO) to fabricate CNT/Inorganic hybrids (91,93,99,100). Hu et al. (91) coated CNT forests with ZnO using ALD and measured its piezoelectric characteristics after transferring it onto a flexible polyurethane substrate. Li et al. (92) also used ALD to coat the plasma enhanced chemical vapor deposition (PECVD) grown vertically aligned CNTs with ZnO nanoparticles and measured its optical properties. Fang et al. (99) sputtered RuO_2 directly on arrayed multi-walled carbon nanotubes and showed a significant enhancement in supercapacitor performance. In another approach, Reddy et al. (101) used porous alumina templates to first make the MnO_2 tubular shells, then filled the inside core with CNTs using the CVD method. Although these methods are great steps toward the fabrication of 3D hybrid CNT/MO structures, they lack generality in terms of structure geometries, oxide types and morphologies. In addition, ALD methods are relatively time consuming and expensive and have limited coating depth. It is

desirable to develop chemical synthesis methods that are cheaper and more versatile in production of various inorganic materials. However, only few studies attempted so far and they were on the CNT forest structures (100,102). Raney et al. (102) have shown that when the empty space among the aligned CNTs in a forest structure is filled with SnO_2 and MnO_2, the foam-like energy dissipative response of the hybrid is higher than a CNT forest alone.

In the current study, a fast and convenient microwave-assisted chemical approach is presented to fabricate a wide variety of complex geometries (through patterning or capillary forces) of three-dimensional (3D) aligned CNT/Inorganic hybrid architectures which is also suitable for making various metal oxide structures; among these are Cobalt oxide, Zinc oxide and Manganese oxide which are demonstrated here (Chapter 3).

3.1.2. Synthesis of Mesoporous Materials

Another significant feature of the presented approach is that CNTs can act as sacrificial templates that can be removed from the CNT/Inorganic hybrid structures leaving behind architectures of mesoporous inorganic materials. Previous attempts at fabricating mesoporous materials used either organic templates, such as surfactants, or inorganic frameworks, such as silica (e.g. MCM-41, SBA-15, and KIT-16) (103–105).

For many applications including sensors and catalysis, 3D ordered mesoporous structures are beneficial and functional since they have higher surface area compared to randomly ordered porous materials. Using soft and hard templates, such structures have been made and reported extensively (103,106–110). For instance, 3D mesoporous silica powders (KIT-6 and SBA-16) were used by Xia and co-workers (106) to prepare cobalt oxide mesoporous ordered structures

with improved catalytic activity. Hard templates should be removed after the synthesis using highly basic solutions or HF (106). However the template removal can affect the structure and porosity of the obtained mesoporous material.

Soft templates are the original source of making the mesoporous materials since the hard templates are also made from highly ordered soft templates. However the micellar ordered structures are not very stable and can be disrupt during the synthesis due to the changes in surface charges or temperature and it's not favored for fabrication of all kinds of mesoporous metal oxides (107).

The new CNT-based synthesis approach presented here can be a unique alternative for the fabrication of 3D mesoporous structures either in the form of CNT/Inorganic hybrids or inorganic nanostructures, which could have significant applications in optoelectronics and energy generation/storage such as photovoltaic, battery and supercapacitors. In another words, aligned CNT patterns not only act as templates with tunable ordering for synthesis of all kinds of mesoporous 3D metal oxides, but also are functional component in the hybrid structure. Therefore 3D mesoporous architectures can be fabricated directly through the process discussed in the current thesis. Also, the template removing step is more convenient as a thermal annealing procedure compared to acid or base washing routes because it's possible to control the annealing atmosphere and temperature to manipulate the metal oxide structure.

3.1.3. Microwave Energy vs CNT Interactions

Microwaves are part of electromagnetic spectrum with frequencies in the range of 0.3-300GHz. They have a broad range of applications including radar and telecommunications.

However in synthetic chemistry and for heating purposes, the instruments operate at 2.45 GHz. Microwave energy has received significant attention in research and industry for the synthesis of organic and inorganic materials due to the advantages it has over the conventional thermal synthesis processes (56,60,111–113). Higher yield and reaction rates as well as uniform heating fashion throughout the solution in comparison with the conventional approaches made the microwave energy a convenient source for materials synthesis. However different materials and species absorb diverse amount of microwave energy due to the various mechanisms govern the absorption of microwave energy. One of them is dipolar mechanism and the other one is ionic conduction.

Dipolar mechanism happens when polar molecules (e.g. water) are irradiated with microwaves. The alternating electric field of the microwaves results in the rotation of polar molecules, trying to follow the alignment of the electric field, thus makes friction and collision among molecules and therefore an increase in the dielectric heating.

The other mechanism which is called ionic conduction is when ionic species travel in the solution in the direction or against the direction of the applied alternating electric field by microwave irradiation. This also results in the rapid temperature increase. The amount of the heat generated by the mentioned mechanisms is governed by the dielectric properties of the irradiated substance (114,115) .

Sp^2-carbon materials such as CNTs and graphene absorb microwave energy through a Joule heating mechanism that is related to their electrical conductivity (116,117). The local heating zones on the sp^2-carbon structures created by the microwave irradiation act as relevant sites for inhomogeneous nucleation of inorganic materials (116) which leads to rapid formation and precise coating of the CNT and graphene architectures with inorganic nanoparticles.

Therefore in this thesis microwave synthesis was used as a convenient route to fabricate inorganic materials on sp^2-carbon materials in situ.

3.2. Experimental Procedures and Results

3.2.1. Synthesis and manipulation of aligned CNTs

Vertically aligned CNTs were grown using the chemical vapor deposition (CVD) method with high purity ethylene, hydrogen and argon as the synthesis gases (70:70:70 sccm) in a 1-inch tube furnace (Lindberg). The growth temperature was 725˚C and the catalyst used was a 4 nm Fe film E-beam evaporated on Si<100>/SiO$_2$ wafers. The Fe film was patterned by standard photolithography using AZ3330 photoresist and LOR15A as the lift-off resist.
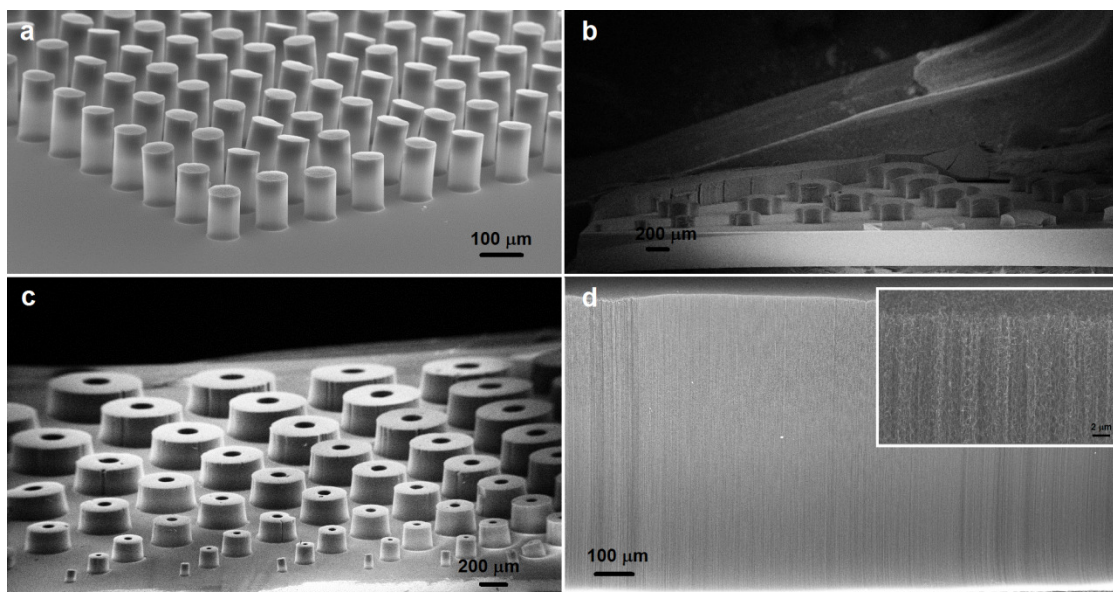
Figure 3.1. SEM images of the aligned CNT patterns obtained by CVD method. (a) Solid pillars, (b) Star-like pillars, (c) Hollow pillars, (d) CNT forest (inset is the high magnification image, scale bar is 2μm). (c&d) are Reprinted with permission from ref. (118)**. Copyright 2013 American Chemical Society)**

Basically, the patterns are transferred from a photo-mask on the photoresist using UV exposure. Then the exposed areas are washed away with a developer and finally Fe thin film is deposited on it. The final pattern is washed with acetone and isopropanol to remove the photoresist. Thus, the Fe pattern remains on the substrate where it's directly deposited on it. If no patterning is done and just a thin Fe layer is deposited on Si/SiO_2 substrate, one can grow aligned CNT forests via CVD. Figure 3.1 illustrates the aligned CNT that can be grown in our CVD synthesis process. The porous nature of the initial CNT patterns and the alignment of the large-aspect ratio CNTs are the key enabling factors for manipulating the CNT through liquid condensation and for deposition of inorganic nanoparticles on the CNT surfaces (Figure 3.1d). With a simple thermal atmospheric CVD system, an extremely high yield of 46 mg/cm^2 with CNT reaching a length of 1mm was achieved (Fig.3.1d).
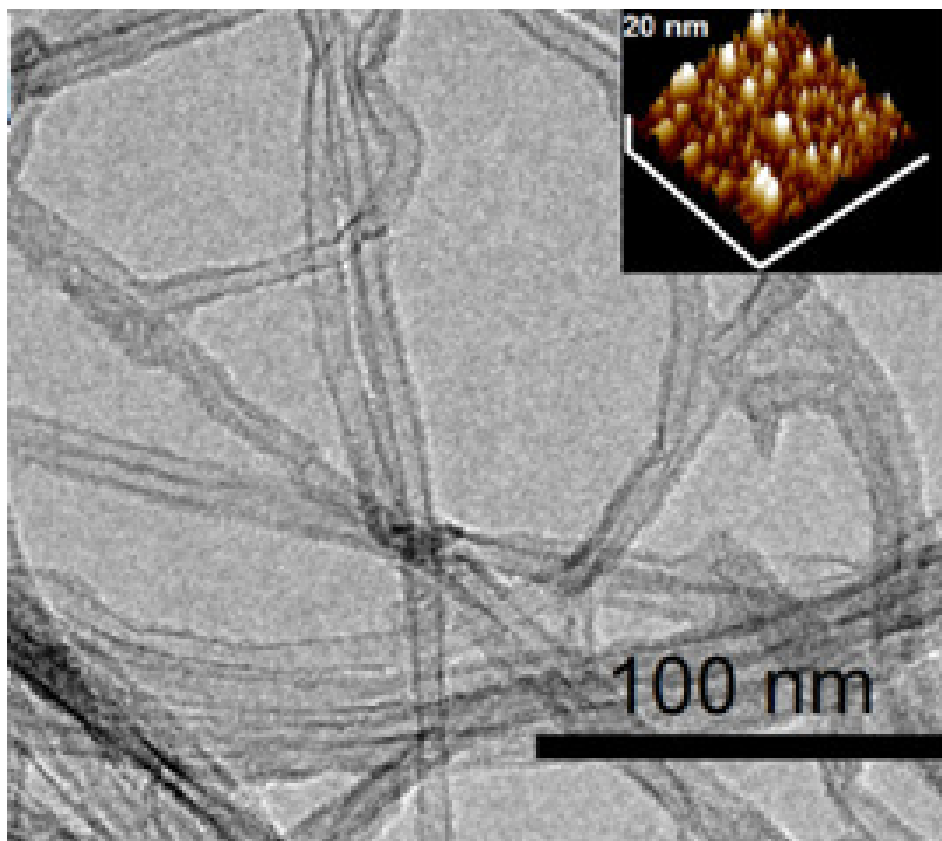
Figure 3.2. TEM image of the CNTs grown by CVD method at 725 ˚C using 4 nm Fe thin film. Inset show the AFM image of the Fe nanoparticles which were annealed at 725˚C (Reprinted with permission from ref. (118)**. Copyright 2013 American Chemical Society).**

TEM image (Figure 3.2) shows that the CNTs grown by CVD have an average outer diameter of 7 nm, which are well correlated to the density and size of the Fe catalyst particles (Figure 3.2; Inset).

Using liquid condensation, one can fabricate new designs of 3D CNT structures. Condensation makes a network of honeycomb like patterns when the CNT forest dries (Figure 3.3a). The patterns with sharp sides, become sharper when condensed (Figure 3.3b&c) and the solid pillars make a needle-like structure (Figure 3.3d). Such condensation and bending feature can be used to manipulate the structure of the 3D architecture when inorganic material is being

synthesized on CNTs through the chemical reaction. Later in this chapter, it is illustrated how aligned CNT walls were used to be coated with cobalt oxide nanoparticles and be bent on the substrate to make continuous strips simultaneously.
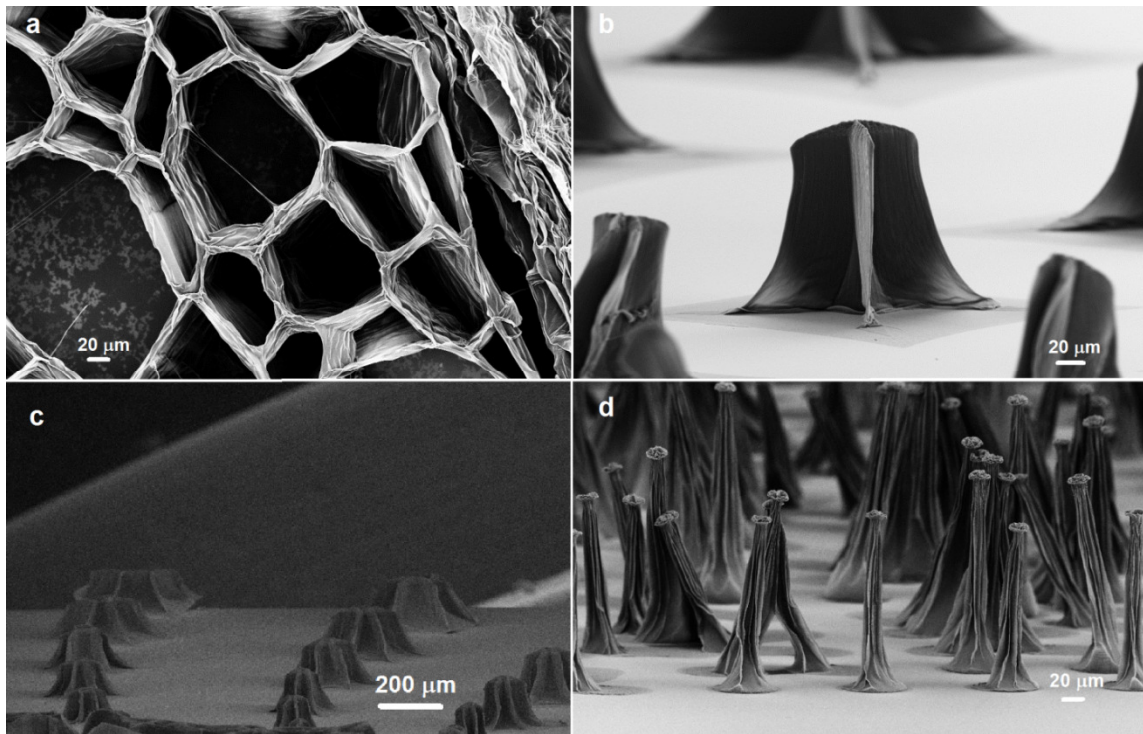
Figure 3.3. Capillary induced condensation of vertically aligned CNT structures.

3.2.2. Metal oxide (MO) Precursors

To demonstrate the CNT-templated synthesis of CNT/Inorganic hybrids, three different metallic precursor solutions were used respectively:

3.2.2.1. Cobalt oxide/CNT

In 30 mL DI water, 10 mL ammonium hydroxide solution (NH_4OH, 30%, ACS GR, Alfa Aesar) was added while stirring. Then 0.11 g cobalt acetate powder ($C_4H_6CoO_4$, ACS GR, Sigma-Aldrich) was added to the mixture. The darkish solution was then used as the precursor solution for the synthesis of Cobalt oxide/CNT hybrid structures.

3.2.2.2. Zinc Oxide/CNT

10 mL ammonium hydroxide solution (NH_4OH, 30%, ACS GR, Alfa Aesar) was mixed with 30 mL deionized (DI) water while stirring. Then 0.2 g zinc acetate dihydrate crystalline powder ($Zn(OOCCH_3)_2.2H_2O$, ACS GR, Alfa Aesar) was added slowly to the solution. The homogenous clear solution was then used as the precursor solution for the fabrication of ZnO/CNT hybrid structures.

3.2.2.3. Manganese oxide/CNT

0.158 g potassium permanganate crystals ($KMnO_4$, ACS GR, EMD chemicals) were dissolved in 40 mL DI water while stirring. Then 1 mL of hydrochloric acid (HCl, 37%, EMD chemicals) was added drop wise to the mixture. The clear blue solution was then used as the precursor solution for the synthesis of Manganese oxide/CNT hybrid structure.

3.2.3. Microwave Synthesis of Aligned CNT/Inorganic hybrids

Figure 3.4 shows the experimental steps involved in this chemical approach for the synthesis of 3D CNT/MO mesoporous architectures using CNT patterns as templates. Three

dimensional CNT patterns were plasma cleaned in an oxygen atmosphere to become more hydrophilic. Then they were immersed into a metallic precursor solution (Figure 3.4, step 1) under mild vacuum conditions (27 inHg Vac.) and left there for 30 minutes in order to have the precursor molecules infiltrate the inter-tube space. The solution is then irradiated in a microwave oven (2.45 GHz, 900W) for 30-60 seconds (Figure 3.4, step 2).

Microwave is known to accelerate the nucleation and formation of MO nanoparticles (52,55,56,119). This quick irradiation step renders a monolayer of crystalline metal oxide nanoparticles (10-30 nm in diameter) grown directly on the surface of individual CNTs, while preserving the overall configuration and shape of the original CNT patterns. Later, the nanoparticle-decorated 3D CNT arrays are taken out of solution and dried at 80 ˚C in air (Figure 3.4, step 3) or annealed at 650 ˚C (Figure 3.4, step 4). With this method, one can fabricate a wide range of 3D architectures.
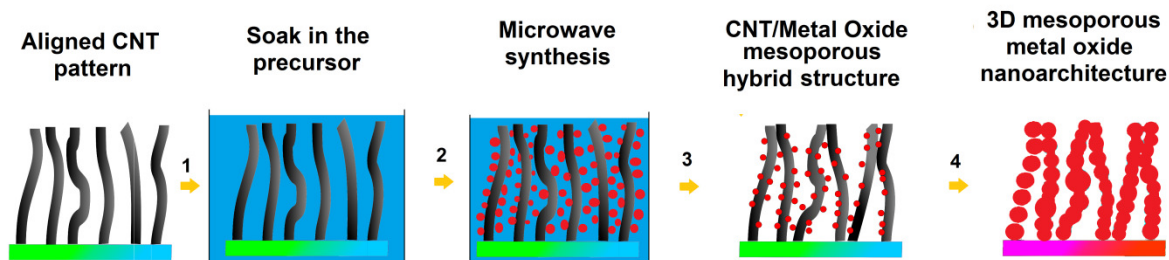
Figure 3. 4. Schematic representation of the experimental steps showing the fabrication of 3D mesoporous hybrid CNT/MO architectures and 3D mesoporous MO structures (Reprinted with permission from ref. (118). Copyright 2013 American Chemical Society).

The detailed chemistry dealing with the synthesis of ZnO nanostructures was discussed in Chapter 2. The chemistry in the synthesis of Co_3O_4 nanoparticles involves the Co^{2+} ions making hexamine complexes $[Co(NH_3)_6]^{2+}$ and $[Co(NH_3)_6]^{3+}$ in aqueous ammonia, which are then

absorbed onto the CNT surfaces and decompose to Co_3O_4 when irradiated with microwaves (120):

$$4[Co(NH_3)_6]^{2+} + O_2 + 2H_2O \rightarrow 4[Co(NH_3)_6]^{3+} + 4OH^- \qquad (6)$$

$$12[Co(NH_3)_6]^{3+} + 36OH^- \rightarrow CO_3O_4 + 72NH_3 + O_2 + 18H_2O \qquad (7)$$
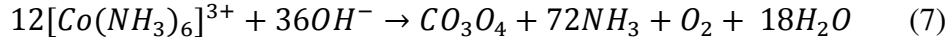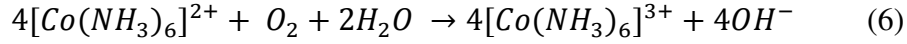
The detailed chemistry for synthesizing MnO_2 nanostructures with microwave irradiation is that in the acidic media, manganate ion (MnO_4^{2-}) is stable and works as the growth unit for synthesis of MnO_2 :

$$3MnO_4^{2-} + 4H^+ \longrightarrow 2MnO_4^- + MnO_2 + 2H_2O \qquad (8)$$
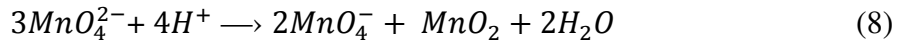
The initial CNT patterns can be defined by standard photolithography. By varying the precursor specie, concentration, pH, as well as the microwave irradiation condition, the MO type, size, and density can be determined. During drying, the CNTs (coated with MO nanoparticles) go through elastocapillary induced densification and thus offer additional flexibility in tuning density and morphology of the final structure. The final annealing step in Figure 3.4 offers another supplementary advantage, which allows further tuning of the hybrid structures via the gas environment and temperature. This annealing step can be used for instance to increase crystallinity and size of MO nanoparticles with CNT preserved (in an inert gas, e.g. Argon) or CNT removed (in O_2 or air), to reduce MO to a metallic phase (e.g. in H_2 atmosphere) or to dope them with desired dopants (e.g. in N_2 gas).

The shape and morphology of the obtained CNT/MO patterns were characterized by scanning electron microscopy (SEM, Zeiss LEO 1550). Depending on the photo-lithographically defined Fe catalyst patterns (typical dimensions of 10 to 500 µm), various geometries of vertically aligned CNT structures can be made, for example walls and hollow pillars as shown in

Fig. 3.5a & 3.5f [1]. Furthermore, the possibility of altering the spatial feature of the 3D CNT structures with liquids, termed elastocapillary condensation, was studied (39,121). CNT walls were bent using DI water to form aligned strips on the surface, which were shown to preserve the CNT alignment after bending (Fig.3.5b &3.5c). It was hypothesized that similar structure modification could be achieved with precursor solutions, which was confirmed experimentally. Fig.3.5d shows the aligned CNT strips laid down on the substrate and coated with cobalt oxide (Co_3O_4) nanoparticles as synthesized. When using patterns of aligned CNTs in the hollow pillar format (Fig.3.5f), the densification during the drying step transforms them to a more condensed and needle-like structure (Fig.3.5g). By manipulating the original size of the CNT hollow pillars, it is possible to obtain various shapes, from needle-like structures (smaller objects) to volcano-like morphologies (larger objects). Recent reports suggest that a wide range of interesting 3D architectures can be fabricated through liquid condensation processes such as these and are potentially applicable in making 3D CNT/MO hybrids (39,121).

---

[1] Photo-Lithography of some of the patterns was performed thanks to the help of my colleague Mrs. Samaneh Shadmehr.
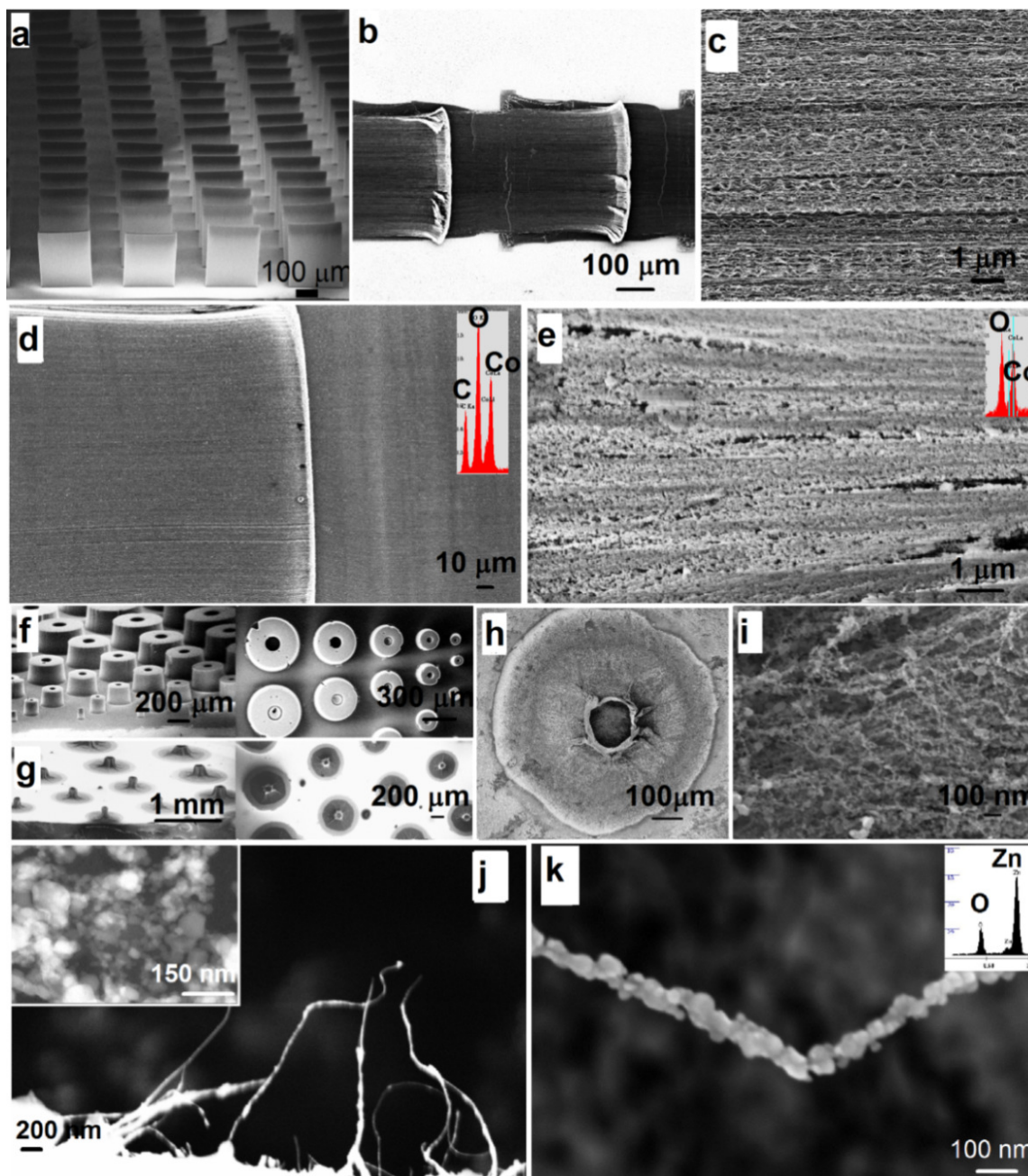
Figure 3.5. SEM images of the aligned CNTs, 3D hybrid CNT/MO architectures and 3D MO architectures. (a) CVD-grown vertically aligned CNT walls, (b) laid down CNT walls to form strips on a SiO$_2$ substrate using DI water, (c) zoomed-in image of the corresponding CNT strips, (d) CNT strip/Co$_3$O$_4$ hybrid(Inset shows EDX), (e) Co$_3$O$_4$ strips after annealing of the corresponding CNT/Co$_3$O$_4$ hybrid in air at 650 °C (Inset shows EDX),(f) Hollow pillars of vertically aligned CNTs, (g) liquid condensed hollow needles, (h) ZnO hollow needle, (i) zoomed-in images of ZnO hollow needle, (j) CNTs decorated with Co$_3$O$_4$ nanoparticles (Inset is the TEM image of Co$_3$O$_4$ nanoparticles), (k) SEM image of a typical fibrous structure made of ZnO nanoparticles after annealing and removal of the CNT template (Reprinted with permission from ref. (118). Copyright 2013 American Chemical Society).

TEM investigation also shows the coverage of individual CNTs with cobalt oxide nanoparticles with average diameter of less than 20 nm. For TEM sample preparation, sonication is necessary to disperse aligned CNTs which are so entangled. Therefore, some of the nanoparticles were detached from the CNT surface during sample preparation with sonication (Figure 3.6).
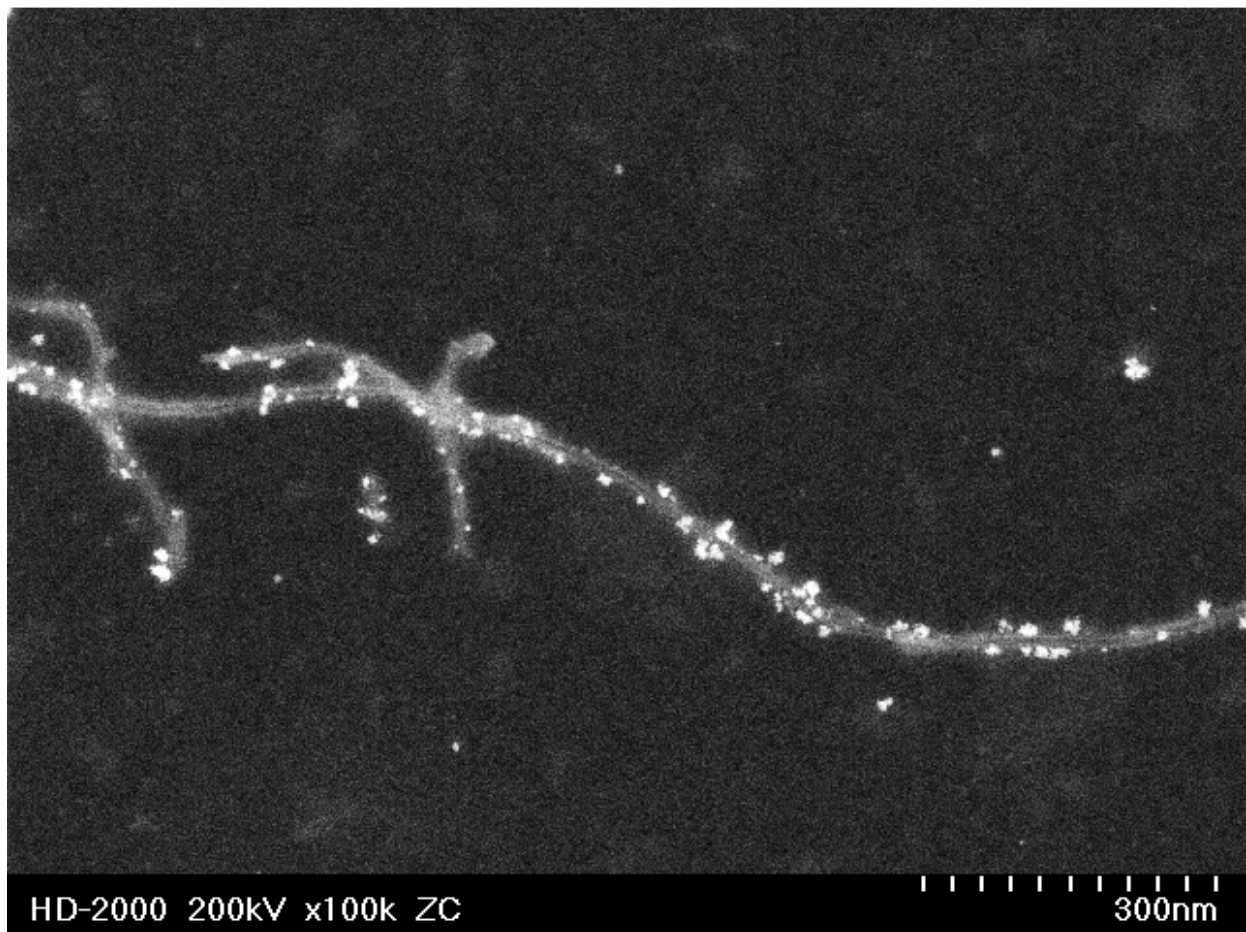
Figure 3.6. TEM image of a single CNT coated with Co_3O_4 nanoparticles.

3.2.4. 3D Mesoporous Inorganic Architectures

As is evident from the energy dispersive X-ray spectroscopy (EDX) analysis and scanning electron microscopy (SEM) images (Figures 3.5d&e and 3.7), annealing of the CNT/Co$_3$O$_4$ and CNT/MnO$_2$ strips in air at 650°C removed the CNTs and increased the size of the Co$_3$O$_4$ and MnO$_2$ nanoparticles and pores, while preserving the original alignment. Figure 3.5h shows that a highly porous, hollow needle-like ZnO architecture can be achieved after annealing of the CNT/ZnO hollow pillars in air.
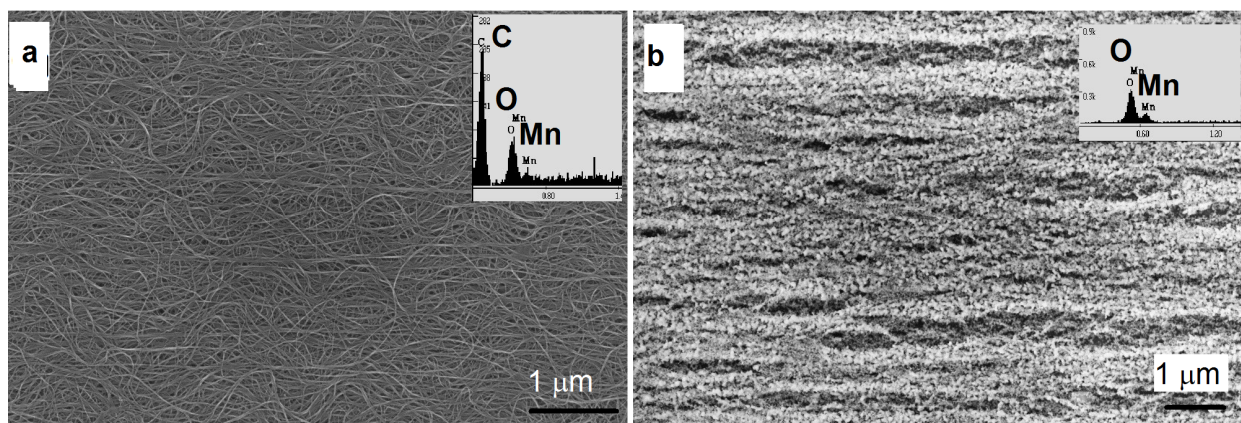
Figure 3.7. (a) Hybrid CNT/MnO$_2$ mesoporous structure. (b) Mn$_2$O$_3$ aligned structure after annealing and removal of CNTs (Reprinted with permission from ref. (118). Copyright 2013 American Chemical Society).

These results suggest that thermal annealing is effective in removing CNT templates and achieve high-porosity 3D architectures of nanoparticulated MOs, applicable to various MO types and geometries. The high fidelity of the remaining MO architectures is only possible when there is a complete and yet uniform layer of MO nanoparticles decorating individual CNTs, as shown in Fig. 3.5j.The inset of Fig. 3.5j is a TEM image of Co$_3$O$_4$ nanoparticles after annealing in air and dispersed in ethanol solution for the purpose of studying their size and shape, which is estimated to be 30 nm in diameter. Fig.3.5k shows a single fibrous structure made of 15-20 nm

ZnO particles after annealing and removal of its single CNT template. It appeared that neighboring ZnO nanoparticles joined together during annealing and therefore became self-supporting after CNT removal. This data indicate that our method could also be a novel approach for the one-dimensional assembly of nanoparticles, which is a subject under intensive research (122).

3.2.5. BET and Pore Size Distribution of the CNT/MO hybrids

The pore characteristics of the initial CNT patterns, CNT/MO hybrids, and the MO architectures were studied. The surface area and pore size distribution measurements were performed by Brunauer-Emmett-Teller (BET) technique using a Quantachrome Autosorb Automated Gas Sorption System. BET measurements showed that the CNT patterns have a specific surface area of 548 m^2/g, which is closely matched to the theoretical specific area of MWNTs with 5 nm inner diameter and 7 nm outer diameter. This indicates the accessibility of individual CNTs devoiding bundles as often encountered in solution dispersed methods. In addition, it is suspected that the alignment of CNTs allowed N_2 gas molecules to penetrate deeper into the structure and thus the higher BET surface area achieved in this study compared to randomly ordered CNTs reported by others (123). The adsorption-desorption curves (inset of Figure 3.8) of the vertically aligned CNTs and aligned CNT/Co_3O_4 hybrid structures both show a typical hysteresis attributed to a mesoporous structure, while having different pore sizes and BET surface areas. The first two peaks in Figure 3.8 are attributed to the intra tubular pores, which were preserved before and after Co_3O_4 synthesis. The size of the mesopores attributed to inter tubular spaces increased after Co_3O_4 formation (refer to the shaded boxes in Figure 3.8). The

BET specific surface area of the nanoparticle decorated aligned CNTs is approximately 357 m^2/g and the pore sizes are between 9-18 nm.

CNTs were able to absorb high levels of microwave energy and cause localized heating, which enabled the rapid decoration of Co_3O_4 nanoparticles on CNT outer surfaces (116,117,124). The nanoparticles that decorate the CNT surfaces can also fill the mesopore spaces in aligned CNT arrays, make new connections between adjacent CNTs and form pores of various sizes that result in the formation of new surface configurations.
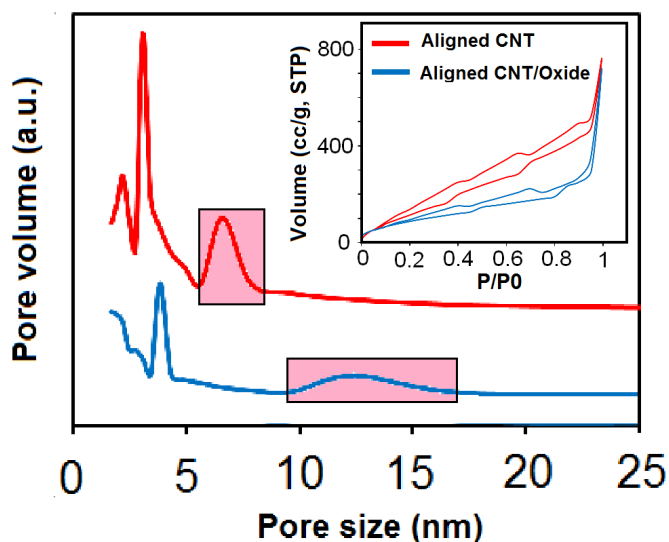
Figure 3.8. Pore size distribution of the aligned CNT structure (red) and aligned CNT decorated with Co_3O_4 nanoparticles (blue). Inset shows the corresponding Adsorption-desorption isotherms (Reprinted with permission from ref. (118)**. Copyright 2013 American Chemical Society).**

3.2.6. X-ray Diffraction Results

Phase and crystalline structures of the oxides were identified with X-ray diffraction analysis (XRD, PANALYTICAL X'Pert Pro MRD X-ray diffractometer). Figures 3.9a&b show the XRD patterns of the CNT/ZnO and CNT/Co_3O_4 hybrid structures after microwave irradiation

46

(before annealing) as well as after annealing in air. It is evident from the differences between the sharpness of the XRD peaks that annealing has increased the crystallinity of the ZnO and Co_3O_4 structures. XRD results show that manganese oxide nanostructures were present after annealing of the synthesized CNT/MnO_2 hybrids in air (Figure 3.10).
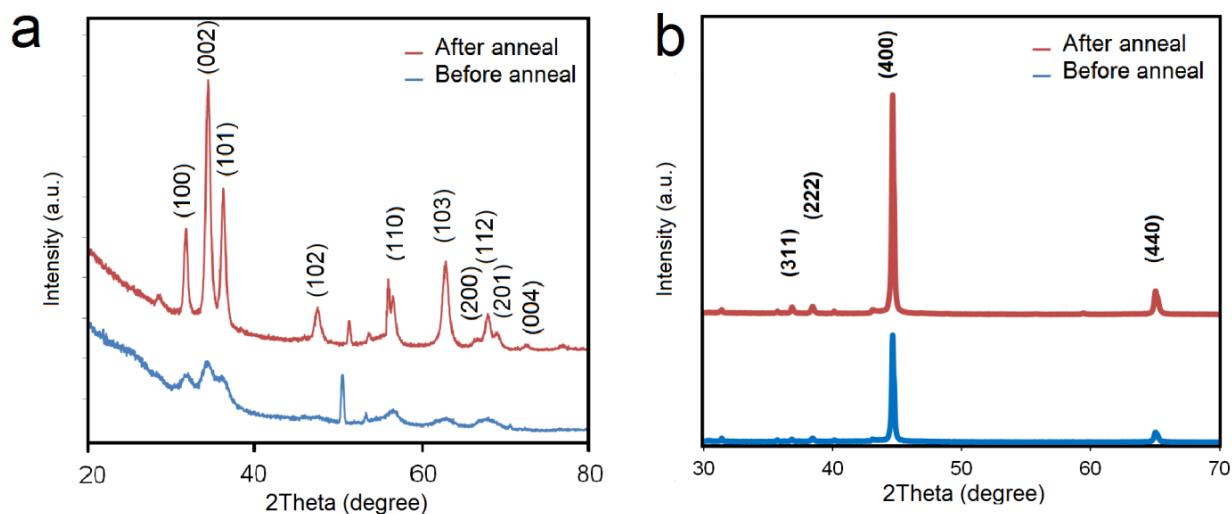
Figure 3.9. (a) XRD spectra of CNT/ZnO hybrid architecture after microwave synthesis (blue) and annealing at 650 °C in air (red). (b) XRD spectra of CNT/Co₃O₄ hybrid architecture after microwave synthesis (blue) and annealing at 650 °C in air (red) (Reprinted with permission from ref. (118). **Copyright 2013 American Chemical Society).**
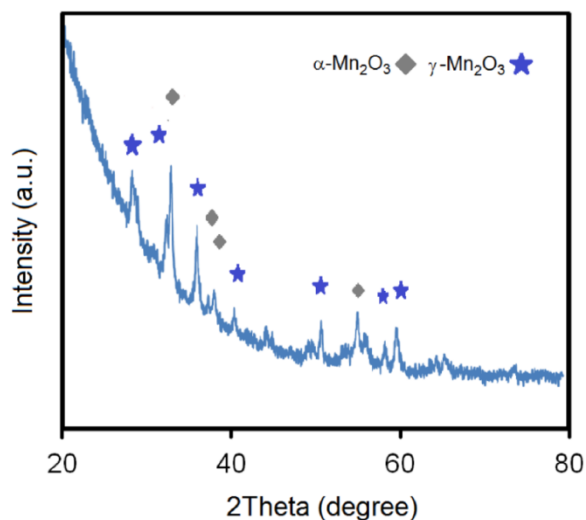
Figure 3.10. XRD of manganese oxide structures after annealing at 650 °C (Reprinted with permission from ref. (118). **Copyright 2013 American Chemical Society).**

3.3. Application of CNT/Co$_3$O$_4$ 3D Hybrid Architecture for Energy Storage

3.3.1. Electrochemical Measurements[1]

Using the BIOLOGIC-VMP3 model potentiostat/galvanostatic apparatus, electrochemical measurements were conducted on as-fabricated aligned strips of CNT/Co$_3$O$_4$ structures laying on a Si/SiO$_2$ substrate. The sample was coated partially with gold to make the proper connection for performing the test. A digital image of the sample is shown in Figure 3.11.
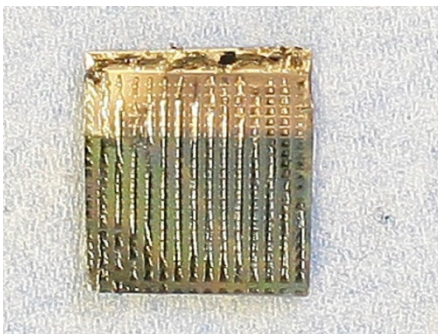
Figure 3.11. CNT/Co$_3$O$_4$ aligned strips laid down on the Si/SiO$_2$ substrate. The top part has been coated with gold to make a connection for the test (Reprinted with permission from ref. (118)**. Copyright 2013 American Chemical Society).**

A 3-electrode cell was utilized for measurements in which the substrate was used as the working electrode, a platinum wire as the counter electrode and a double junction Ag/AgCl electrode filled with 3.5M potassium chloride (KCl) half-cell served as the reference electrode. The electrolyte used was an aqueous solution of 2M potassium hydroxide (KOH). Galvanostatic cycling and cyclovoltametric with potential limitation (-0.2V to +0.3V vs Ag/Agcl) were used to measure the capacitance and charging/discharging current density of the CNT/Co$_3$O$_4$ strips.

---

[1] E-Chem tests were performed thanks to the help of Mr. Yverick Rangom, PhD. student at Dr. Linda Nazar's Lab (our collaborative).

Galvanostatic and cyclic voltammetric (CV) tests were performed to illustrate the capacitive characteristics of the aligned CNT/Co_3O_4 strips. CV tests were conducted at scan rates of 10, 30, 50 and 100 mV/s, between 0 and 0.5 Volts (vs. NHE) in 2M KOH aqueous electrolyte. The CV curve (Figure 3.12) reveals two peaks: an oxidation peak around 0.3V and the corresponding reduction peak around 0.25V for 10 mV/s scan rate. This is in agreement with results for Co_3O_4 electrodes (125,126) where the same quasi-reversible redox reaction takes place at the same potentials. Reduction-oxidation of cobalt oxide Co_3O_4 is as follows (125,126):
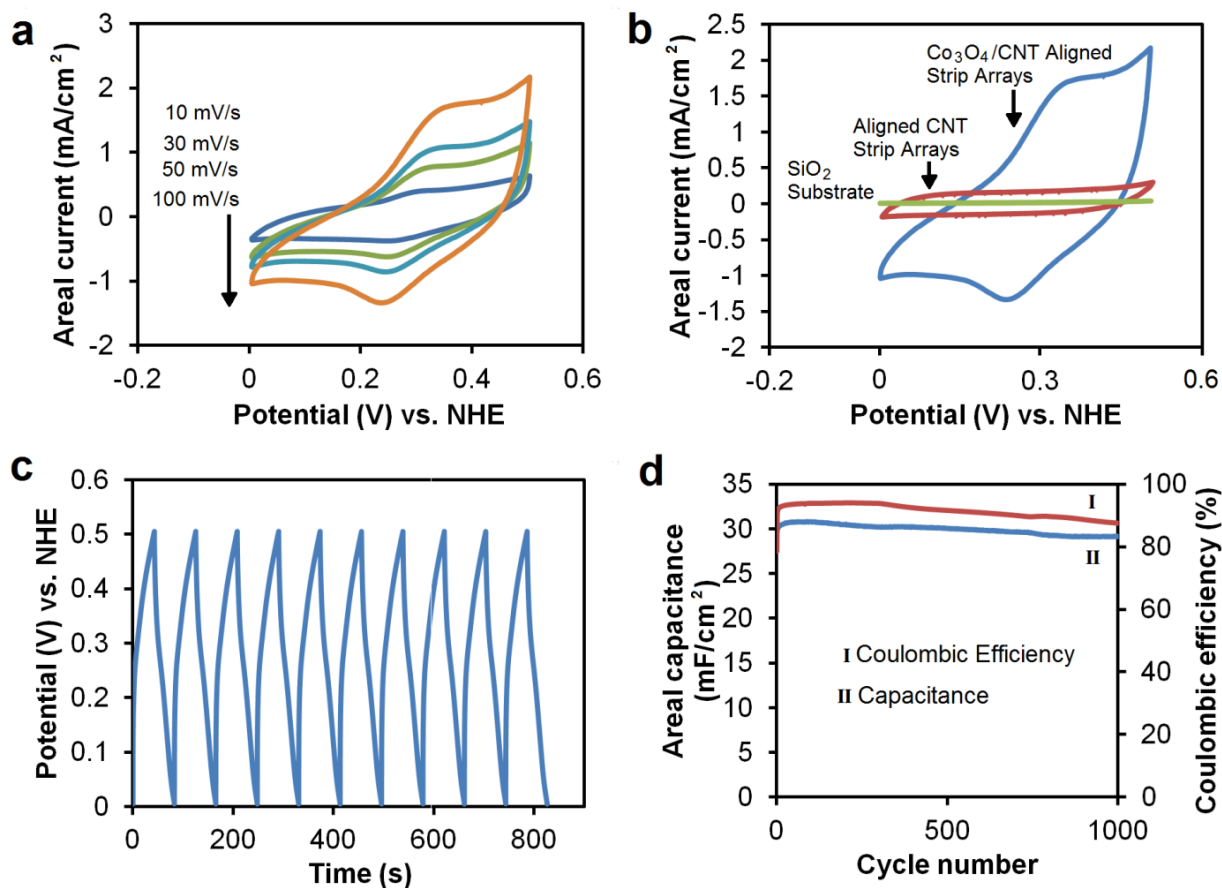
Figure 3.12. Electrochemical measurement data of aligned strips of hybrid CNT/Co_3O_4 in a 2M KOH electrolyte. (a) Cyclic voltammograms at scan rates of 10, 30, 50 and 100 mV/s. (b) Cyclic voltammograms of SiO$_2$ substrate, pristine aligned CNT, and aligned CNT/Co_3O_4 hybrid strips at a scan rate of 100 mV/s. (c) Galvanostatic charge-discharge vs. time at 200 μA constant current. (d) Areal capacitance and Coulombic efficiency during 1000 charge-discharge cycles (Reprinted with permission from ref. (118). Copyright 2013 American Chemical Society).

49

$$Co_3O_4 + H_2O + OH^- \leftrightarrow 3CoOOH + e^- \qquad\qquad (9)$$

In CNT/Co$_3$O$_4$ hybrid mesoporous architectures, aligned CNTs act as the current collector and transfer the charge from the CNT surfaces and CNT/Co$_3$O$_4$ interfaces during the electrochemical measurements. The oxidation and reduction of Co$_3$O$_4$ occured at a fast pace, measured as up to 100 mV/s. Furthermore the oxidation/reduction peak potentials did not change significantly when the cycles were performed at higher scan rates (compare 10 and 100 mV/s in Figure 3.12a), indicating the ease at which the ions diffuse to the electrode surface. This is due to the highly mesoporous nature of the CNT/Co$_3$O$_4$ electrode. Another important feature of such hybrid electrodes is that both electric double layer capacitance and pseudocapacitance occurs. In another word, charges are stored both in a double layer of electrons and holes inside the mesopores and through the redox Faradaic reaction of Co$_3$O$_4$ nanoparticles on the CNT surfaces. Figure 3.12 shows the huge change occurred in the capacitance and mechanism when CNTs were coated with Co$_3$O$_4$ nanoparticles, indicating that pseudocapacitance had a greater effect in this case. The shape of the CV curve when the electrode has only aligned CNTs (without Co$_3$O$_4$) is typical of electric double layer capacitors, whereas the CNT/Co$_3$O$_4$ shows significant pseudocapacitance behavior. The contribution from the supporting SiO$_2$ substrate is negligible.

The aligned CNT/Co$_3$O$_4$ strips showed excellent stability in the Galvanostatic Cycling test, with a fixed charge and discharge current of 200 µA (Figure 3.12c) after approximately 1000 cycles. At 200 µA (377 µA/cm^2), the CNT/Co$_3$O$_4$ strips managed a consistent and repeatable areal capacitance of 30.84 mF/cm^2, and specific capacitance of 168.22 F/g (based on weight of Co$_3$O$_4$) or 123.94 F/g (based on weight of CNT/Co$_3$O$_4$). The measured thickness of the CNT/Co$_3$O$_4$ strips was about 10 µm, which makes the volumetric capacitance 30.84 F/cm^3. The Coulombic efficiency was about 87 to 92% and the capacitance did not change significantly

(within 5%) during the 1000 cycles, suggesting the stability of such an electrode in capacitor applications (Figure 3.12d).

The capacitance of cobalt oxide structures in the forms of mesoporous composites or thin films ranges from 70 to 400 F/g (126). These numbers are much less than the theoretical specific capacitance of Co_3O_4 (3560 F/g). Researchers worldwide are striving to improve the capacitance value achievable experimentally. Proposed recently is an approach that calls for the use of binder free hybrid materials as they provide direct contact between the metal oxide and the current collector without blocking the electrical conductivity of the electrode. In this regard, Yuan and co-workers (127) recently made a free standing Co_3O_4/reduced Graphene oxide/CNT paper electrode and measured its electrochemical capacitance to be 378 F/g at 2 A/g and 297 F/g at 8 A/g. The method presented in this thesis can be another approach to achieve such binder-free hybrid materials with compatible or superior capacitance, and it is applicable to a variety of oxides besides Co_3O_4. It is anticipated that an order of amplitude improvement can be achieved through optimization of the test setup and the architecture geometry.

3.4. Conclusion

In conclusion the template effect of aligned 3D CNT patterns in fabricating mesoporous CNT/MO hybrid structures as well as 3D mesoporous MO architectures using a microwave-assisted chemical technique was shown. The porous nature of aligned CNT patterns along with their high specific surface area (548 m^2/g) allowed the decoration of single nanotubes with MO nanoparticles in this microwave-chemical coating process. The fabricated CNT/MO hybrid structures preserved the alignment, three dimensional morphology and porous nature of the

original CNT patterns while still having a high surface area (e.g. 350 m^2/g for CNT/Co_3O_4) and a slightly larger pore size of 9-18 nm. It was demonstrated that this microwave-chemical approach is highly universal in terms of oxide type and architecture geometry. It is also shown that such mesoporous structures are relevant candidates for use as electrodes in energy storage applications. An example electrode composed of CNT/Co_3O_4 aligned strips exhibited an areal capacitance of 30.84 mF/cm^2, specific capacitance of 123.94 F/g and a Coulombic efficiency of about 87-92% over 1000 charge-discharge cycles.

CHAPTER 4. Bio-inspired Graphene Oxide (GO)/Inorganic Layered Hybrids

4.1. Introduction to Bio-inspired Materials

Nature is always a wonder for researchers in how it fabricates the materials with extraordinary characteristics and structures coming from several interrelated features including the self-assembly of the counter-parts, multi-functionality of the structural frameworks and hierarchy of the building blocks. Therefore a lot of research activities pursue mimicking the mechanisms that enable the duplication of such naturally formed assemblies (128). Bio-inspired materials, as they are named, have been developed through mimicking the structure of the biological systems or mechanisms that they use in making the living organisms and structures, for fabricating the engineering materials.

Seashell nacre for instance inspired researchers due to its high stiffness and toughness arising from the layered brick-and-mortar (B&M) order of aragonite ($CaCO_3$) platelets (0.5µm thick) and chitin fibers (~30nm thick) which act as a cushion for damping the propagation of micro-cracks and therefore elevates the toughness of the material (6)(5)(129). Figure 4.1 illustrates the optical and SEM images of the Abalone nacre which confirms the layered structure composed of aragonite platelets bridging together with chitin fibers and the protrusions of the ceramic component. The organic layer in nacre structure has pores of about 50 nm in diameter which enables the formation of mineral bridges between the aragonite layers (130). Mimicking the nacre structure in materials fabrication and design results in developing advanced layered ceramics with superior mechanical properties (5).

In an attempt to mimic the layered structure of nacre and producing novel layered hybrid ceramics, an ice-templated approach was presented in 2008 by Munch and co-workers (6). They

53
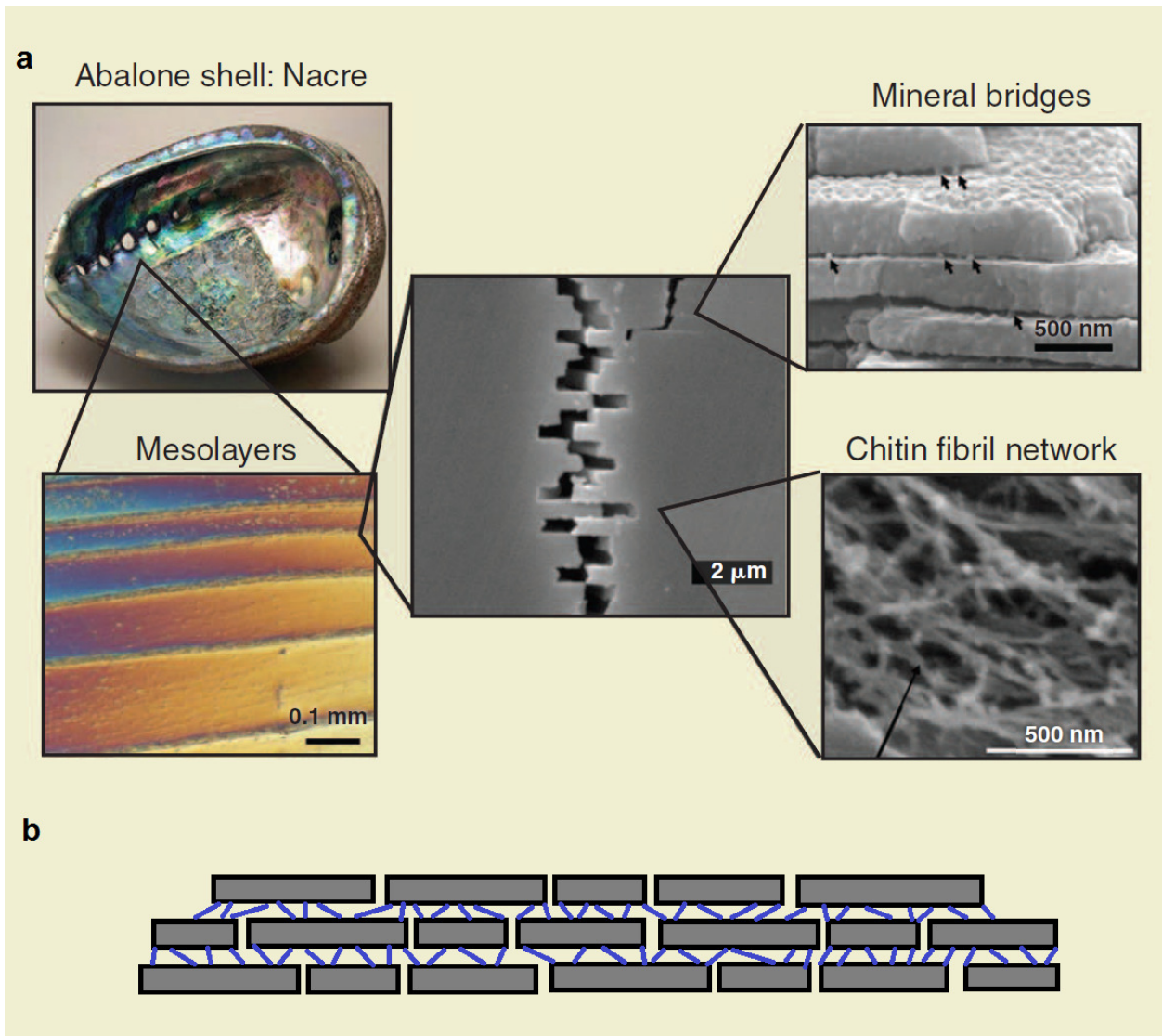
Figure 4.1. (a) Optical and electron microscopy images of the Abalone nacre showing the layered structure (Adopted from ref. (5,131,132) **with permission). (b) the schematic drawing of the nacre layered structure.**

basically made a layered ice template by directional rapid cooling of ceramic slurries. When cooling, ice crystals make layered branches and at the same time the ceramic particles precipitate out of the solution and trap between the ice layers (6). Then the ice template is removed by lyophilization (133) and finally the structure can be sintered to increase the mechanical

interconnection of ceramic or infiltrate with a polymer to make a ceramic-polymer hybrid (Figure 4.2) (6,129,133,134).

Although the ice template method is a simple and inexpensive top-down method, it is limited by the thickness of the layers which can be controlled by freezing rate to values not lower than 10 µm (134). Also for the preparation of slurries surfactants should be used to stabilize the particles in the colloids which is not very bio-favorable. On the other hand, sintering the final structure is needed which can affect the size and morphology of the ceramic particles.

Another approach is layer by layer assembly of thin films to obtain the layered structure at the end. For instance nacre-like heparin (HEP)/layered double hydroxide (LDH) ultrathin film was made by Shu and co-workers (135) through alternative coating of HEP solution and LDL colloidal solutions on a silicon substrate. The layered HEP/LDH film showed improved mechanical properties and blood compatibility.

The approach which is developed and presented in the current thesis is to use a bottom-up approach and in-situ synthesis of layered materials using GO films as templates. The GO film as what was discussed previously in this thesis (Chapter 1), has a fine layered structure which can be fabricated in different sizes and shapes. Also the GO surface is hydrophilic and due to the presence of epoxy, hydroxyl groups and vacancies, it provides a relevant site for nucleation and growth of nanoparticles. This method can be used to directly synthesize various types of bio-inspired GO/Inorganic layered hybrids having diverse technological applications. In addition, the GO film can later be eliminated from the structure while sintering the ceramic counter-part, leaving a porous layered ceramic structure with very small layer thickness (as low as a GO single sheet thickness ~ 10-20 nm).
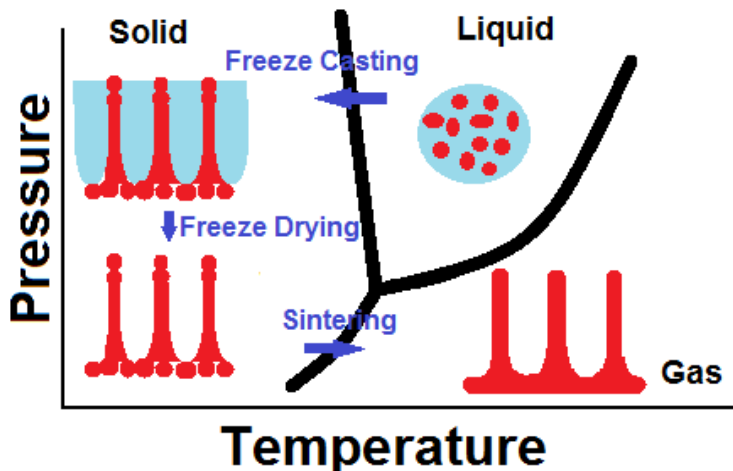
Figure 4.2. Schematic drawing of the ice-templated fabrication of layered ceramics.

4.2. Synthesis of Graphene Oxide (GO) Films[1]

The GO solution was prepared by using a modified Hummer's method. First, 30g NaCl was mixed with 3.6g graphite flakes and the mixture was grounded for 20 minutes. Then, NaCl was washed and filtered away from the mixture using plenty amount of water and filtration. The so obtained graphite was dried at 60°C for 1.5 h and about 3.0g of it, was added into a solution of potassium persulfate ($K_2S_2O_8$, 2.5 g), phosphorus pentoxide (P_2O_5, 2.5 g) and concentrated sulfuric acid (H_2SO_4, 12 mL). After 4h of stirring the mixture at 80°C in an oil bath, the dark blue mixture was cooled to room temperature, DI water was added, followed by filtration and rinsing with lots of water and then drying at 60 °C for 1.5 h. The as obtained pre-oxidized graphite was treated later by Hummers method.

In a typical procedure, 69 mL of concentrated H_2SO_4 was added to the pre-oxidized graphite and the mixture was kept in a 0°C ice bath. Then 9g of potassium permanganate

---

[1] GO solution was made by my colleague Mr. Xiguang Gao.

56

(KMnO$_4$) was added to the solution slowly while stirring to keep the temperature of the mixture below 20 °C. The mixture later was kept at 35~40 °C and stirred for 1 h. The mixture was diluted with 560 ml water followed by addition of 30 mL H$_2$O$_2$ (30%) and suddenly the color of the suspension turned bright yellow. Repeated steps of centrifugation (at 11,000 rpm), washing with HCl (5%) and water was performed and each time the precipitate was collected. Then obtained precipitate was re-dispersed in DI water (350 mL) and stirred for 5 minutes followed by sonication for 40 min. After sonication, a suspension is obtained that was centrifuged repeatedly for 4~5 times at 4000 rpm to remove any insoluble particles. After each centrifugation the supernatant was collected. The brown homogenous solution thus made was dialyzed against Milli-Q water for 1 week and stored for future use (Figure 4.3).
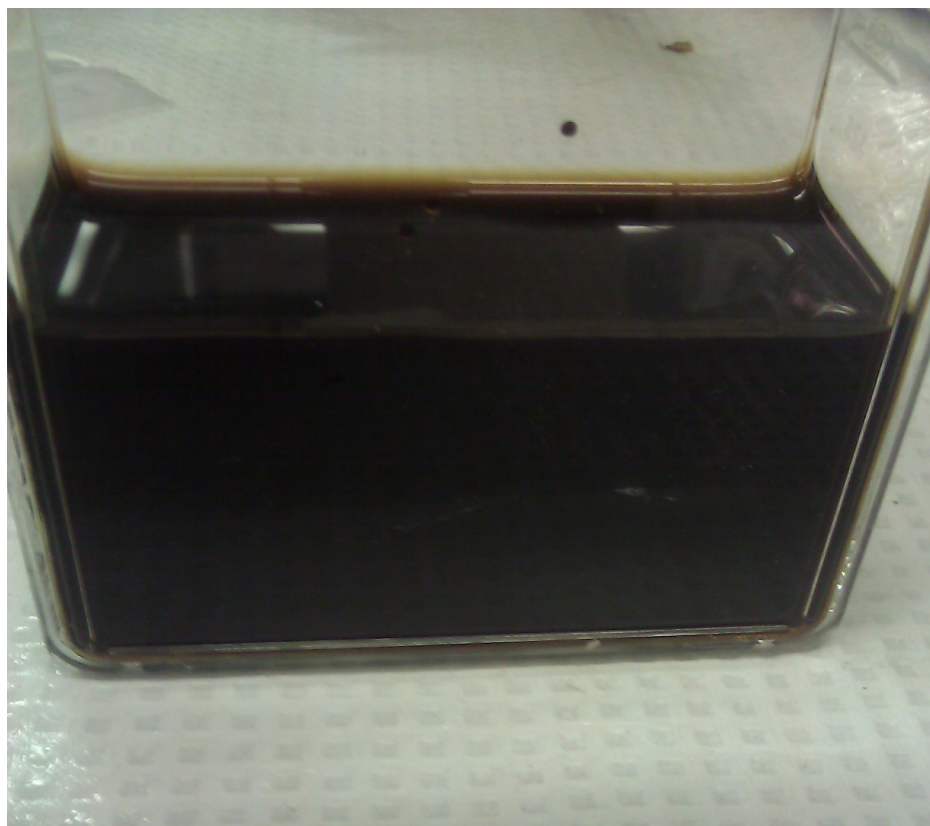
Figure 4.3. The obtained GO solution through the modified Hummer's method.
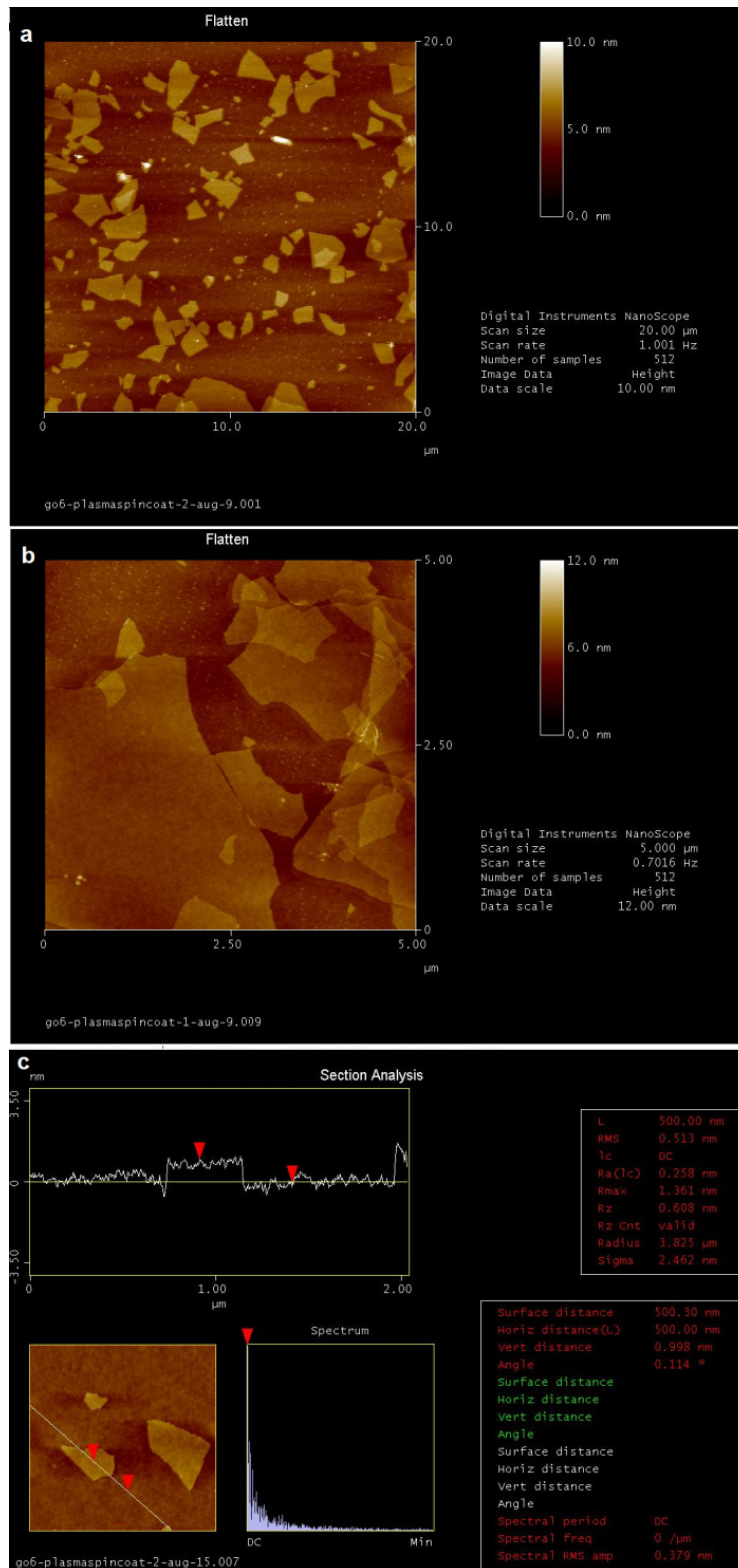
Figure 4.4. AFM images of the GO flakes obtained in our synthesis process using a modified Hummers method.

The concentration was determined by filtering 8.0 mL GO stock solution using a 0.02 μm Anodic alumina membrane filter (Whatman) and weighing the mass of resultant GO film. The concentration of GO solution is about 3.0~4.0 mg/mL using the preparation method described above.

The thickness of the as-synthesized graphene oxide flakes was characterized using atomic force microscopy (AFM, Figure 4.4). The size of the GO flakes shown in Figure 4.4a&b is below 5μm. The thickness of the GO flakes (Figure 4.4c) is about 1 nm, suggesting that the obtained GO flakes are single-layered. It has been shown that the distance between the graphene sheets in graphite structure is about 0.34 nm which transforms to about 0.78-1nm when oxidized. The oxidized graphene is thicker than pristine graphene since the oxygen-containing groups attaching to the graphene plane increases the thickness (136,137).

4.3. Synthesis of Layered GO/Inorganic Hybrids and Inorganic Thin Films

To make the free-standing GO films, 5mg of the as-obtained GO solution was filtered using vacuum filtration and polycarbonate (PC) membranes with pore size of 100 nm to get the GO thin film. The filtration was done overnight at room temperature. The free-standing film was taken out later to do the interlayer synthesis of inorganic nanoparticles (Figure 4.5).
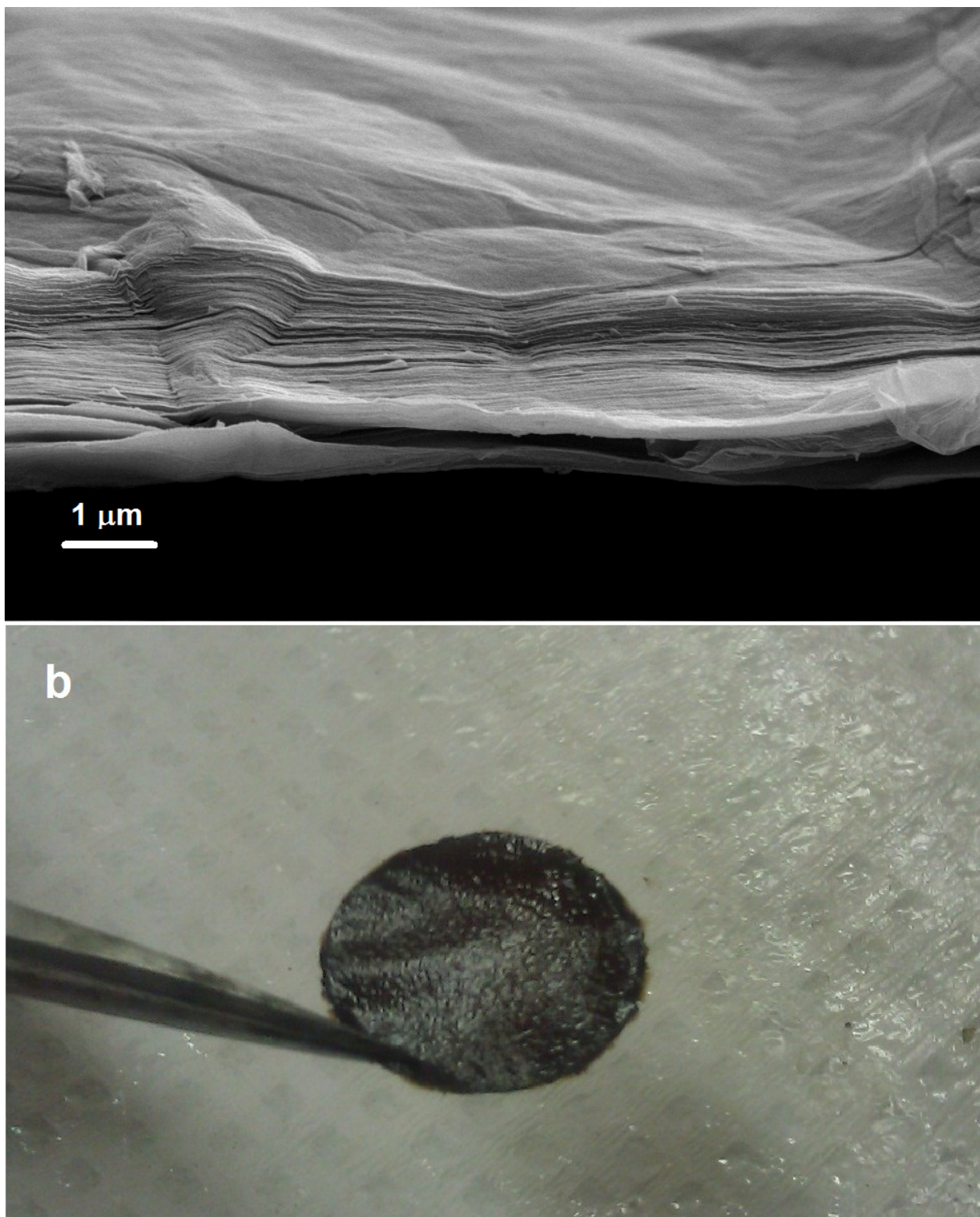
Figure 4.5. (a) SEM image of the vacuum filtered GO thin film, (b) Digital image of the free-standing GO film.

In a general procedure to fabricate the layered GO/Inorganic hybrids, the GO film soaked in a precursor solution of desired material under vacuum so that the solution infiltrates between the layered structures of GO film. The whole solution was then irradiated in the microwave (900W, 2.45 GHz) oven for 30-60 seconds. Figure 4.6 shows schematically the steps involved in in-situ fabrication of the GO/Inorganic layered hybrids.
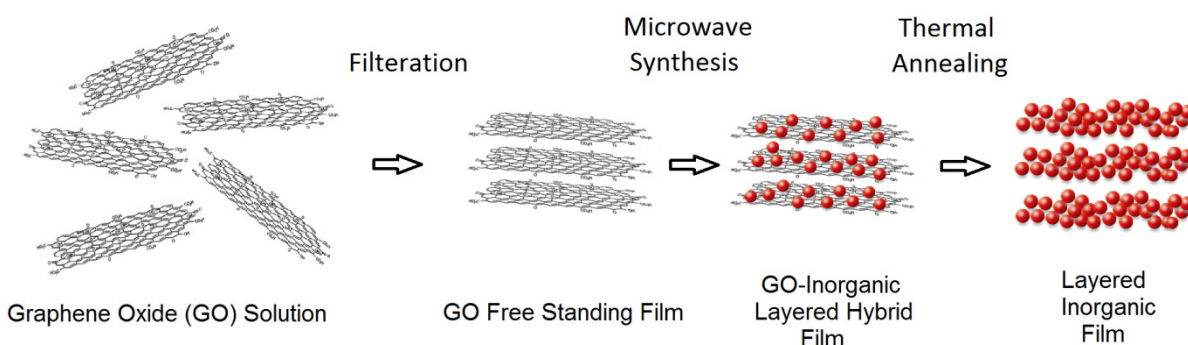
Figure 4.6. Schematic representation of the synthesis steps involving the formation of layered GO/Inorganic hybrids and layered inorganic free-standing films.

As what was mentioned previously, the GO template can be removed through a thermal annealing process leaving a porous layered inorganic film behind (Figure 4.6). Such approach is very novel in fabricating free-standing inorganic thin films and can be beneficial in design and development of devices based on inorganic thin films such as energy storage applications (138).

The method described here can be used to fabricate various GO/Inorganic layered hybrids. For example GO/Ag, GO/ZnO, GO/Fe$_3$O$_4$ and GO/Hydroxyapatite (HA) layered hybrids are produced and described in this thesis.

4.3.1. Synthesis of Layered GO/Ag Hybrids and Ag Thin Film

The precursor solution for making the GO/Ag hybrids was prepared as follows. In a 200 ml beaker, 10 ml ammonium hydroxide solution (NH$_4$OH, 30% NH$_3$) was mixed with 50 ml DI water and then 50 mg AgNO$_3$ was added into the mixture and stirred vigorously to completely dissolve. Afterwards, 2ml H$_2$O$_2$ was added to the as obtained clear solution and stirred again to homogenize. Later, the GO film (as what was described before) soaked in the solution under vacuum to infiltrate the solution between the layers. Then the whole solution together with the GO film was irradiated in a microwave oven (900W, 2.45 GHz) for 30-60 seconds. The GO/Ag film was then taken out and dried at 80 ˚C. In order to make the free-standing layered silver thin film, a GO/Ag film was annealed in air at 650 ˚C for 10 minutes. Figure 4.7 shows the typical digital images of the obtained free standing Ag film after annealing and removing GO from the hybrid structure.
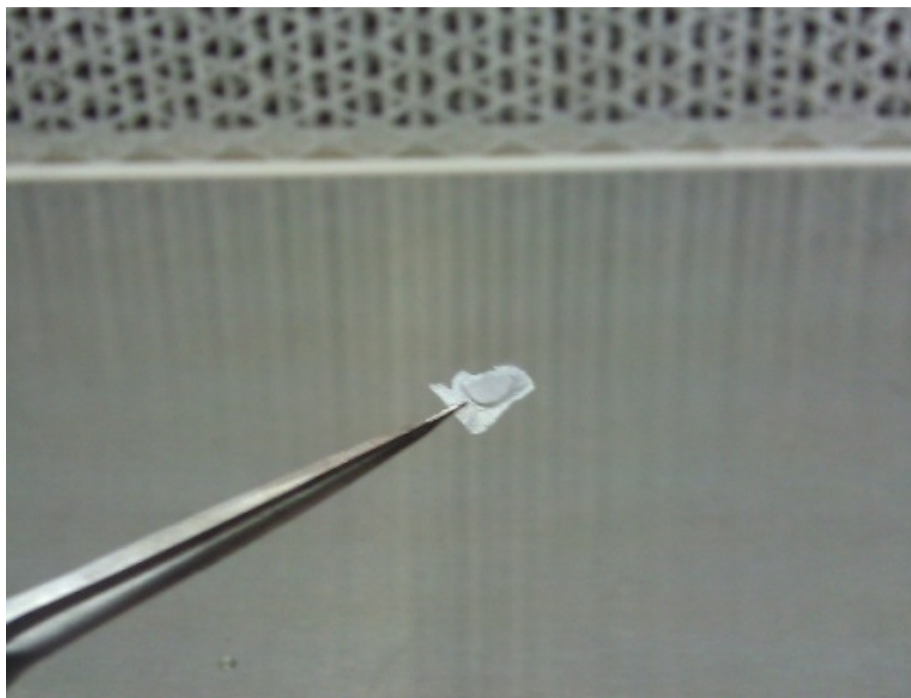
Figure 4.7. Digital image of the typical free-standing Ag film after GO burn out.

62

X-ray diffraction characterization was performed on the obtained inorganic materials after microwave synthesis to find out the phase and crystal structure of the obtained materials. In Figure 4.8 the intensity of peaks reflected the high degree of crystallinity of the silver nanoparticles fabricated through the microwave assisted technique. All the peaks are assigned with Miller indices (hkl) correspond to pure silver metal with face centered cubic (FCC) symmetry (139).
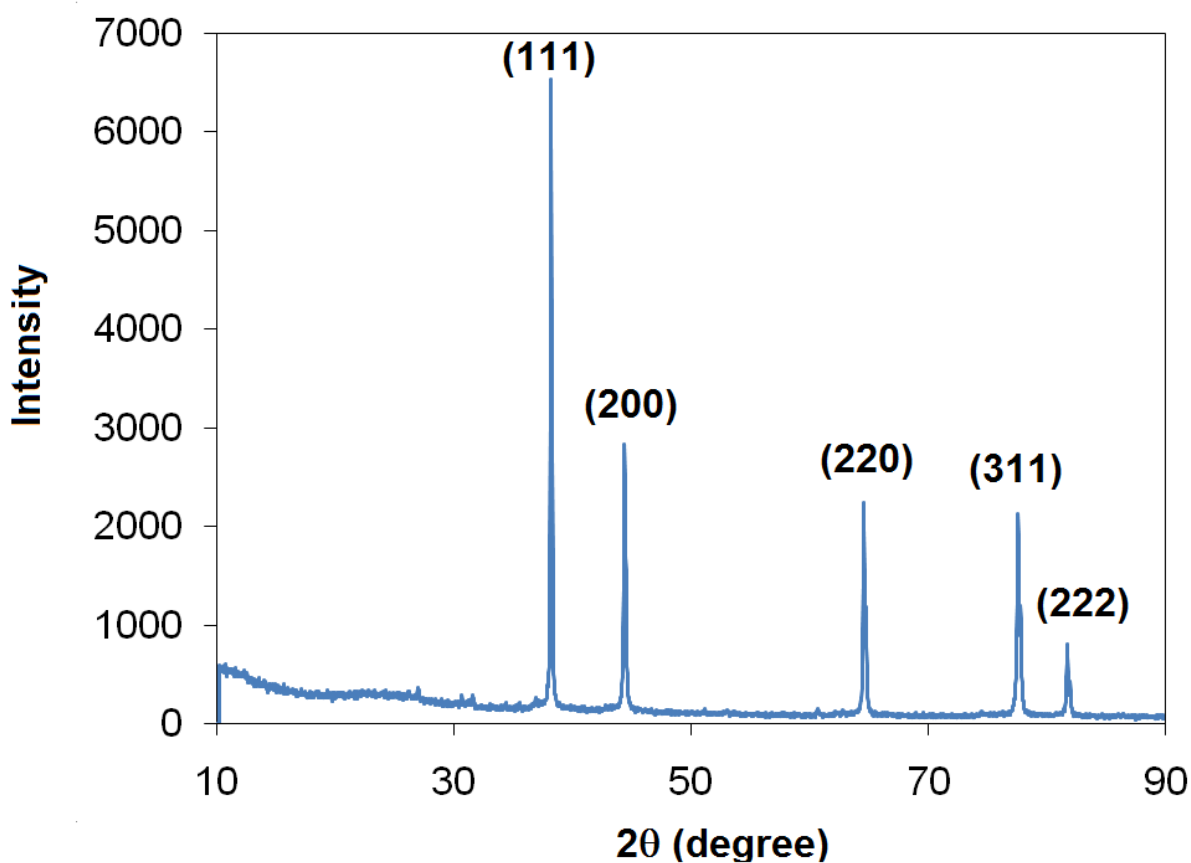
Figure 4.8. XRD pattern of the Ag nanoparticles synthesized by microwave chemical process.

The SEM images (Figure 4.9) show that the GO film is covered with silver particles (less than 1μm in diameter) and they grow and bind together when annealed to make the free-standing
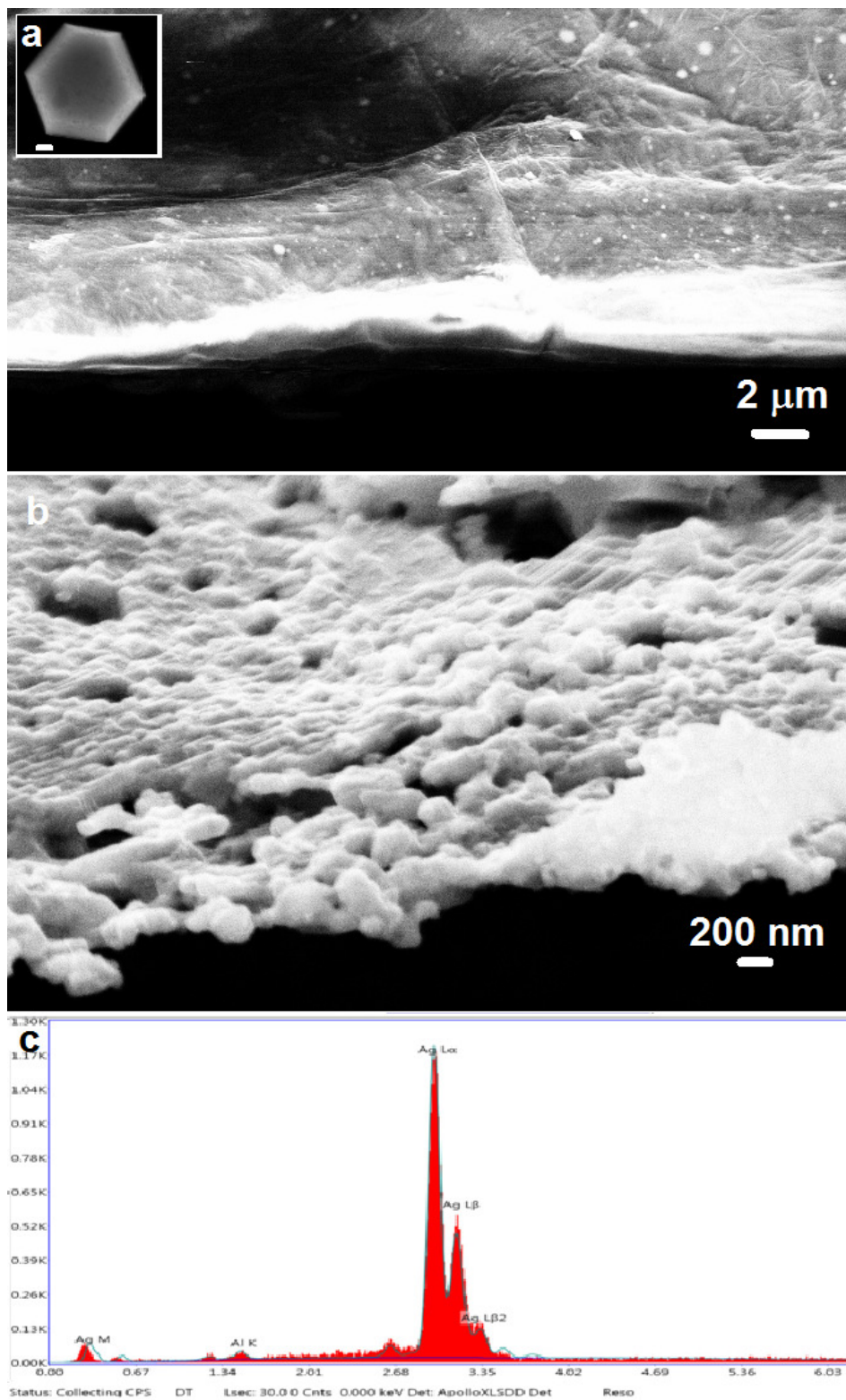
Figure 4.9. SEM images of (a) the GO/Ag hybrid film (inset is a single Ag nanoparticles, the scale bar is 100nm), (b) Ag free standing thin film and (c) EDS analysis of the Ag nanoparticles.

film with layer thickness of about 200 nm. Also the SEM images prove the porous structure of the Ag thin film after annealing and GO removal. The EDS analysis further confirms the fabrication of Ag nanoparticles with this method.

The chemistry involved in synthesis of silver nanoparticles with microwave energy is described below:

$$AgNO_3 + NH_4OH \rightarrow AgOH_{(aq)} + NH_4NO_3 \qquad (1)$$

$$2AgOH_{(aq)} + H_2O_2 \xrightarrow{microwave} 2Ag + 2H_2O + O_{2(g)} \qquad (2)$$
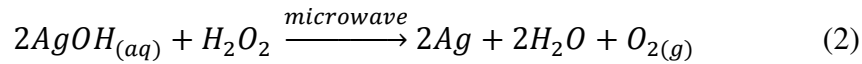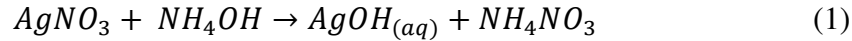
The oxygen bubbles and the yellow color of the solution (due to presence of silver nanoparticles in the solution) after the experiment confirms the reaction happen.

4.3.2. Synthesis of GO/ZnO Layered Hybrids and ZnO Thin Film

The precursor solution for making the GO/ZnO hybrids was prepared as follows. In a 200 ml beaker, 25 ml ammonium hydroxide solution (NH_4OH, 30% NH_3) was mixed with 40 ml DI water and then 1 g zinc acetate dehydrate ($Zn(O_2CCH_3)_2(H_2O)_2$) was added into the mixture and stirred vigorously to completely dissolve. Later, the GO film (as what was made before) soaked in the solution under vacuum to infiltrate the solution between the layers. Then the whole solution together with the GO film was irradiated in a microwave oven (900W, 2.45 GHz) for 30-60 seconds. The GO/ZnO film was then taken out and dried at 80 ˚C. In order to make the free-standing layered ZnO thin film, a GO/ZnO film was annealed in air at 650 ˚C for 10 minutes. The synthesis mechanism of ZnO nanoparticles is the same as what was discussed in Chapter 2. However the morphology of the nanostructures here shows an interesting feature.
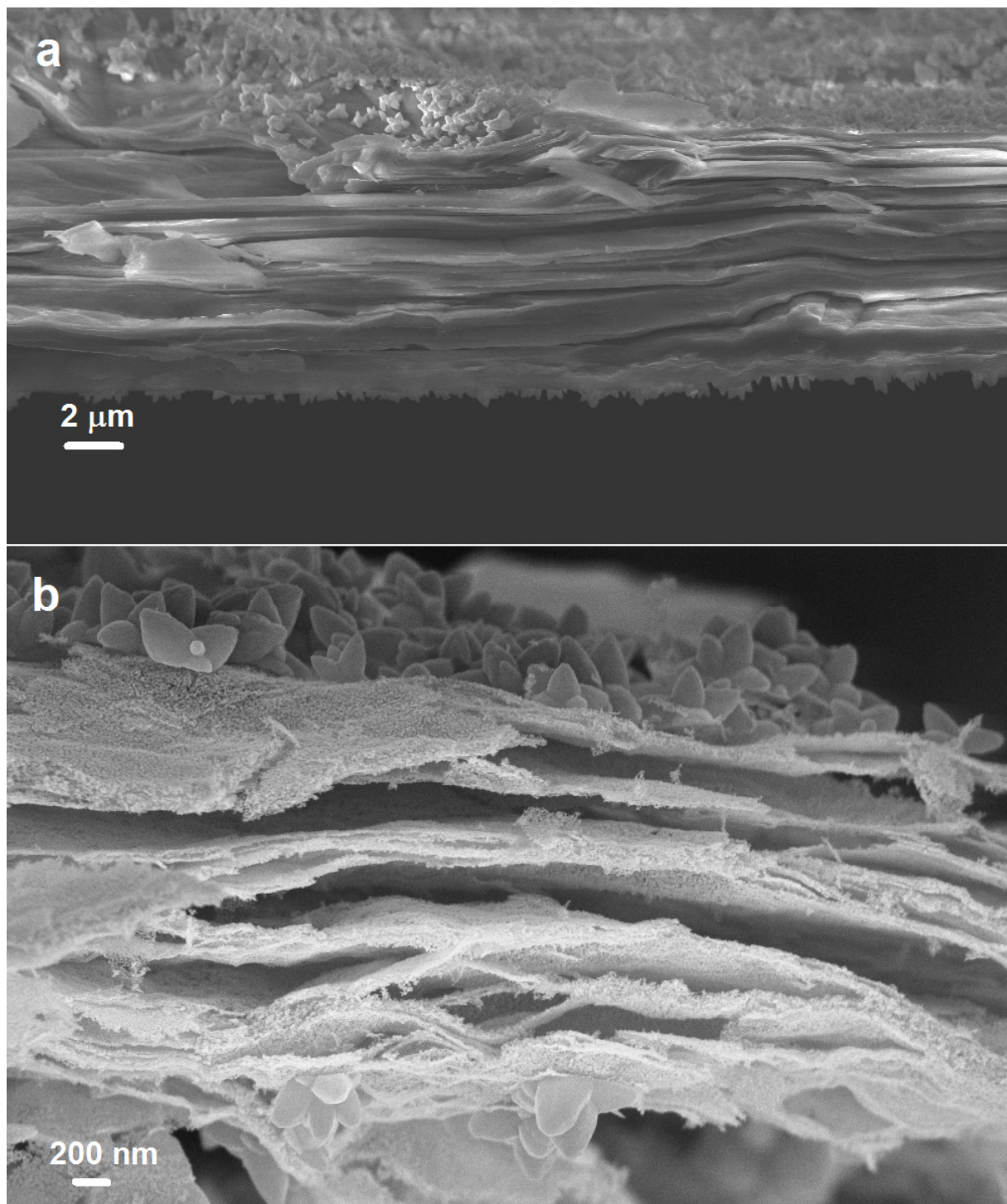
Figure 4.10. SEM images of (a) GO/ZnO layered hybrid, (b) ZnO layered thin film.

The SEM images in Figure 4.10 illustrate the coverage of the outer surfaces of GO film with flower-like ZnO structures while the inter-layer sections are coated with small nanoparticles. In another words, the morphology and growth of ZnO nanoparticles is affected by the packing characteristics of the inter-layer sheets of GO film. The packing density of the GO layers can block the diffusion of precursor solution while the rapid synthesis happens during microwave irradiation. Therefore the nucleated seeds that occur on the surface have the possibility to grow more due to the direct contact with the precursor solution but the nucleation sites between the layers can't be fed with fresh precursor and they don't grow larger. This phenomenon can be beneficial in controlling the shape and size of nanomaterials and therefore affect their physical properties and derive different characteristics out of the surface and interlayer spaces of the hybrid material. The highly porous free-standing ZnO thin film can be used in thin film optoelectronic devices. Its empty spaces can be infiltrate with polymers to increase the mechanical properties.

4.3.3. Synthesis of GO/Fe$_3$O$_4$ Layered Hybrids

The precursor solution for making the GO/Fe$_3$O$_4$ hybrids was prepared as follows. In a 200 ml beaker, 10 ml ammonium hydroxide solution (NH$_4$OH, 30% NH$_3$) was mixed with 50 ml DI water and then 17 mg Iron(III) acetylacetonate (Fe(C$_5$H$_7$O$_2$)$_3$, AKA Fe(acac)$_3$) was added into the mixture and stirred vigorously to completely dissolve. Then 2ml hydrazine solution (N$_2$H$_4$) was added to the solution and stirred to homogenize. Later, the GO film (as what was made before) soaked in the solution under vacuum to infiltrate the solution between the layers. Then

the whole solution together with the GO film was irradiated in a microwave oven (900W, 2.45 GHz) for 30-60 seconds. The GO/Fe$_3$O$_4$ film was then taken out and dried at 80 ˚C.

The phase and crystallinity of the obtained material was confirmed with XRD (Figure 4.11). The resulting XRD pattern shows the peaks attributed to the magnetite (Fe$_3$O$_4$) phase with an FCC crystal structure (JCPDS Card No. (79-0417)). The peaks are broad which shows the small crystallite size of the nanoparticles.
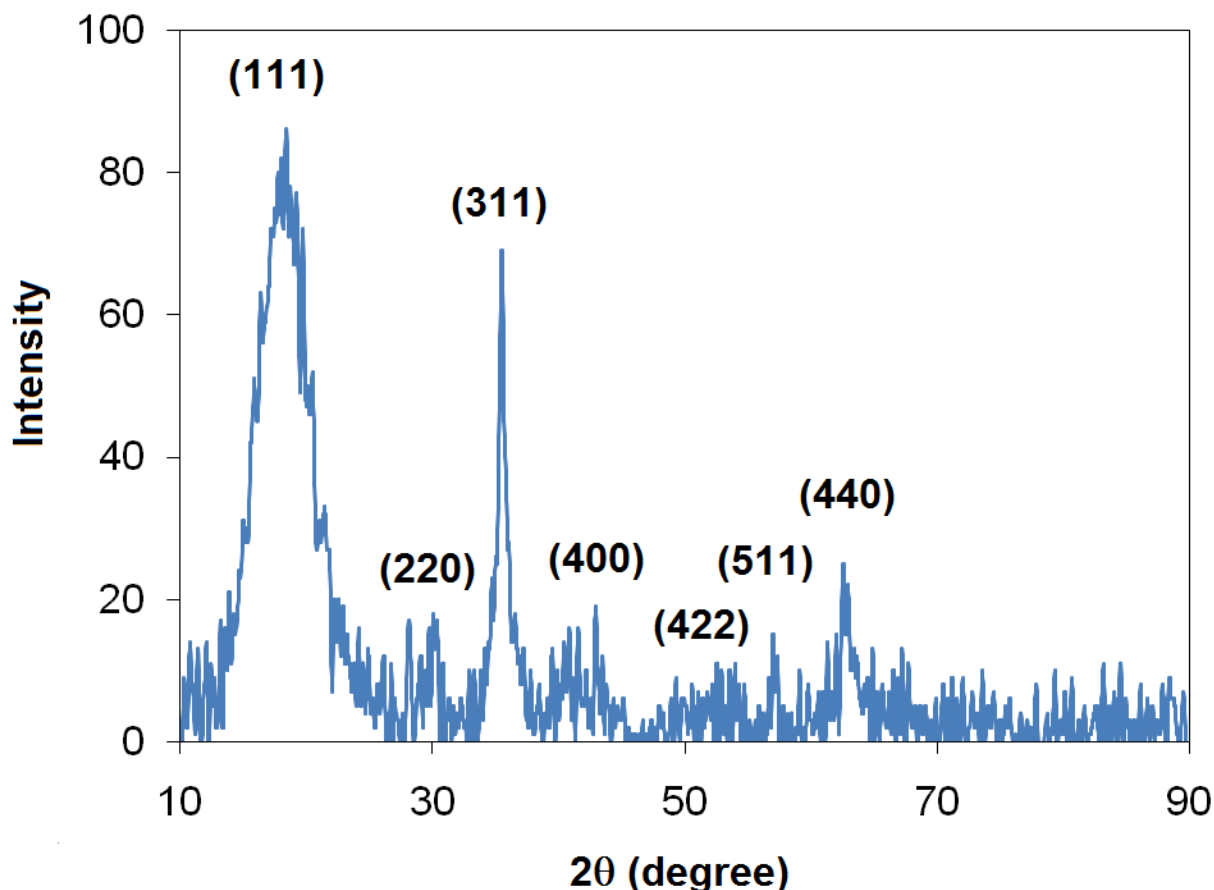
Figure 4.11. XRD pattern of the obtained iron oxide through the microwave synthesis process.

The obtained free-standing GO/Fe$_3$O$_4$ hybrid film was utilized to synthesize carbon nanotubes on it using CVD method with parameters that were described in chapter 3. In order to

make Fe catalyst nanoparticles for CNT growth, the GO/Fe$_3$O$_4$ film was pretreated with H$_2$ gas for 30 min at 750 ˚C before the CNT growth step. During annealing with hydrogen gas, the iron oxide nanoparticles reduce partially (depending on annealing time and hydrogen gas flow) and transform into iron nanoparticles.
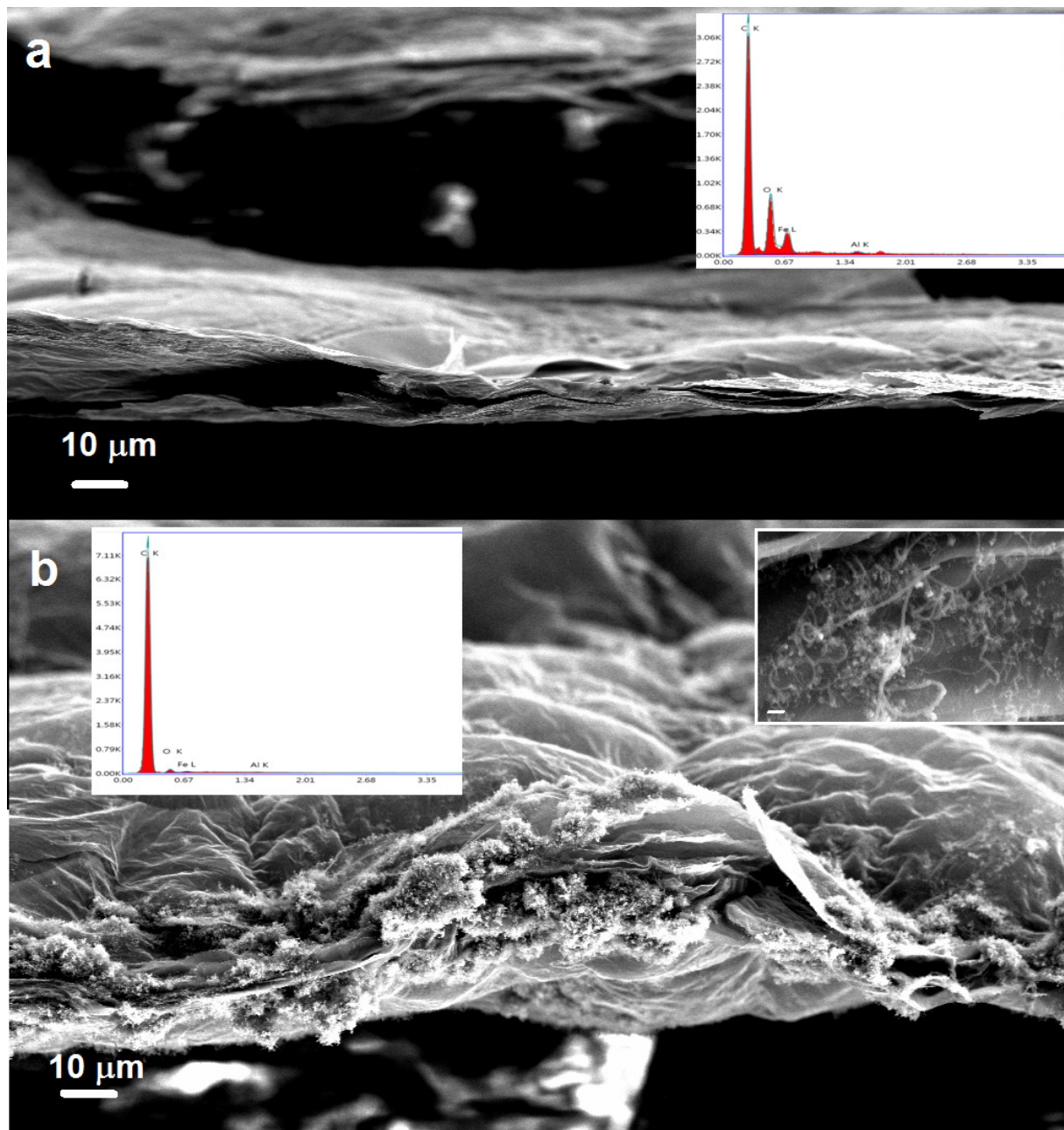
Figure 4.12. SEM images of (a) GO/Fe$_3$O$_4$ hybrid film (the inset shows the EDS of the film), (b) the CNT grown on GO/Fe$_3$O$_4$ hybrid film. The inset show the zoomed in image and the scale bar is 200 nm.

Fe nanoparticles act as catalysts during the CNT growth step. Also the GO film reduced to some extend to the graphene. Figure 4.12 reveals the SEM images of the GO/Fe_3O_4 hybrid film and $rGO/rFe_3O_4/CNT$ hybrid film. The iron oxide nanoparticles covered all around the surface and between the layers in the GO/Fe_3O_4 hybrid film (Figure 4.12a). EDS analysis (inset of Figure 4.12) confirms the presence of iron oxide on the film. After CVD growth, CNTs grow randomly on the iron oxide particles which covered the hybrid film. The nanotubes are fluffy and have diameters about 50 nm (Figure 4.12b). The EDS analysis after CNT growth reveals the increase in the carbon content and decrease in oxygen content of the hybrid film that further confirms the partial reduction of GO and Fe_3O_4 components.

It has been shown previously that the GO/CNT composites are useful in energy storage applications since they provide high dielectric constant, enhanced breakdown strength and maximum energy storage density as well as low dielectric loss (9). Therefore the obtained free-standing $rGO/rFe_3O_4/CNT$ hybrid film can have potential applications in flexible energy storage devices.

4.3.4. Synthesis of GO/Hydroxyapatite (HA) Layered Hybrids

In order to make the GO/HA layered hybrids, two separate solutions were made. In a 200 ml beaker, 30 mg calcium hydroxide powder ($Ca(OH)_2$) was added to 50ml DI water and stirred vigorously to dissolve (solution **A**). Then GO film soaked in solution A to infiltrate the solution between the layers. The other solution (**B**) was made in a 100 ml beaker by adding 27 mg ammonium phosphate dibasic ((NH_4)H_2PO_4) into 50 ml DI water. Then solution **B** was added drop-wise to solution **A** while slowly stirring. The pH of the mixture was about 10.8 after adding

solution **B** to **A**. The whole mixture was irradiated in a microwave oven (900W, 2.45 GHz) for 30-60 seconds. The GO/HA film was then taken out and dried at 80 ˚C.
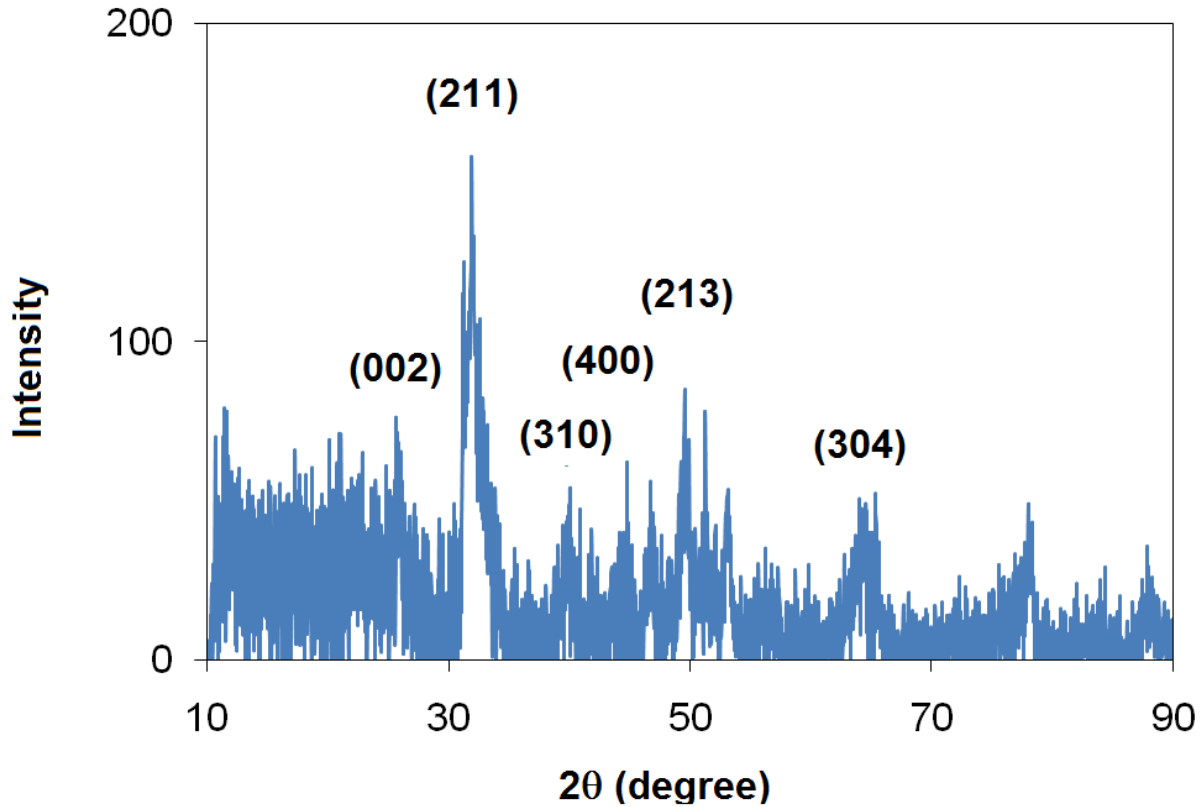
Figure 4.13. XRD pattern of the obtained hydroxyapatite.

The XRD pattern (Figure 4.13) is attributed to the hexagonal HA [$Ca_5(PO_4)_3OH$] structure and reveals that the obtained HA has crystalline structure due to the presence of sharp peaks at higher degrees which are not usually very sharp in amorphous HA (60,119,140). However the broad peaks are related to the nano sized particles.
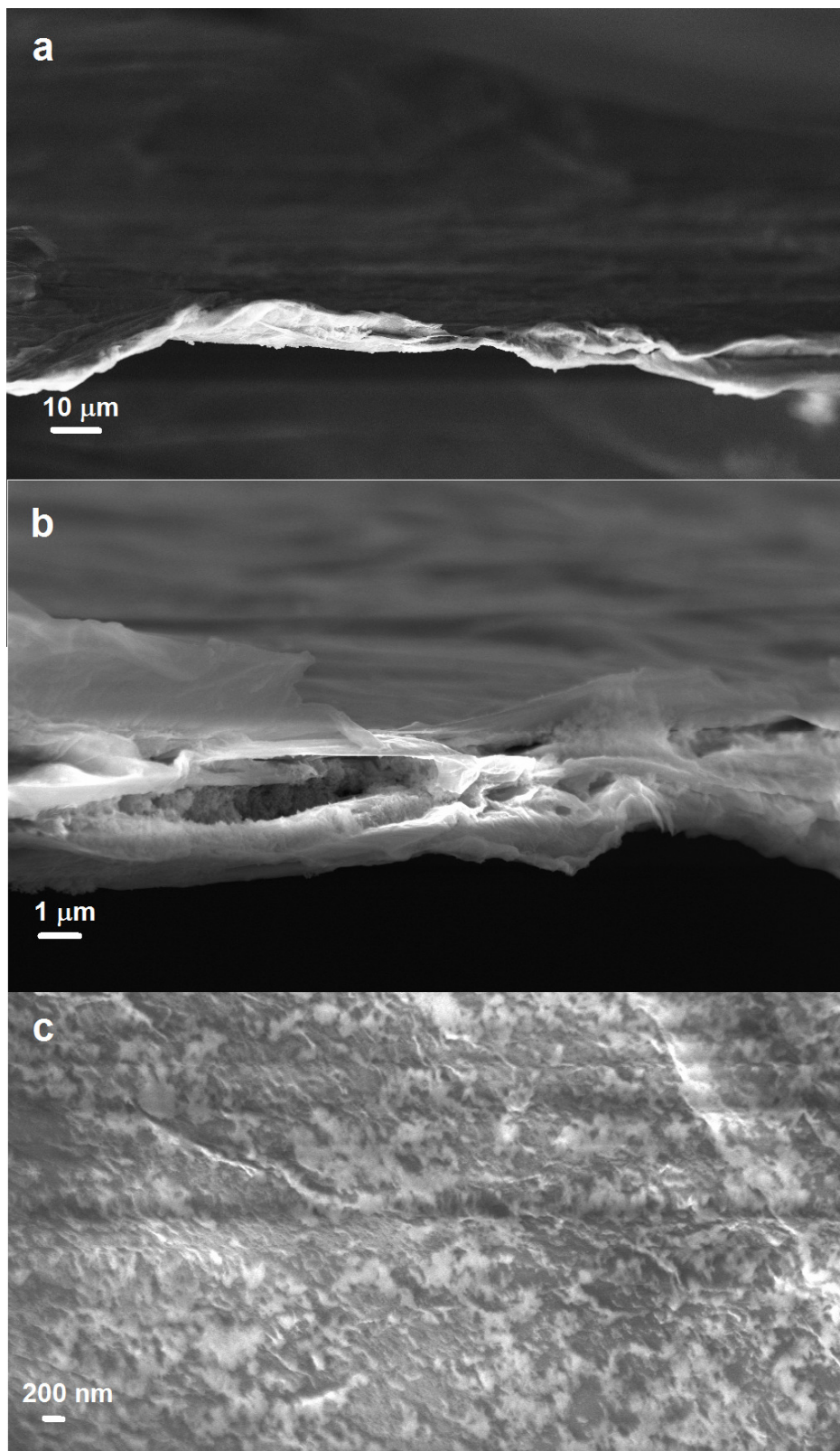
Figure 4.14. SEM images of the GO/HA hybrid film (a & b) side view, (c) top view.

The SEM images (Figure 4.14) show that the GO film is covered homogenously with nano sized needle shaped HA particles in between the layers and on the surface of the GO film. The HA nanoparticles have lengths of about 100 nm and diameter of about 20 nm.

The GO/HA hybrids can be used as templates for bone cell growth and proliferation because of its composition similarity to the human bone tissue. It has been shown that GO and reduced GO can improve the mechanical property of the HA ceramics and therefore increase their application in the load bearing conditions similar to the natural bone (141). So in the next section the mechanical properties of the GO film and GO/HA film are investigated and the results are compared with other materials for reference.

4.4. Mechanical Property of Bio-inspired Layered GO and GO/HA Hybrids

Hydroxyapatite ($Ca_{10}(PO_4)_6(OH)_2$, HA), is the naturally occurring mineral form of calcium apatite and is the main constitute of the hard tissues (i.e. bones and teeth) in human. Owing to its excellent bioactivity, biocompatibility and osteoconductivity, it has been extensively used as an implant material for bone tissue replacement and in orthopedic surgeries for enhancing the fixation of bony tissues (58,60,119). However the main drawback of HA in its mineral form is its weak mechanical properties as a result of its poorly crystallized structure. In order to increase the mechanical properties, one approach is to crystallize and sinter the HA nanoparticles. Also it's possible to use HA nanoparticles in a composite to make it stronger. Recently, graphene and graphene oxide have been used as reinforcing components to enhance the HA mechanical properties (141,142). In other attempts to mimic the bone and nacre 3D

73

structure and making layered ceramics, freeze-casting was used to make the layered HA scaffolds which was infiltrated with polymers later (133). The approach that is taken in this thesis is novel since GO films not only increase the mechanical properties of the HA nanoparticles but also orient them in layered structures to further increase the strength.

4.4.1. Cantilever Flexure Test

In order to examine the mechanical behavior of the GO and GO/HA samples cantilever beam bending tests were carried out on the narrow strips cut out of the films. All specimens were cut using razor blades to sizes between 1 and 3 mm wide. The mechanical bending test was performed using MicroSquisher instrument at CellScale Biomaterials Testing.
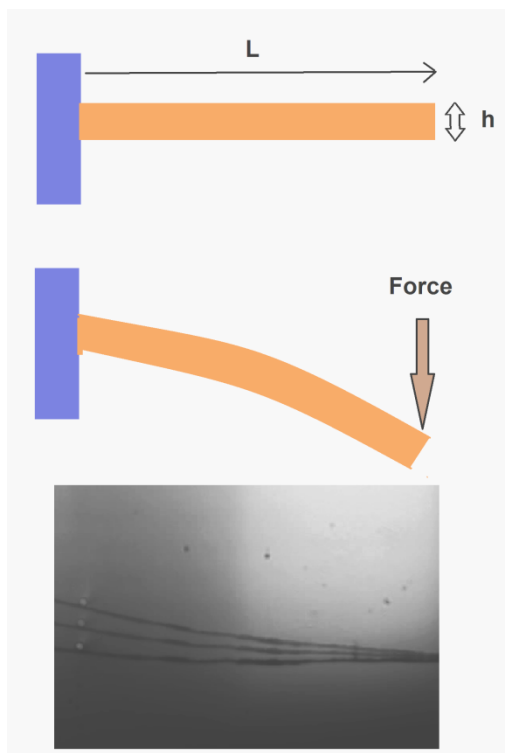
Figure 4.15. (Top) Schematic drawing of the cantilever beam bending test, (Bottom) Digital image of the GO strip during the beam bending test.

When an end load **F** is applied to a flat beam of length **L**, width **w** and height **h**, it starts to bend while **L**, **w** and **F** are constant (Figure 4.15). The height **h** is a variable and the bending moment **M** at the root of the beam is given by:

$$M = FL \quad (3)$$

The second moment of area (**I**) is given by:

$$I = \frac{wh^3}{12} \quad (4)$$

The deflection of the end point of the beam when a simple bending happens is:

$$\delta = \frac{FL^3}{3EI} \quad (5)$$

Therefore from substituting eq. 4 to 5, the deflection is:

$$\delta = \frac{4FL^3}{Ewh^3} \quad (6)$$

in which **E** is the Young modulus of the material.

In the tests that were performed on the GO and GO/HA films, force and deflection were recorded by the MicroSquisher instrument. Length and width of the strips were measured with a vernier caliper and the thickness of the films (**h**) was measured by SEM characterization. The thickness of the GO film is about 26.23 µm and the GO/HA hybrid film is about 8.58 µm thick. Using these data, the average value of the Young's modulus for the GO and GO/HA free-standing films are 0.985 GPa and 251.82 GPa respectively.

As it can be seen in Figure 4.16, the Young's modulus of the GO thin film is close to polymeric materials and for the GO/HA layered hybrids is above metals and close to dense sintered ceramics considering the fact that GO/HA is still flexible. The GO-HA hybrid is clearly far above the composite materials. Therefore we can conclude that the nacre-like layered structure of the GO-HA hybrids resulted to a huge improvement in the mechanical properties.
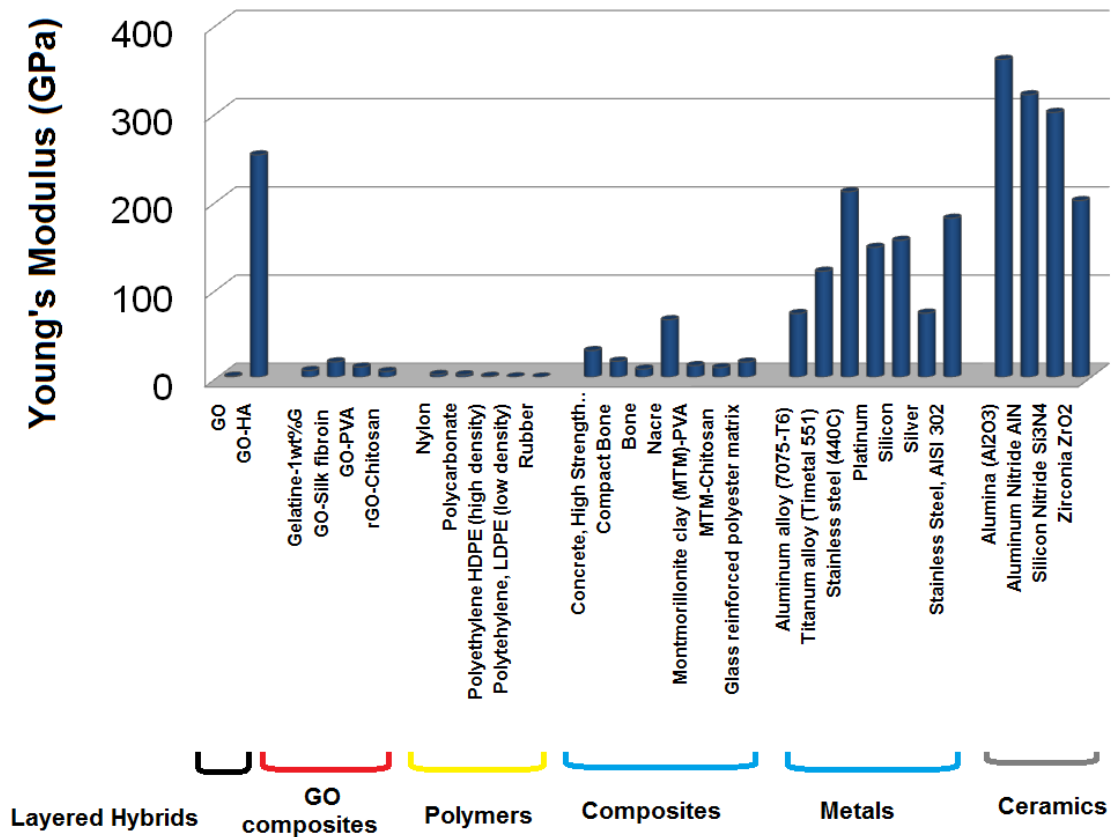
Figure 4.16. Young's modulus comparison of different category of materials with GO and GO/HA layered hybrid materials.

In other words, the bio-inspired nacre-like layered hybrids fabricated and introduced in this thesis, not only can be made in various structures and phases but also their shape, morphology and mechanical properties can be affected with such ordered design. Therefore highly mechanically improved hybrids can be made and depending on their inorganic phase they can be beneficial in different applications such as energy storage and optoelectronics.

CHAPTER 5. Summary and Future Work

5.1. Summary

Manipulating the structure and properties of materials at nano scale has brought important advances to almost all aspects of modern technologies including medicine, electronics, aerospace, transportation and communication. The new materials and designs resulted from nanotechnology, from efficient diagnostic and treatment ways in medicine to more light-weight and fast-processing laptops and cellphones, are continually improving our quality of life. Material scientists around the world are therefore the modern gods/goddesses who "magically" make the modern human's wishes come true by manipulating the structure and properties of the materials.

Nanotechnology offers new approaches to develop bio-inspired materials mimicing natural mechanisms. Hybrid structures are extensively been used by natural systems to not only reinforce mechanically the whole complex system but also implement multi-functionality. For example bones in the endoskeleton of vertebrates tolerate the forces applied by body weight and at the same time produce the red and white blood cells and store minerals. It's basically a hybrid structure composed of organic and inorganic materials (i.e. mineralized bone tissues and living cells). Another example is mollusks nacre. It's a layered hybrid structure of mineralized inorganic platelets and organic inter-layers. The layered structure not only supports the mollusks against the external forces and attacks, but also makes the smooth inner surface for binding the soft tissue to the outer shell. From the technological point of view, the hybrid structures are new classes of 3D functional materials with potential applications in various fields.

In this thesis, synthetic processes have been proposed to fabricate 3D hybrid structures composed of CNT or GO and various types of inorganic nanostrcutures. In chapter 1, the literature data have been assessed on the synthetic and design strategies of fabricating 3D structures of CNT and GO materials. CVD method was discussed as a relevant technique for the catalytic synthesis of aligned CNTs with high yield. Photolitography was mentioned as a tool to design the shape and pattern of the catalysts on the substrate and therefore influence the growth and spatial configuration of the obtained aligned CNTs in CVD method. Capillary condensation and bending of the aligned CNTs is also a useful tool to affect the final 3D shape of the structure for making features which are unattainable in regular microfabrication processes. Graphene and GO were also discussed as interesting materials in lots of industrial applications such as electronics, energy storage and catalytic applications. GO has attracted a lot of attentions since it can be chemically functionalized and be utilized as an organic material in fabricating novel hybrid materials.

Chapter 2 devotes to the patterned synthesis of ZnO nanostructures using a microwave assisted chemical approach. The flower-like ZnO nanostructures coated the area between the electrodes on a device making bridges between the Pt electrodes for electron transport. Under UV light and green light, the ZnO bridges show Schottkey barrier behavior.

Chapter 3 discusses the fabrication of 3D mesoporous structures of CNT/Inorganic hybrids using a chemical microwave-synthesis approach. Various aligned CNT shapes were made though initial photolithographical catalyst patterning and later CNT growth via CVD method. In nanoscale, the obtained aligned CNT patterns are like a bundle of free-standing vertical carbon nanotubes which have huge surface area to be covered with inorganic materials (for instance here the synthesis of CNT/ZnO, CNT/MnO$_2$ and CNT/Co$_3$O$_4$ were shown). Such

78

CNT bundles can be used as capacitors and current collectors in an electrochemical process. While coated with inorganic materials, they are shown to persist high capacitance with fast charge/discharge cycles. The energy storage application is just an example for this new type of 3D hybrids. Depending on the inorganic phase, the application could be different. Also various designs can be made by photolithography to further lead to the achievement of complicated 3D devices.

Chapter 4 discusses a bio-inspired nacre-like 3D hybrid material that is composed of layered hybrid constituents. The layered materials have been made previously using a freeze-casting technique. However in this study a direct bottom up process was introduced for in-situ synthesis of GO/Inorganic 3D free-standing hybrid films. The approach is based on making the layered template with a GO film and then in-situ synthesis of inorganic material in between and on the surface of the layers. Therefore a sequential order of GO/Inorganic phases is obtained. The process was shown to be effective for in-situ synthesis of metal oxides (e.g. ZnO, Fe_3O_4), metals (e.g. Ag) and ceramics (e.g. hydroxyapatite). Inspired by the nacre structure, this type of hybrid structures are designed to enhance mechanical properties. It has been shown that the obtained GO/HA has a high Young's modulus compared to different categories of materials (e.g. metals, composites,…). The same as CNT/Inorganic hybrids, the inorganic constitutes in the GO/Inorganic free-standing hybrid films largely define the overall properties and final application of the hybrids. Our approach offers the flexibility to select from a remarkably wide range of inorganic constitutes best fitting targeted applications.

5.2. Future Work

Generally, there are a lot of ways that can be taken to further research on the CNT/Inorganic and GO/Inorganic hybrid structures. Different synthesis conditions can be tested to affect the morphology of the inorganic constituents that later influence the properties of the hybrid. For example inorganic nanowires and nanotubes can be grown on the aligned CNTs or between the GO layers. Some of the examples that can lead to potential breakthroughs in developing hybrid structures are discussed as following.

5.2.1. Free-standing CNT/Inorganic Thin Films

The CNT/Inorganic hybrids which were fabricated and shown in this thesis were placed on hard Si/SiO_2 substrates. In order to integrate these hybrid structures in flexible electronic and optoelectronic devices, one should be able to transfer them on soft polymeric substrates (33,143,144). This is possible by simple taping or by stamping the structures on a polymeric substrate. Another approach is embedding the surface of the hybrid in a polymer matrix.
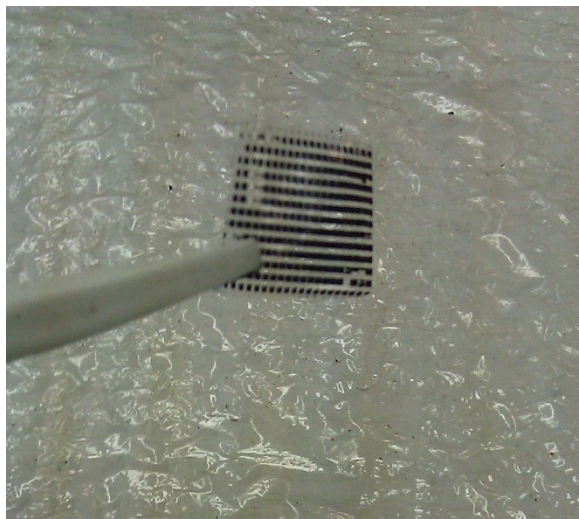
Figure 5.1. CNT/Co_3O_4 hybrid strips transferred on flexible PMMA substrate.

Figure 5.1 exhibits the transferred CNT/Co_3O_4 on PMMA. The transfer was performed by spin coating PMMA solution on the as-synthesized hybrid and later cures the polymer and detaches it in an HF environment. However this process needs to be developed in order to maintain the phase and composition of CNTs and inorganic phase.

5.2.2. 3D Metallic Porous Thin Films

Porous metallic thin films are very useful in light-weight applications, in tissue engineering where the porous structure is needed for tissue growth inside the pores and in catalysis (145,146). Using the approaches described in this thesis, metals can be deposited on various 3D CNT architectures or on GO thin films and later by removal of the carbon constituent, the porous metallic thin film remains (for instance refer to chapter 4 for porous Ag thin films).

5.2.3. Magnetically oriented GO/Inorganic Hybrid Structures

Inspired from the various mineral configurations in the endo- and exoskeletons (5), research can be performed on mimicking such 3D orientations using CNT and GO as templates. For instance the GO flakes in the solution are firstly coated with magnetite nanoparticles so they can be oriented and patterned using regular magnets. Then the flakes are coated again with hydroxyapatite nanoparticles. The whole system can still be manipulated with magnets to construct the desired orientation. To make such biomimetic complex structures, freeze casting has been used recently and magnetic particles were added to the slurry for controlling the

orientation at micro scale during freezing (133). The approach suggested here can be applied as an in-situ process to make CNT or GO/Inorganic hybrids with different orientations using magnetic field.

Letters of Copyright Permission

1- NATURE PUBLISHING GROUP LICENSE

TERMS AND CONDITIONS, Aug 14, 2013

This is a License Agreement between Mahyar Mazloumi ("You") and Nature Publishing Group ("Nature Publishing Group") provided by Copyright Clearance Center ("CCC"). The license consists of your order details, the terms and conditions provided by Nature Publishing Group, and the payment terms and conditions.

All payments must be made in full to CCC. For payment instructions, please see information listed at the bottom of this form.

License Number: 3207830178057

License date: Aug 14, 2013

Licensed content publisher: Nature Publishing Group

Licensed content publication: Nature

Licensed content title: Helical microtubules of graphitic carbon

Licensed content author: Sumio Iijima

Licensed content date: Nov 7, 1991

Volume number: 354

Issue number: 6348

Type of Use: reuse in a thesis/dissertation

Requestor type: academic/educational

Format: print and electronic

Portion: figures/tables/illustrations

Number of figures/tables/illustrations: 1

Figures: Figure 1

Author of this NPG article: no

Title of your thesis/dissertation: Fabrication of 3D Hybrid Architectures Composed of sp^2-Carbon and Inorganic Materials

Expected completion date: Sep 2013

Estimated size (number of pages): 100

Total 0.00 USD

2- TERMS AND CONDITIONS, Aug 14, 2013

This is a License Agreement between Mahyar Mazloumi ("You") and Springer ("Springer") provided by Copyright Clearance Center ("CCC"). The license consists of your order details, the terms and conditions provided by Springer, and the payment terms and conditions. All payments must be made in full to CCC. For payment instructions, please see information listed at the bottom of this form.

License Number: 3207830339927

License date: Aug 14, 2013

Licensed content publisher: Springer

Licensed content publication: Springer eBook

Licensed content title: Introduction to Carbon Materials Research

Licensed content author: Mildred S. Dresselhaus

Licensed content date: Jan 1, 2001

Type of Use: Thesis/Dissertation

Portion: Figures

Author of this Springer article: No

Title of your thesis/dissertation: Fabrication of 3D Hybrid Architectures Composed of sp^2-Carbon and Inorganic Materials

Expected completion date: Sep 2013

Estimated size (pages): 100

Total 0.00 CAD

3- ELSEVIER LICENSE TERMS AND CONDITIONS, Aug 14, 2013

This is a License Agreement between Mahyar Mazloumi ("You") and Elsevier ("Elsevier") provided by Copyright Clearance Center ("CCC"). The license consists of your order details, the terms and conditions provided by Elsevier, and the payment terms and conditions. All payments must be made in full to CCC. For payment instructions, please see information listed at the bottom of this form.

Supplier: Elsevier Limited, The Boulevard, Langford Lane, Kidlington,Oxford,OX5 1GB,UK

Registered Company

Number: 1982084

Customer name: Mahyar Mazloumi

Customer address: Apt. 1213, 50 Mooregate Cres, Kitchener, ON N2M 5G6

License number: 3207850581889

License date: Aug 14, 2013

Licensed content publisher: Elsevier

Licensed content publication: Carbon

Licensed content title: Effect of catalyst pattern geometry on the growth of vertically aligned carbon nanotube arrays

Licensed content author: Goo-Hwan Jeong, Niklas Olofsson, Lena K.L. Falk, Eleanor E.B. Campbell

Licensed content date: March 2009

Licensed content volume number: 47

Licensed content issue number: 3

Number of pages: 9

Start Page: 696

End Page: 704

Type of Use: reuse in a thesis/dissertation

Intended publisher of new work: other

Portion: figures/tables/illustrations

Number of figures/tables/illustrations: 2

Format: both print and electronic

Are you the author of this Elsevier article?: No

Will you be translating?: No

Title of your thesis/dissertation: Fabrication of 3D Hybrid Architectures Composed of sp^2-Carbon and Inorganic Materials

Expected completion date: Sep 2013

Estimated size (number of pages): 100

Elsevier VAT number: GB 494 6272 12

Permissions price: 0.00 USD

VAT/Local Sales Tax: 0.0 USD / 0.0 GBP

Total: 0.00 US

4- AIP PUBLISHING LLC LICENSE TERMS AND CONDITIONS, Aug 14, 2013

All payments must be made in full to CCC. For payment instructions, please see information listed at the bottom of this form.

License Number: 3207841091117

Order Date: Aug 14, 2013

Publisher: AIP Publishing LLC

Publication: Applied Physics Letters

Article Title: Effect of catalyst film thickness on carbon nanotube growth by selective area chemical vapor deposition

Author: Y. Y. Wei, Gyula Eres, V. I. Merkulov, D. H. Lowndes et al.

Online Publication Date: Mar 5, 2001

Volume number: 78

Issue number: 10

Type of Use: Thesis/Dissertation

Requestor type: Student

Format: Print and electronic

Portion: Figure/Table

Number of figures/tables: 1

Title of your thesis/dissertation: Fabrication of 3D Hybrid Architectures Composed of sp^2-Carbon and Inorganic Materials

Expected completion date: Sep 2013

Estimated size (number of pages): 100

Total: 0.00 USD

Terms and Conditions

AIP Publishing LLC -- Terms and Conditions: Permissions Uses

AIP Publishing LLC ("AIPP"") hereby grants to you the non-exclusive right and license to use and/or distribute the Material according to the use specified in your order, on a one-time basis, for the specified term, with a maximum distribution equal to the number that you have ordered. Any links or other content accompanying the Material are not the subject of this license.

5- ELSEVIER LICENSE TERMS AND CONDITIONS, Aug 14, 2013

This is a License Agreement between Mahyar Mazloumi ("You") and Elsevier ("Elsevier") provided by Copyright Clearance Center ("CCC"). The license consists of your order details, the terms and conditions provided by Elsevier, and the payment terms and conditions. All payments must be made in full to CCC. For payment instructions, please see information listed at the bottom of this form.

Supplier: Elsevier Limited, The Boulevard, Langford Lane Kidlington, Oxford, OX5 1GB, UK

Registered Company

Number: 1982084

Customer name: Mahyar Mazloumi

Customer address: Apt. 1213, 50 Mooregate Cres, Kitchener, ON N2M 5G6

License number: 3207851389293

License date: Aug 14, 2013

Permissions price: 0.00 USD

VAT/Local Sales Tax: 0.0 USD / 0.0 GBP

Total: 0.00 USD

6- Nanotechnology

ISSN: 0957-4484

Publication year(s):1990 - present

Publication type: Journal

Publisher: IOP Publishing

Language: English

Country of publication: United Kingdom of Great Britain and Northern Ireland

Rights holder: IOP PUBLISHING, LTD

Covered by CCC Annual License - Academic

7- Title: Structurally Programmed Capillary Folding of Carbon Nanotube Assemblies

Author: Sameh Tawfick, Michael De Volder, and A. John Hart

Publication: Langmuir

Publisher: American Chemical Society

Date: May 1, 2011

PERMISSION/LICENSE IS GRANTED FOR YOUR ORDER AT NO CHARGE

This type of permission/license, instead of the standard Terms & Conditions, is sent to you because no fee is being charged for your order. Please note the following:

Permission is granted for your request in both print and electronic formats, and translations.

If figures and/or tables were requested, they may be adapted or used in part.

Please print this page for your records and send a copy of it to your publisher/graduate school.

Appropriate credit for the requested material should be given as follows: "Reprinted (adapted) with permission from (COMPLETE REFERENCE CITATION). Copyright (YEAR) American Chemical Society." Insert appropriate information in place of the capitalized words. One-time permission is granted only for the use specified in your request. No additional uses are granted (such as derivative works or other editions). For any other uses, please submit a new request.

8- JOHN WILEY AND SONS LICENSE TERMS AND CONDITIONS, Aug 14, 2013

This is a License Agreement between Mahyar Mazloumi ("You") and John Wiley and Sons ("John Wiley and Sons") provided by Copyright Clearance Center ("CCC"). The license consists of your order details, the terms and conditions provided by John Wiley and Sons, and the payment terms and conditions.

All payments must be made in full to CCC. For payment instructions, please see information listed at the bottom of this form.

License Number: 3207870927154

License date: Aug 14, 2013

Licensed content publisher: John Wiley and Sons

Licensed content publication: Advanced Materials

Licensed content title: Diverse 3D Microarchitectures Made by Capillary Forming of Carbon Nanotubes

Licensed copyright line Copyright © 2010 WILEY-VCH Verlag GmbH & Co. KGaA, Weinheim

Licensed content author: Michael De Volder, Sameh H. Tawfick, Sei Jin Park, Davor Copic, Zhouzhou Zhao, Wei Lu, A. John Hart

Licensed content date: Sep 2, 2010

Start page: 4384

End page: 4389

Type of use: Dissertation/Thesis

Requestor type: University/Academic

Format: Print and electronic

Portion: Figure/table

Number of figures/tables: 1

Original Wiley figure/table number(s): Figure 1c

Will you be translating?: No

Total 0.00 USD

9- Title: Corrugated Carbon Nanotube Microstructures with Geometrically Tunable Compliance

Author: Michaël F. L. De Volder, Sameh Tawfick, Sei Jin Park, and A. John Hart

Publication: ACS Nano

Publisher: American Chemical Society

Date: Sep 1, 2011

PERMISSION/LICENSE IS GRANTED FOR YOUR ORDER AT NO CHARGE

This type of permission/license, instead of the standard Terms & Conditions, is sent to you because no fee is being charged for your order. Please note the following:

Permission is granted for your request in both print and electronic formats, and translations.

If figures and/or tables were requested, they may be adapted or used in part.

Please print this page for your records and send a copy of it to your publisher/graduate school.

Appropriate credit for the requested material should be given as follows: "Reprinted (adapted) with permission from (COMPLETE REFERENCE CITATION). Copyright (YEAR) American Chemical Society." Insert appropriate information in place of the capitalized words. One-time permission is granted only for the use specified in your request. No additional uses are granted (such as derivative works or other editions). For any other uses, please submit a new request.

10- NATURE PUBLISHING GROUP LICENSE TERMS AND CONDITIONS, Aug 14, 2013

This is a License Agreement between Mahyar Mazloumi ("You") and Nature Publishing Group ("Nature Publishing Group") provided by Copyright Clearance Center ("CCC"). The license consists of your order details, the terms and conditions provided by Nature Publishing Group, and the payment terms and conditions.

All payments must be made in full to CCC. For payment instructions, please see information listed at the bottom of this form.

License Number: 3207981502530

License date: Aug 14, 2013

Licensed content publisher: Nature Publishing Group

Licensed content publication: Nature

Licensed content title: Preparation and characterization of graphene oxide paper

Licensed content author: Dmitriy A. Dikin, Sasha Stankovich, Eric J. Zimney, Richard D. Piner, Geoffrey H. B. Dommett et al.

Licensed content date: Jul 26, 2007

Volume number: 448

Issue number: 7152

Type of Use: reuse in a thesis/dissertation

Requestor type: academic/educational

Format: print and electronic

Portion: figures/tables/illustrations

Number of figures/tables/illustrations: 1

High-res required: no

Figures: Figure 1

Author of this NPG article: no

Title of your thesis/dissertation: Fabrication of 3D Hybrid Architectures Composed of sp^2-Carbon and Inorganic Materials

Expected completion date: Sep 2013

Estimated size (number of pages): 100

Total: 0.00 USD

11- Title: Fabrication of optical device arrays using patterned growth of ZnO nanostructures

Author: Mazloumi, M.; Mandal, H.S.; Xiaowu Tang

Publication: Nanotechnology, IEEE Transactions on

Publisher: IEEE

Date: May 2012

Thesis / Dissertation Reuse

The IEEE does not require individuals working on a thesis to obtain a formal reuse license, however, you may print out this statement to be used as a permission grant:

Requirements to be followed when using any portion (e.g., figure, graph, table, or textual material) of an IEEE copyrighted paper in a thesis:

1) In the case of textual material (e.g., using short quotes or referring to the work within these papers) users must give full credit to the original source (author, paper, publication) followed by the IEEE copyright line © 2011 IEEE.

2) In the case of illustrations or tabular material, we require that the copyright line © [Year of original publication] IEEE appear prominently with each reprinted figure and/or table.

3) If a substantial portion of the original paper is to be used, and if you are not the senior author, also obtain the senior author's approval.

Requirements to be followed when using an entire IEEE copyrighted paper in a thesis:

1) The following IEEE copyright/ credit notice should be placed prominently in the references: © [year of original publication] IEEE. Reprinted, with permission, from [author names, paper title, IEEE publication title, and month/year of publication]

2) Only the accepted version of an IEEE copyrighted paper can be used when posting the paper or your thesis on-line.

3) In placing the thesis on the author's university website, please display the following message in a prominent place on the website: In reference to IEEE copyrighted material which is used with permission in this thesis, the IEEE does not endorse any of [university/educational entity's name goes here]'s products or services. Internal or personal use of this material is permitted. If interested in reprinting/republishing IEEE copyrighted material for advertising or promotional purposes or for creating new collective works for resale or redistribution, please go to

http://www.ieee.org/publications_standards/publications/rights/rights_link.html to learn how to obtain a License from RightsLink.

12- Title: Fabrication of Three- Dimensional Carbon Nanotube and Metal Oxide Hybrid Mesoporous Architectures

Author: Mahyar Mazloumi, Samaneh Shadmehr, Yverick Rangom, Linda F. Nazar, and Xiaowu (Shirley) Tang

Publication: ACS Nano

Publisher: American Chemical Society

Date: May 1, 2013

PERMISSION/LICENSE IS GRANTED FOR YOUR ORDER AT NO CHARGE

References

1.   Bhushan B, editor. Springer Handbook of Nanotechnology. Berlin, Heidelberg: Springer Berlin Heidelberg; 2004.

2.   Sun D-M, Liu C, Ren W-C, Cheng H-M. A review of carbon nanotube- and graphene-based flexible thin-film transistors. Small. 2013 Apr 22;9(8):1188–205.

3.   Eder D. Carbon nanotube-inorganic hybrids. Chem. Rev. [Internet]. 2010 Mar 10;110(3):1348–85. Available from: http://www.ncbi.nlm.nih.gov/pubmed/20108978

4.   Zhou D, Cui Y, Han B. Graphene-based hybrid materials and their applications in energy storage and conversion. Chinese Sci. Bull. [Internet]. 2012 Aug 4 [cited 2013 Jun 10];57(23):2983–94. Available from: http://link.springer.com/10.1007/s11434-012-5314-9

5.   Meyers MA, McKittrick J, Chen P-Y. Structural biological materials: critical mechanics-materials connections. Science [Internet]. 2013 Feb 15 [cited 2013 May 22];339(6121):773–9. Available from: http://www.ncbi.nlm.nih.gov/pubmed/23413348

6.   Munch E, Launey ME, Alsem DH, Saiz E, Tomsia a P, Ritchie RO. Tough, bio-inspired hybrid materials. Science [Internet]. 2008 Dec 5;322(5907):1516–20. Available from: http://www.ncbi.nlm.nih.gov/pubmed/19056979

7.   Cheng H, Dong Z, Hu C, Zhao Y, Hu Y, Qu L, et al. Textile electrodes woven by carbon nanotube-graphene hybrid fibers for flexible electrochemical capacitors. Nanoscale

[Internet]. 2013 Apr 21 [cited 2013 Jun 10];5(8):3428–34. Available from: http://www.ncbi.nlm.nih.gov/pubmed/23475309

8.   Mohana Reddy AL, Gowda SR, Shaijumon MM, Ajayan PM. Hybrid nanostructures for energy storage applications. Adv. Mater. [Internet]. 2012 Sep 25 [cited 2013 Feb 15];24(37):5045–64. Available from: http://www.ncbi.nlm.nih.gov/pubmed/22740354

9.   Wu C, Huang X, Wu X, Xie L, Yang K, Jiang P. Graphene oxide-encapsulated carbon nanotube hybrids for high dielectric performance nanocomposites with enhanced energy storage density. Nanoscale [Internet]. 2013 May 7 [cited 2013 Jun 10];5(9):3847–55. Available from: http://www.ncbi.nlm.nih.gov/pubmed/23525168

10.   Wang H, Liang Y, Mirfakhrai T, Chen Z, Casalongue HS, Dai H. Advanced asymmetrical supercapacitors based on graphene hybrid materials. Nano Res. [Internet]. 2011 Apr 12 [cited 2013 Feb 25];4(8):729–36. Available from: http://www.springerlink.com/index/10.1007/s12274-011-0129-6

11.   Joselevich E, Dai H, Liu J, Hata K, Windle AH. Carbon Nanotube Synthesis and Organization. Top. Appl. Phys. 2008;111:101–64.

12.   Yamada T, Namai T, Hata K, Futaba DN, Mizuno K, Fan J, et al. Size-selective growth of double-walled carbon nanotube forests from engineered iron catalysts. Nat. Nanotechnol. [Internet]. 2006 Nov [cited 2013 Feb 13];1(2):131–6. Available from: http://www.ncbi.nlm.nih.gov/pubmed/18654165

13. Futaba D, Hata K, Yamada T, Mizuno K, Yumura M, Iijima S. Kinetics of Water-Assisted Single-Walled Carbon Nanotube Synthesis Revealed by a Time-Evolution Analysis. Phys. Rev. Lett. [Internet]. 2005 Jul [cited 2013 Feb 25];95(5):056104. Available from: http://link.aps.org/doi/10.1103/PhysRevLett.95.056104

14. Yun Y, Shanov V, Tu Y, Subramaniam S, Schulz MJ. Growth mechanism of long aligned multiwall carbon nanotube arrays by water-assisted chemical vapor deposition. J. Phys. Chem. B [Internet]. 2006 Nov 30 [cited 2013 Feb 25];110(47):23920–5. Available from: http://www.ncbi.nlm.nih.gov/pubmed/17125359

15. Belin T, Epron F. Characterization methods of carbon nanotubes: a review. Mater. Sci. Eng. B [Internet]. 2005 May [cited 2013 Feb 11];119(2):105–18. Available from: http://linkinghub.elsevier.com/retrieve/pii/S0921510705001315

16. Iijima S. Helical microtubules of graphitic carbon. Nature. 1991;354:56–8.

17. Dresselhaus MS, Avouris P. Introduction to Carbon Materials Research. Top. Appl. Phys. 2001. p. 1–9.

18. Avouris P, Chen Z, Perebeinos V. Carbon-based electronics. Nat. Nanotechnol. [Internet]. 2007 Oct;2(10):605–15. Available from: http://www.ncbi.nlm.nih.gov/pubmed/18654384

19. Journet C, Maser WK, Bernier P, Loiseau A. Large-scale production of single-walled carbon nanotubes by the electric-arc technique. Nature. 1997;388(August):756–8.

20. Journet C, Bernier P. Production of carbon nanotubes. Appl. Phys. A Mater. Sci. Process. [Internet]. 1998 Jul 1;67(1):1–9. Available from: http://link.springer.com/10.1007/s003390050731

21. Lamura G, Andreone A, Yang Y, Barbara P, Vigolo B, He C, et al. High-Crystalline Single- and Double-Walled Carbon Nanotube Mats Grown by Chemical Vapor Deposition. J. Phys. Chem. C. 2007;111:15154–9.

22. Zhong X-H, Li Y-L, Feng J-M, Kang Y-R, Han S-S. Fabrication of a multifunctional carbon nanotube "cotton" yarn by the direct chemical vapor deposition spinning process. Nanoscale [Internet]. 2012 Sep 21 [cited 2013 Jun 27];4(18):5614–8. Available from: http://www.ncbi.nlm.nih.gov/pubmed/22864939

23. Hart AJ, Slocum AH. Rapid growth and flow-mediated nucleation of millimeter-scale aligned carbon nanotube structures from a thin-film catalyst. J. Phys. Chem. B [Internet]. 2006 Apr 27 [cited 2013 Feb 13];110(16):8250–7. Available from: http://www.ncbi.nlm.nih.gov/pubmed/16623503

24. Huang S, Cai X, Liu J. Growth of millimeter-long and horizontally aligned single-walled carbon nanotubes on flat substrates. J. Am. Chem. Soc. [Internet]. 2003 May 14;125(19):5636–7. Available from: http://www.ncbi.nlm.nih.gov/pubmed/12733894

25. Jeong G-H, Olofsson N, Falk LKL, Campbell EEB. Effect of catalyst pattern geometry on the growth of vertically aligned carbon nanotube arrays. Carbon N. Y. [Internet]. Elsevier

Ltd; 2009 Mar [cited 2013 Feb 25];47(3):696–704. Available from: http://linkinghub.elsevier.com/retrieve/pii/S0008622308005952

26.   Meyyappan M. A review of plasma enhanced chemical vapour deposition of carbon nanotubes. J. Phys. D. Appl. Phys. [Internet]. 2009 Nov 7 [cited 2013 May 28];42(21):213001. Available from: http://stacks.iop.org/0022-3727/42/i=21/a=213001?key=crossref.1d8bf93e98ecbab5eb978c3028d6749f

27.   Hata K, Futaba DN, Mizuno K, Namai T, Yumura M, Iijima S. Water-assisted highly efficient synthesis of impurity-free single-walled carbon nanotubes. Science [Internet]. 2004 Nov 19 [cited 2013 May 21];306(5700):1362–4. Available from: http://www.ncbi.nlm.nih.gov/pubmed/15550668

28.   Wei YY, Eres G, Merkulov VI, Lowndes DH. Effect of catalyst film thickness on carbon nanotube growth by selective area chemical vapor deposition. Appl. Phys. Lett. [Internet]. 2001 [cited 2013 Jun 28];78(10):1394. Available from: http://link.aip.org/link/APPLAB/v78/i10/p1394/s1&Agg=doi

29.   Amama PB, Pint CL, Kim SM, McJilton L, Eyink KG, Stach E a, et al. Influence of alumina type on the evolution and activity of alumina-supported Fe catalysts in single-walled carbon nanotube carpet growth. ACS Nano [Internet]. 2010 Feb 23;4(2):895–904. Available from: http://www.ncbi.nlm.nih.gov/pubmed/20131855

30.   Zhang C, Pisana S, Wirth CT, Parvez a., Ducati C, Hofmann S, et al. Growth of aligned millimeter-long carbon nanotube by chemical vapor deposition. Diam. Relat. Mater.

[Internet]. 2008 Jul [cited 2013 Feb 25];17(7-10):1447–51. Available from: http://linkinghub.elsevier.com/retrieve/pii/S0925963508001544

31.   Wu T-C, Chang S-H. Temperature enhanced growth of ultralong multi-walled carbon nanotubes forest. Curr. Appl. Phys. [Internet]. Elsevier B.V.; 2009 Sep [cited 2013 Feb 25];9(5):1117–21.   Available   from: http://linkinghub.elsevier.com/retrieve/pii/S1567173908002927

32.   Zhu Y, Lim X, Sim MC, Lim CT, Sow CH. Versatile transfer of aligned carbon nanotubes with polydimethylsiloxane as the intermediate. Nanotechnology [Internet]. 2008 Aug 13 [cited   2013   Feb   25];19(32):325304.   Available   from: http://www.ncbi.nlm.nih.gov/pubmed/21828811

33.   Tsai TY, Lee CY, Tai NH, Tuan WH. Transfer of patterned vertically aligned carbon nanotubes onto plastic substrates for flexible electronics and field emission devices. Appl. Phys. Lett. [Internet]. 2009 [cited 2013 Feb 25];95(1):013107. Available from: http://link.aip.org/link/APPLAB/v95/i1/p013107/s1&Agg=doi

34.   Sunden E, Moon JK, Wong CP, King WP, Graham S. Microwave assisted patterning of vertically aligned carbon nanotubes onto polymer substrates. J. Vac. Sci. Technol. B Microelectron. Nanom. Struct. [Internet]. 2006 [cited 2013 Feb 25];24(4):1947. Available from: http://link.aip.org/link/JVTBD9/v24/i4/p1947/s1&Agg=doi

35.   Chakrapani N, Wei B, Carrillo A, Ajayan PM, Kane RS. Capillarity-driven assembly of two-dimensional cellular carbon nanotube foams. Proc. Natl. Acad. Sci. U. S. A.

[Internet]. 2004 Mar 23;101(12):4009–12. Available from: http://www.pubmedcentral.nih.gov/articlerender.fcgi?artid=384686&tool=pmcentrez&rendertype=abstract

36. Futaba DN, Hata K, Yamada T, Hiraoka T, Hayamizu Y, Kakudate Y, et al. Shape-engineerable and highly densely packed single-walled carbon nanotubes and their application as super-capacitor electrodes. Nat. Mater. [Internet]. 2006 Dec [cited 2013 Feb 10];5(12):987–94. Available from: http://www.ncbi.nlm.nih.gov/pubmed/17128258

37. De Volder MFL, Park SJ, Tawfick SH, Vidaud DO, Hart a J. Fabrication and electrical integration of robust carbon nanotube micropillars by self-directed elastocapillary densification. J. Micromechanics Microengineering [Internet]. 2011 Apr 1;21(4):045033. Available from: http://stacks.iop.org/0960-1317/21/i=4/a=045033?key=crossref.6cde12036c8d45c8d171c9e07dcd3b9b

38. Tawfick S, De Volder M, Hart a J. Structurally programmed capillary folding of carbon nanotube assemblies. Langmuir [Internet]. 2011 May 17;27(10):6389–94. Available from: http://www.ncbi.nlm.nih.gov/pubmed/21504164

39. De Volder M, Tawfick SH, Park SJ, Copic D, Zhao Z, Lu W, et al. Diverse 3D microarchitectures made by capillary forming of carbon nanotubes. Adv. Mater. [Internet]. 2010 Oct 15 [cited 2013 Feb 4];22(39):4384–9. Available from: http://www.ncbi.nlm.nih.gov/pubmed/20814919

40. De Volder MFL, Tawfick S, Park SJ, Hart a J. Corrugated carbon nanotube microstructures with geometrically tunable compliance. ACS Nano [Internet]. 2011 Sep 27;5(9):7310–7. Available from: http://www.ncbi.nlm.nih.gov/pubmed/21800907

41. Geim AK, Novoselov KS. The rise of graphene. Nat. Mater. [Internet]. Nature Publishing Group; 2007;6(3):183–91. Available from: http://www.ncbi.nlm.nih.gov/pubmed/17330084

42. Novoselov KS, Geim a K, Morozov S V, Jiang D, Zhang Y, Dubonos S V, et al. Electric field effect in atomically thin carbon films. Science [Internet]. 2004 Oct 22 [cited 2013 May 21];306(5696):666–9. Available from: http://www.ncbi.nlm.nih.gov/pubmed/15499015

43. Zhu Y, Murali S, Cai W, Li X, Suk JW, Potts JR, et al. Graphene and graphene oxide: synthesis, properties, and applications. Adv. Mater. [Internet]. 2010 Sep 15 [cited 2013 Feb 13];22(35):3906–24. Available from: http://www.ncbi.nlm.nih.gov/pubmed/20706983

44. Li X, Cai W, Jung I, An J, Yang D, Velamakanni A, et al. Synthesis, Characterization, and Properties of Large-Area Graphene Films. ECS Trans. 2009;19(5):41–52.

45. Jayasena B, Subbiah S. A novel mechanical cleavage method for synthesizing few-layer graphenes. Nanoscale Res. Lett. [Internet]. Springer Open Ltd; 2011 Jan [cited 2013 Jul 8];6(1):95. Available from: http://www.pubmedcentral.nih.gov/articlerender.fcgi?artid=3212245&tool=pmcentrez&rendertype=abstract

46. Li D, Kaner RB. Materials science. Graphene-based materials. Science [Internet]. 2008 May 30 [cited 2013 May 30];320(5880):1170–1. Available from: http://www.ncbi.nlm.nih.gov/pubmed/18511678

47. Kelly KF, Billups WE. Synthesis of soluble graphite and graphene. Acc. Chem. Res. [Internet]. 2013 Jan 15;46(1):4–13. Available from: http://www.ncbi.nlm.nih.gov/pubmed/23116420

48. Park S, Ruoff RS. Chemical methods for the production of graphenes. Nat. Nanotechnol. [Internet]. 2009 Apr [cited 2013 May 21];4(4):217–24. Available from: http://www.ncbi.nlm.nih.gov/pubmed/19350030

49. Chen C-M, Huang J-Q, Zhang Q, Gong W-Z, Yang Q-H, Wang M-Z, et al. Annealing a graphene oxide film to produce a free standing high conductive graphene film. Carbon N. Y. [Internet]. Elsevier Ltd; 2012 Feb [cited 2013 May 23];50(2):659–67. Available from: http://linkinghub.elsevier.com/retrieve/pii/S0008622311007639

50. Dikin D a, Stankovich S, Zimney EJ, Piner RD, Dommett GHB, Evmenenko G, et al. Preparation and characterization of graphene oxide paper. Nature [Internet]. 2007 Jul 26 [cited 2013 May 22];448(7152):457–60. Available from: http://www.ncbi.nlm.nih.gov/pubmed/17653188

51. Mazloumi M, Attarchi M, Lak A, Mohajerani MS, Kajbafvala A, Zanganeh S, et al. Boehmite nanopetals self assembled to form rosette-like nanostructures. Mater. Lett.

[Internet]. 2008 Oct [cited 2013 Jul 10];62(26):4184–6. Available from: http://linkinghub.elsevier.com/retrieve/pii/S0167577X08005417

52. Mazloumi M, Shahcheraghi N, Kajbafvala A, Zanganeh S, Lak A, Mohajerani MS, et al. 3D bundles of self-assembled lanthanum hydroxide nanorods via a rapid microwave-assisted route. J. Alloys Compd. [Internet]. 2009 Apr [cited 2013 Jul 10];473(1-2):283–7. Available from: http://linkinghub.elsevier.com/retrieve/pii/S0925838808008323

53. Mazloumi M, Zanganeh S, Kajbafvala A, Ghariniyat P, Taghavi S, Lak A, et al. Ultrasonic induced photoluminescence decay in sonochemically obtained cauliflower-like ZnO nanostructures with surface 1D nanoarrays. Ultrason. Sonochem. [Internet]. ELSEVIER SCIENCE BV; 2009;16(1):11–4. Available from: http://www.ncbi.nlm.nih.gov/pubmed/18603463

54. Arami H, Mazloumi M, Khalifehzadeh R, Lak A, Sadrnezhaad SK. Self-assembled dahlia-like cadmium hydrogen phosphate hydrate nanostructures as templates for cadmium hydroxyapatite hexagonal prisms. J. Cryst. Growth [Internet]. 2007 Nov [cited 2013 Jul 10];309(1):37–42. Available from: http://linkinghub.elsevier.com/retrieve/pii/S0022024807007427

55. Mohajerani MS, Mazloumi M, Lak A, Kajbafvala A, Zanganeh S, Sadrnezhaad SK. Self-assembled zinc oxide nanostructures via a rapid microwave-assisted route. J. Cryst. Growth [Internet]. 2008 Jul [cited 2013 Feb 25];310(15):3621–5. Available from: http://linkinghub.elsevier.com/retrieve/pii/S0022024808003436

56. Mazloumi M, Mandal HS, Tang XS. Fabrication of Optical Device Arrays Using Patterned Growth of ZnO Nanostructures. IEEE Trans. Nanotechnol. 2012;11(3):444 – 447. © 2012 IEEE. Reprinted, with permission, from Mazloumi M, Mandal HS, Tang XS, Fabrication of Optical Device Arrays Using Patterned Growth of ZnO Nanostructures, IEEE Trans. Nanotechnology, 2012.

57. Arami H, Mazloumi M, Khalifehzadeh R, Sadrnezhaad SK. Bundles of self-assembled boehmite nanostrips from a surfactant free hydrothermal route. J. Alloys Compd. [Internet]. 2008 Aug [cited 2013 Jul 10];461(1-2):551–4. Available from: http://linkinghub.elsevier.com/retrieve/pii/S0925838807015551

58. Lak A, Mazloumi M, Mohajerani M, Kajbafvala A, Zanganeh S, Arami H, et al. Self-Assembly of Dandelion-Like Hydroxyapatite Nanostructures Via Hydrothermal Method. J. Am. Ceram. Soc. [Internet]. 2008 Oct [cited 2013 Jul 10];91(10):3292–7. Available from: http://doi.wiley.com/10.1111/j.1551-2916.2008.02600.x

59. Arami H, Mazloumi M, Khalifehzadeh R, Sadrnezhaad SK. Surfactant free hydrothermal formation of Pb3O4 nanorods. J. Alloys Compd. [Internet]. 2008 Oct [cited 2013 Jul 10];466(1-2):323–5. Available from: http://linkinghub.elsevier.com/retrieve/pii/S0925838807021512

60. Lak A, Mazloumi M, Mohajerani MS, Zanganeh S, Shayegh MR, Kajbafvala A, et al. Rapid Formation of Mono-Dispersed Hydroxyapatite Nanorods with Narrow-Size Distribution via Microwave Irradiation. J. Am. Ceram. Soc. [Internet]. 2008;91(11):3580–

4.   Available   from: http://blackwell-synergy.com/doi/abs/10.1111/j.1551-2916.2008.02690.x

61.   Mazloumi M, Taghavi S, Arami H, Zanganeh S, Kajbafvala A, Shayegh MR, et al. Self-assembly of ZnO nanoparticles and subsequent formation of hollow microspheres. J. Alloys Compd. [Internet]. 2009 Jan [cited 2013 Feb 25];468(1-2):303–7. Available from: http://linkinghub.elsevier.com/retrieve/pii/S0925838807023870

62.   Kim Y-J, Lee C-H, Hong YJ, Yi G-C, Kim SS, Cheong H. Controlled selective growth of ZnO nanorod and microrod arrays on Si substrates by a wet chemical method. Appl. Phys. Lett. [Internet]. 2006 [cited 2013 Feb 25];89(16):163128. Available from: http://link.aip.org/link/APPLAB/v89/i16/p163128/s1&Agg=doi

63.   Law M, Greene LE, Johnson JC, Saykally R, Yang P. Nanowire dye-sensitized solar cells. Nat. Mater. [Internet]. 2005 Jun [cited 2013 Feb 11];4(6):455–9. Available from: http://www.ncbi.nlm.nih.gov/pubmed/15895100

64.   Yang K-Y, Yoon K-M, Choi K-W, Lee H. The direct nano-patterning of ZnO using nanoimprint lithography with ZnO-sol and thermal annealing. Microelectron. Eng. [Internet]. Elsevier B.V.; 2009 Nov [cited 2013 Feb 19];86(11):2228–31. Available from: http://linkinghub.elsevier.com/retrieve/pii/S0167931709002524

65.   Hu X, Masuda Y, Ohji T, Kato K. Micropatterning of ZnO nanoarrays by forced hydrolysis of anhydrous zinc acetate. Langmuir [Internet]. 2008 Jul 15;24(14):7614–7. Available from: http://www.ncbi.nlm.nih.gov/pubmed/18547075

66.   Liu C, Masuda Y, Li Z, Zhang Q, Li T. Site-Selective Growth of Highly Oriented ZnO Rod Arrays on Patterned Functionalized Si Substrates from Aqueous Solution. Cryst. Growth Des. [Internet]. 2009 May 6;9(5):2168–72. Available from: http://pubs.acs.org/doi/abs/10.1021/cg800810r

67.   Wang X, Zhu H, Wang Z, Yang F, Yang X. Spontaneously patterned ZnO nanoarrays. Chemistry [Internet]. 2009 Nov 2 [cited 2013 Feb 25];15(43):11473–7. Available from: http://www.ncbi.nlm.nih.gov/pubmed/19780124

68.   Zhang J. Control of ZnO Morphology via a Simple Solution Route. Chem. Mater. [Internet]. 2002 Oct;14(10):4172–7. Available from: http://pubs.acs.org/doi/abs/10.1021/cm020077h

69.   Fang X, Bando Y, Gautam UK, Zhai T, Zeng H, Xu X, et al. ZnO and ZnS Nanostructures: Ultraviolet-Light Emitters, Lasers, and Sensors [Internet]. Crit. Rev. Solid State Mater. Sci. 2009 [cited 2013 May 21]. p. 190–223. Available from: http://www.tandfonline.com/doi/abs/10.1080/10408430903245393

70.   Zhang H, Yang D, Ma X, Ji Y, Xu J, Que D. Synthesis of flower-like ZnO nanostructures by an organic-free hydrothermal process. Nanotechnology [Internet]. 2004 May 1 [cited 2013 Feb 25];15(5):622–6. Available from: http://stacks.iop.org/0957-4484/15/i=5/a=037?key=crossref.322aceea37e92f82f0e2bfa8c22bddb2

71.   Zhang H, Yang D, Ji Y, Ma X, Xu J, Que D. Low Temperature Synthesis of Flowerlike ZnO Nanostructures by Cetyltrimethylammonium Bromide-Assisted Hydrothermal

Process. J. Phys. Chem. B [Internet]. 2004 Apr;108(13):3955–8. Available from: http://pubs.acs.org/doi/abs/10.1021/jp036826f

72.   Wang Z, Qian X, Yin J, Zhu Z. Large-scale fabrication of tower-like, flower-like, and Tube-like ZnO Arrays by a Simple Chemical Solution Route. Langmuir. 2004;20:3441–8.

73.   Min C, Shen X, Sheng W. Microwave-assisted aqueous synthesis of ultralong ZnO nanowires: photoluminescence and photovoltaic performance for dye-sensitized solar cell. Appl. Phys. A [Internet]. 2009 Jun 30 [cited 2013 Feb 25];96(4):799–803. Available from: http://www.springerlink.com/index/10.1007/s00339-009-5299-7

74.   Zhu P, Zhang J, Wu Z, Zhang Z. Microwave-Assisted Synthesis of Various ZnO Hierarchical Nanostructures: Effects of Heating Parameters of Microwave Oven. Cryst. Growth Des. [Internet]. 2008 Sep 3;8(9):3148–53. Available from: http://pubs.acs.org/doi/abs/10.1021/cg0704504

75.   Kajbafvala A, Shayegh M, Mazloumi M, Zanganeh S, Lak A, Mohajerani M, et al. Nanostructure sword-like ZnO wires: Rapid synthesis and characterization through a microwave-assisted route. J. Alloys Compd. [Internet]. 2009;469(1-2):293–7. Available from: http://linkinghub.elsevier.com/retrieve/pii/S0925838808001606

76.   Baruah S, Dutta J. Hydrothermal growth of ZnO nanostructures. Sci. Technol. Adv. Mater. [Internet]. 2009 Jan 1 [cited 2013 Feb 20];10(1):013001. Available from: http://stacks.iop.org/1468-6996/10/i=1/a=013001?key=crossref.d25e0ce78c9331246c61a9786d5aafdf

77.   Heo YW, Tien LC, Norton DP, Pearton SJ, Kang BS, Ren F, et al. Pt/ZnO nanowire Schottky diodes. Appl. Phys. Lett. [Internet]. 2004 [cited 2013 Feb 25];85(15):3107. Available from: http://link.aip.org/link/APPLAB/v85/i15/p3107/s1&Agg=doi

78.   Ip K, Heo YW, Baik KH, Norton DP, Pearton SJ, Kim S, et al. Temperature-dependent characteristics of Pt Schottky contacts on n-type ZnO. Appl. Phys. Lett. [Internet]. 2004 [cited 2013 Feb 20];84(15):2835. Available from: http://link.aip.org/link/APPLAB/v84/i15/p2835/s1&Agg=doi

79.   Liu J, Fei P, Song J, Wang X, Lao C, Tummala R, et al. Carrier density and Schottky barrier on the performance of DC nanogenerator. Nano Lett. [Internet]. 2008 Jan;8(1):328–32. Available from: http://www.ncbi.nlm.nih.gov/pubmed/18085814

80.   Yang R, Qin Y, Dai L, Wang ZL. Power generation with laterally packaged piezoelectric fine wires. Nat. Nanotechnol. 2009;4:34–9.

81.   Kim S, Kang BS, Ren F, Ip K, Heo YW, Norton DP, et al. Sensitivity of Pt/ZnO Schottky diode characteristics to hydrogen. Appl. Phys. Lett. [Internet]. 2004 [cited 2013 Feb 25];84(10):1698. Available from: http://link.aip.org/link/APPLAB/v84/i10/p1698/s1&Agg=doi

82.   Lu M-P, Song J, Lu M-Y, Chen M-T, Gao Y, Chen L-J, et al. Piezoelectric nanogenerator using p-type ZnO nanowire arrays. Nano Lett. [Internet]. 2009 Mar [cited 2013 Feb 5];9(3):1223–7. Available from: http://www.ncbi.nlm.nih.gov/pubmed/19209870

83.   Wang ZL, Song J. Piezoelectric nanogenerators based on zinc oxide nanowire arrays. Science [Internet]. 2006 Apr 14 [cited 2013 Feb 17];312(5771):242–6. Available from: http://www.ncbi.nlm.nih.gov/pubmed/16614215

84.   Ajayan PM, Stephan O, Redlich P, Colliex C. Carbon Nanotubes as Removable Templates for Metal Oxide Nanocomposites and Nanostructures. Nature. 1995;375:564–7.

85.   Hao C, Du Y, Li L. Microwave-Assisted Heating Method for the Decoration of Carbon Nanotubes with Zinc Sulfide Nanoparticles. J. Dispers. Sci. Technol. [Internet]. 2009 Apr 20 [cited 2013 Feb 25];30(5):691–3. Available from: http://www.tandfonline.com/doi/abs/10.1080/01932690701688821

86.   Lin C-C, Chu BTT, Tobias G, Sahakalkan S, Roth S, Green MLH, et al. Electron transport behavior of individual zinc oxide coated single-walled carbon nanotubes. Nanotechnology [Internet]. 2009 Mar 11 [cited 2013 Feb 25];20(10):105703. Available from: http://www.ncbi.nlm.nih.gov/pubmed/19417531

87.   Khanderi J, Hoffmann RC, Gurlo A, Schneider JJ. Synthesis and sensoric response of ZnO decorated carbon nanotubes. J. Mater. Chem. [Internet]. 2009 [cited 2013 Feb 25];19(28):5039. Available from: http://xlink.rsc.org/?DOI=b904822g

88.   Guo G, Guo J, Tao D, Choy WCH, Zhao L, Qian W, et al. A Simple method to prepare multi-walled carbon nanotube/ZnO nanoparticle composites. Appl. Phys. A [Internet]. 2007 Jun 20 [cited 2013 Feb 25];89(2):525–8. Available from: http://www.springerlink.com/index/10.1007/s00339-007-4098-2

89.   Luo Y-S, Ren Q-F, Li J-L, Jia Z-J, Dai Q-R, Zhang Y, et al. Synthesis and optical properties of multiwalled carbon nanotubes beaded with Cu 2 O nanospheres. Nanotechnology [Internet]. 2006 Dec 14 [cited 2013 Feb 25];17(23):5836–40. Available from: http://stacks.iop.org/0957-4484/17/i=23/a=020?key=crossref.407c57e76801ad776e6b94b95194c19b

90.   Sun Z, Zhang X, Han B, Wu Y, An G, Liu Z, et al. Coating carbon nanotubes with metal oxides in a supercritical carbon dioxide–ethanol solution. Carbon N. Y. [Internet]. 2007 Nov   [cited   2013   Feb   25];45(13):2589–96.   Available   from: http://linkinghub.elsevier.com/retrieve/pii/S0008622307003971

91.   Hu CJ, Lin YH, Tang CW, Tsai MY, Hsu WK, Kuo HF. ZnO-coated carbon nanotubes: flexible piezoelectric generators. Adv. Mater. [Internet]. 2011 Jul 12 [cited 2013 Feb 6];23(26):2941–5. Available from: http://www.ncbi.nlm.nih.gov/pubmed/21567478

92.   Lin Y-H, Lee P-S, Hsueh Y-C, Pan K-Y, Kei C-C, Chan M-H, et al. Atomic Layer Deposition of Zinc Oxide on Multiwalled Carbon Nanotubes for UV Photodetector Applications. J. Electrochem. Soc. [Internet]. 2011 [cited 2013 Feb 25];158(2):K24. Available from: http://jes.ecsdl.org/cgi/doi/10.1149/1.3522764

93.   Li XL, Li C, Zhang Y, Chu DP, Milne WI, Fan HJ. Atomic Layer Deposition of ZnO on Multi-walled Carbon Nanotubes and Its Use for Synthesis of CNT-ZnO Heterostructures. Nanoscale Res. Lett. [Internet]. 2010 Jan [cited 2013 Feb 25];5(11):1836–40. Available from:

http://www.pubmedcentral.nih.gov/articlerender.fcgi?artid=2964460&tool=pmcentrez&rendertype=abstract

94.   Wang X, Zhang F, Zhu X, Xia B, Chen J, Qiu S, et al. Decoration of multiwalled carbon nanotubes with CoO and NiO nanoparticles and studies of their magnetism properties. J. Colloid Interface Sci. [Internet]. Elsevier Inc.; 2009 Sep 1 [cited 2013 Feb 25];337(1):272–7. Available from: http://www.ncbi.nlm.nih.gov/pubmed/19523647

95.   Liu Y, Jiang W, Li S, Li F. Electrostatic self-assembly of Fe3O4 nanoparticles on carbon nanotubes. Appl. Surf. Sci. [Internet]. 2009 Jun [cited 2013 Feb 25];255(18):7999–8002. Available from: http://linkinghub.elsevier.com/retrieve/pii/S0169433209005947

96.   Chen CS, Chen XH, Yi B, Liu TG, Li WH, Xu LS, et al. Zinc oxide nanoparticle decorated multi-walled carbon nanotubes and their optical properties. Acta Mater. [Internet]. 2006 Dec [cited 2013 Feb 25];54(20):5401–7. Available from: http://linkinghub.elsevier.com/retrieve/pii/S1359645406005131

97.   Huang Y, Lin J, Ding XX, Tang C, Gu CZ, Qi SR. Coating carbon nanotubes with iron oxide using methanol–thermal reaction. Mater. Lett. [Internet]. 2007 Feb [cited 2013 Feb 19];61(3):697–700.   Available   from: http://linkinghub.elsevier.com/retrieve/pii/S0167577X06006434

98.   Lin J, Huang Y, Ding XX, Cheng C, Tang C, Qi SR. Metal Oxide Coating on Carbon Nanotubes by a Methanol-Thermal Method. J. Nanosci. Nanotechnol. [Internet]. 2005 Jun

1 [cited 2013 Feb 25];5(6):932–6. Available from: http://www.ingentaselect.com/rpsv/cgi-bin/cgi?ini=xref&body=linker&reqdoi=10.1166/jnn.2005.120

99.   Fang W, Chyan O, Sun C, Wu C, Chen C, Chen K, et al. Arrayed CNx NT–RuO2 nanocomposites directly grown on Ti-buffered Si substrate for supercapacitor applications. Electrochem. commun. [Internet]. 2007 Feb [cited 2013 Jul 10];9(2):239–44. Available from: http://linkinghub.elsevier.com/retrieve/pii/S1388248106004152

100.   Neocleus S, Pattinson SW, Moisala Motta a. M, Windle a. H, Eder D. Hierarchical Carbon Nanotube-Inorganic Hybrid Structures Involving Cnt Arrays and Cnt Fibers. Funct. Mater. Lett. [Internet]. 2011 Mar [cited 2013 Jul 10];04(01):83–9. Available from: http://www.worldscientific.com/doi/abs/10.1142/S1793604711001609

101.   Reddy A, Shaijumon MM, Gowda SR, Ajayan PM. Multisegmented Au-MnO2/Carbon Nanotube Hybrid Coaxial Arrays for High-Power Supercapacitor Applications. J. Phys. Chem. C. 2010;114:658–63.

102.   Raney JR, Zhang H-L, Morse DE, Daraio C. In situ synthesis of metal oxides in carbon nanotube arrays and mechanical properties of the resulting structures. Carbon N. Y. [Internet]. Elsevier Ltd; 2012 Oct [cited 2013 Jun 21];50(12):4432–40. Available from: http://linkinghub.elsevier.com/retrieve/pii/S0008622312004502

103.   Li D, Zhou H, Honma I. Design and synthesis of self-ordered mesoporous nanocomposite through controlled in-situ crystallization. Nat. Mater. [Internet]. 2004 Jan [cited 2013 Feb 13];3(1):65–72. Available from: http://www.ncbi.nlm.nih.gov/pubmed/14704786

104. Che S, Garcia-Bennett AE, Yokoi T, Sakamoto K, Kunieda H, Terasaki O, et al. A novel anionic surfactant templating route for synthesizing mesoporous silica with unique structure. Nat. Mater. [Internet]. 2003 Dec [cited 2013 Feb 25];2(12):801–5. Available from: http://www.ncbi.nlm.nih.gov/pubmed/14634644

105. Hui C, Shen C, Tian J, Bao L, Ding H, Li C, et al. Core-shell Fe3O4@SiO2 nanoparticles synthesized with well-dispersed hydrophilic Fe3O4 seeds. Nanoscale [Internet]. 2011 Feb [cited 2013 Feb 25];3(2):701–5. Available from: http://www.ncbi.nlm.nih.gov/pubmed/21103488

106. Xia Y, Dai H, Jiang H, Zhang L. Three-dimensional ordered mesoporous cobalt oxides: Highly active catalysts for the oxidation of toluene and methanol. Catal. Commun. [Internet]. Elsevier B.V.; 2010 Sep [cited 2013 Feb 25];11(15):1171–5. Available from: http://linkinghub.elsevier.com/retrieve/pii/S1566736710002025

107. Dahal N, Ibarra I a., Humphrey SM. High surface area mesoporous Co3O4 from a direct soft template route. J. Mater. Chem. [Internet]. 2012 [cited 2013 Feb 25];22(25):12675. Available from: http://xlink.rsc.org/?DOI=c2jm30460k

108. Lee B, Lu D, Kondo JN, Domen K. Three-dimensionally ordered mesoporous niobium oxide. J. Am. Chem. Soc. [Internet]. 2002 Sep 25;124(38):11256–7. Available from: http://www.ncbi.nlm.nih.gov/pubmed/12236725

109. Wang G, Liu H, Horvat J, Wang B, Qiao S, Park J, et al. Highly ordered mesoporous cobalt oxide nanostructures: synthesis, characterisation, magnetic properties, and

applications for electrochemical energy devices. Chemistry [Internet]. 2010 Sep 24 [cited 2013 Feb 25];16(36):11020–7. Available from: http://www.ncbi.nlm.nih.gov/pubmed/20690118

110. Xia Y, Dai H, Jiang H, Deng J, He H, Au CT. Mesoporous chromia with ordered three-dimensional structures for the complete oxidation of toluene and ethyl acetate. Environ. Sci. Technol. [Internet]. 2009 Nov 1;43(21):8355–60. Available from: http://www.ncbi.nlm.nih.gov/pubmed/19924969

111. Yan J, Fan Z, Wei T, Cheng J, Shao B, Wang K, et al. Carbon nanotube/MnO2 composites synthesized by microwave-assisted method for supercapacitors with high power and energy densities. J. Power Sources [Internet]. 2009 Dec [cited 2013 Feb 25];194(2):1202–7. Available from: http://linkinghub.elsevier.com/retrieve/pii/S0378775309010192

112. Society AC. Microwave-assisted chemical synthesis and integration of ZnO nanostructures Microwave-assisted chemical synthesis and integration of patterned ZnO nanostructures.

113. Bai J, Xu Z, Zheng Y. Microwave-polyol Process for Functionalizing Carbon Nanotubes with SnO2 and CeO2 Coating. Chem. Lett. [Internet]. 2006 [cited 2013 Feb 25];35(1):96–7. Available from: http://joi.jlc.jst.go.jp/JST.JSTAGE/cl/2006.96?from=CrossRef

114. Gabriel C, Gabriel S, H. Grant E, S. J. Halstead B, Michael P. Mingos D. Dielectric parameters relevant to microwave dielectric heating. Chem. Soc. Rev. [Internet]. 1998;27(3):213. Available from: http://xlink.rsc.org/?DOI=a827213z

115. Nadagouda MN, Speth TF, Varma RS. Microwave-assisted green synthesis of silver nanostructures. Acc. Chem. Res. [Internet]. 2011 Jul 19;44(7):469–78. Available from: http://www.ncbi.nlm.nih.gov/pubmed/21526846

116. Vazquez E, Prato M. Carbon Nanotubes and Microwaves: Interactions, responses and applications. ACS Nano. 2009;3(12):3819–24.

117. Lin Y, Baggett DW, Kim J-W, Siochi EJ, Connell JW. Instantaneous formation of metal and metal oxide nanoparticles on carbon nanotubes and graphene via solvent-free microwave heating. ACS Appl. Mater. Interfaces [Internet]. 2011 May;3(5):1652–64. Available from: http://www.ncbi.nlm.nih.gov/pubmed/21517032

118. Mazloumi M, Shadmehr S, Rangom Y, Nazar LF, Tang XS. Fabrication of three-dimensional carbon nanotube and metal oxide hybrid mesoporous architectures. ACS Nano [Internet]. 2013 May 28;7(5):4281–8. Available from: http://www.ncbi.nlm.nih.gov/pubmed/23544883

119. Arami H, Mohajerani M, Mazloumi M, Khalifehzadeh R, Lak A, Sadrnezhaad S. Rapid formation of hydroxyapatite nanostrips via microwave irradiation. J. Alloys Compd. [Internet]. 2009;469(1-2):391–4. Available from: http://linkinghub.elsevier.com/retrieve/pii/S0925838808001886

120. Dong Y, He K, Yin L, Zhang A. A facile route to controlled synthesis of Co 3 O 4 nanoparticles and their environmental catalytic properties. Nanotechnology [Internet]. 2007 Oct 31 [cited 2013 Feb 25];18(43):435602. Available from: http://stacks.iop.org/0957-4484/18/i=43/a=435602?key=crossref.5f75e2498b450d0d439326cedf431dae

121. Zhao Z, Tawfick SH, Park SJ, De Volder M, Hart a. J, Lu W. Bending of nanoscale filament assemblies by elastocapillary densification. Phys. Rev. E [Internet]. 2010 Oct [cited 2013 Feb 25];82(4):041605. Available from: http://link.aps.org/doi/10.1103/PhysRevE.82.041605

122. Li X, Qin Y, Picraux ST, Guo Z-X. Noncovalent assembly of carbon nanotube-inorganic hybrids. J. Mater. Chem. [Internet]. 2011 [cited 2013 Feb 25];21(21):7527. Available from: http://xlink.rsc.org/?DOI=c1jm10516g

123. Zilli D, Bonelli PR, Cukierman a L. Effect of alignment on adsorption characteristics of self-oriented multi-walled carbon nanotube arrays. Nanotechnology [Internet]. 2006 Oct 28 [cited 2013 Feb 25];17(20):5136–41. Available from: http://stacks.iop.org/0957-4484/17/i=20/a=016?key=crossref.b9a27c34ae59e9fb2eab28050675b89a

124. Sherrell PC, Chen J, Razal JM, Nevirkovets IP, Crean C, Wallace GG, et al. Advanced microwave-assisted production of hybrid electrodes for energy applications. Energy Environ. Sci. [Internet]. 2010 [cited 2013 Feb 25];3(12):1979. Available from: http://xlink.rsc.org/?DOI=c0ee00352b

125. Kong L-B, Lang J-W, Liu M, Luo Y-C, Kang L. Facile approach to prepare loose-packed cobalt hydroxide nano-flakes materials for electrochemical capacitors. J. Power Sources [Internet]. 2009 Dec [cited 2013 Feb 25];194(2):1194–201. Available from: http://linkinghub.elsevier.com/retrieve/pii/S037877530901026X

126. Zhu T, Liu Y, Hu Z, Wang C, Wen Z. Preparation and characterization of mesoporous Co3O4 electrode material. J. Mater. Sci. Mater. Electron. [Internet]. 2011 Mar 23 [cited 2013 Feb 25];22(11):1649–55. Available from: http://www.springerlink.com/index/10.1007/s10854-011-0340-y

127. Yuan C, Yang L, Hou L, Li J, Sun Y, Zhang X, et al. Flexible Hybrid Paper Made of Monolayer Co3O4 Microsphere Arrays on rGO/CNTs and Their Application in Electrochemical Capacitors. Adv. Funct. Mater. [Internet]. 2012 Jun 20 [cited 2013 Jul 12];22(12):2560–6. Available from: http://doi.wiley.com/10.1002/adfm.201102860

128. Saavedra Flores EI, Friswell MI, Xia Y. Variable stiffness biological and bio-inspired materials. J. Intell. Mater. Syst. Struct. [Internet]. 2012 Dec 5 [cited 2013 Jun 10];24(5):529–40. Available from: http://jim.sagepub.com/cgi/doi/10.1177/1045389X12461722

129. Hunger PM, Donius AE, Wegst UGK. Platelets self-assemble into porous nacre during freeze casting. J. Mech. Behav. Biomed. Mater. [Internet]. Elsevier; 2013 Mar [cited 2013 May 23];19:87–93. Available from: http://www.ncbi.nlm.nih.gov/pubmed/23313642

130. Meyers MA, Lin AY-M, Chen P-Y, Muyco J. Mechanical strength of abalone nacre: role of the soft organic layer. J. Mech. Behav. Biomed. Mater. [Internet]. 2008 Jan [cited 2013 Jun 3];1(1):76–85. Available from: http://www.ncbi.nlm.nih.gov/pubmed/19627773

131. Lin AY-M, Meyers MA. Interfacial shear strength in abalone nacre. J. Mech. Behav. Biomed. Mater. [Internet]. Elsevier Ltd; 2009 Dec [cited 2013 Sep 26];2(6):607–12. Available from: http://www.ncbi.nlm.nih.gov/pubmed/19716105

132. Meyers MA, Chen P-Y, Lin AY-M, Seki Y. Biological materials: Structure and mechanical properties. Prog. Mater. Sci. [Internet]. 2008 Jan [cited 2013 Sep 20];53(1):1–206. Available from: http://linkinghub.elsevier.com/retrieve/pii/S0079642507000254

133. Porter MM, Mckittrick J, Meyers M a. Biomimetic Materials by Freeze Casting. Jom (The J. Miner. Met. Mater. Soc. [Internet]. 2013 Apr 13 [cited 2013 Jun 21];65(6):720–7. Available from: http://link.springer.com/10.1007/s11837-013-0606-3

134. Launey ME, Munch E, Alsem DH, Saiz E, Tomsia AP, Ritchie RO. A novel biomimetic approach to the design of high-performance ceramic-metal composites. J. R. Soc. Interface [Internet]. 2010 May 6 [cited 2013 May 27];7(46):741–53. Available from: http://www.pubmedcentral.nih.gov/articlerender.fcgi?artid=2874234&tool=pmcentrez&rendertype=abstract

135. Shu Y, Yin P, Liang B, Wang S, Gao L, Wang H, et al. Layer by layer assembly of heparin/layered double hydroxide completely renewable ultrathin films with enhanced

strength and blood compatibility. J. Mater. Chem. [Internet]. 2012 [cited 2013 Jun 10];22(40):21667. Available from: http://xlink.rsc.org/?DOI=c2jm34728h

136. Mcallister MJ, Li J, Adamson DH, Schniepp HC, Abdala AA, Liu J, et al. Single sheet functionalized graphene by oxidation and thermal expansion of graphite. Chem. Mater. 2007;19(4):4396–404.

137. Schniepp HC, Li J-L, McAllister MJ, Sai H, Herrera-Alonso M, Adamson DH, et al. Functionalized single graphene sheets derived from splitting graphite oxide. J. Phys. Chem. B [Internet]. 2006 May 4;110(17):8535–9. Available from: http://www.ncbi.nlm.nih.gov/pubmed/16640401

138. Dudney NJ. Thin Film Micro-Batteries. Interface. 2008;17(3):44–8.

139. Theivasanthi T, Alagar M. Electrolytic Synthesis and Characterizations of Silver Nanopowder. Nano Biomed. Eng. [Internet]. 2012 Apr 18;4(2). Available from: http://nanobe.org/index.php?journal=nbe&page=article&op=view&path%5B%5D=176

140. Pramanik S, Kar KK. Nanohydroxyapatite synthesized from calcium oxide and its characterization. Int. J. Adv. Manuf. Technol. [Internet]. 2012 Jul 26 [cited 2013 Jul 15];66(5-8):1181–9. Available from: http://link.springer.com/10.1007/s00170-012-4401-z

141. Liu Y, Huang J, Li H. Synthesis of hydroxyapatite–reduced graphite oxide nanocomposites for biomedical applications: oriented nucleation and epitaxial growth of hydroxyapatite. J. Mater. Chem. B [Internet]. 2013 [cited 2013 Jun 10];1(13):1826. Available from: http://xlink.rsc.org/?DOI=c3tb00531c

142. Kim S, Ku SH, Lim SY, Kim JH, Park CB. Graphene-biomineral hybrid materials. Adv. Mater. [Internet]. 2011 May 3 [cited 2013 Jun 10];23(17):2009–14. Available from: http://www.ncbi.nlm.nih.gov/pubmed/21413084

143. Pint CL, Xu ḰY, Moghazy S, Cherukuri ḰT, Alvarez ḰNT, Haroz ḰEH, et al. Dry Contact Transfer Printing of Aligned Carbon Nanotube Patterns and characterization of their optical properties for diameter distribution and alignment. ACS Nano. 2010;4(2):1131–45.

144. Li F, Son DI, Cho SH, Kim WT, Kim TW. Flexible photovoltaic cells fabricated utilizing ZnO quantum dot/carbon nanotube heterojunctions. Nanotechnology [Internet]. 2009 Apr 15 [cited 2013 Feb 25];20(15):155202. Available from: http://www.ncbi.nlm.nih.gov/pubmed/19420541

145. Attarchi M, Mazloumi M, Behckam I, Sadrnezhaad SK. EIS study of porous NiTi biomedical alloy in simulated body fluid. Mater. Corros. [Internet]. 2009 Nov [cited 2013 Jun 15];60(11):871–5. Available from: http://doi.wiley.com/10.1002/maco.200905212

146. Jung HY, Kim DH, Chun HK, Kim SH, Lim CS, Byun JY, et al. Towards Engineering Nanoporous Platinum Thin Films for Highly Efficient Catalytic Applications. Adv. Energy Mater. [Internet]. 2011 Nov 7 [cited 2013 Jul 16];1(6):1126–32. Available from: http://doi.wiley.com/10.1002/aenm.201100402